FORCE AND VIBRATION ANALYSIS IN MECHANICAL PREPARATION OF ROOT CANALS USING ENDODONTIC FILES

Ph.D. Thesis

By

VINOD SINGH THAKUR

DISCIPLINE OF MECHANICAL ENGINEERING

INDIAN INSTITUTE OF TECHNOLOGY INDORE

DECEMBER 2022

FORCE AND VIBRATION ANALYSIS IN MECHANICAL PREPARATION OF ROOT CANALS USING ENDODONTIC FILES

A THESIS

*Submitted in partial fulfillment of the
requirements for the award of the degree*
of
DOCTOR OF PHILOSOPHY

by

VINOD SINGH THAKUR

1906103001

DISCIPLINE OF MECHANICAL ENGINEERING

INDIAN INSTITUTE OF TECHNOLOGY INDORE

DECEMBER 2022

INDIAN INSTITUTE OF TECHNOLOGY INDORE

I hereby certify that the work which is being presented in the thesis entitled **FORCE AND VIBRATION ANALYSIS IN MECHANICAL PREPARATION OF ROOT CANALS USING ENDODONTIC FILES** in the partial fulfillment of the requirements for the award of the degree of **DOCTOR OF PHILOSOPHY** and submitted in the **DEPARTMENT OF MECHANICAL ENGINEERING, INDIAN INSTITUTE OF TECHNOLOGY INDORE**, is an authentic record of my own work carried out during the time period from July, 2019 to December, 2022 under the supervision of **Dr. PAVAN KUMAR KANKAR**, Associate Professor, Department of Mechanical Engineering and **Prof. ANAND PAREY**, Professor, Department of Mechanical Engineering.

The matter presented in this thesis has not been submitted by me for the award of any other degree of this or any other institute.

29/12/22

VINOD SINGH THAKUR

This is to certify that the above statement made by the candidate is correct to the best of my/our knowledge.

29.12.2022

29/12/2022

Dr. PAVAN KUMAR KANKAR

Prof. ANAND PAREY

VINOD SINGH THAKUR has successfully given his/her Ph.D. Oral Examination held on **April 6, 2023.**

06/04/2023

06/04/2023

Dr. PAVAN KUMAR KANKAR

Prof. ANAND PAREY

----

iii

ACKNOWLEDGEMENTS

DEDICATION

To my parents, family, and friends

for their endless love, care, and encouragement

ABSTRACT

Endodontics is a branch of clinical dentistry that deals with diagnosing and treating inflammation and infection pulp and their repercussions. The primary objective of endodontic therapy includes saving and curing the tooth with infected and inflamed pulp. Endodontics treatment has been described as a clinical dental specialty that combines art and science. It is so because even though endodontics is based on scientific facts, providing a perfect root canal treatment (RCT) is still an art. Various approaches have been used to predict the failure or fracture of endodontic files during root canal treatment. These approaches include fractographic analysis, optical micrographs, scanning electron microscopic images, etc. Most of the previous studies utilized the simulated root canal with the help of endodontic blocks, which deviates highly from real-world practice. Every human has a different tooth structure and a different root canal anatomy. This effect cannot be noticed in simulated root canal preparation. Therefore, this study attempts to define the approaches for failure prediction of endodontic files using human-extracted teeth obtained with due procedures by following clinical ethics. A newly conceptualized and established root canal treatment setup capable of performing the root canal in-vitro experimental research work is developed for laboratory-based experiments. The endodontic files are used to prepare the root canal structure, which is one of the essential stages in canal preparation. The purpose of RCT is to remove all the debris and smear layers from the face of the inner layer of the root canal using an endodontic file. Thus, the designated root canal preparation method allows the endodontic instrument to reach the center portion of the pulp to remove infected and decayed tissue. The endodontic file sometimes fractures during the root canal treatment, usually without any visual degradation. The consequences of these fractured instrument fragments influence the success rate of root canal treatment. Therefore, early detection of such degradation is required during the initial phase of development of such failure.

Further, the present thesis describes a finite element approach to analyze the mechanical behaviour of endodontic instruments when penetrated inside the root canal. Explicit dynamic simulations have been carried out for three different endodontic files: TwoShape (TS1 and TS2) and WaveOne Gold (WOG). It was observed that the TS2 and WOG endodontic files are better suited for RCT than the TS1 endodontic file. The force and vibration analysis has been studied during RCT utilizing reciprocating and rotary motion endodontic instruments. Furthermore, a curve-fitting model has been established to analyze the correlation between force and vibration. A higher magnitude of vibration and force is generated during canal preparation due to overloading in the uneven anatomy of the root canal.

A comprehensive assessment and decision support system for an endodontist may avoid several failures. This research proposes a machine learning-based approach that can help to diagnose the endodontic instrument. The synthetic minority oversampling technique (SMOTE) is employed to balance the minority class. The ensemble bagged tree (EBT), and fine k-nearest neighbor (FKNN) performed well, with accuracies of 98.95% and 97.56% for balanced and imbalanced data. An intelligent health prediction and fault prognosis of the endodontic file during RCT has been proposed using the recorded force signals. Linear support vector machine (LSVM), quadratic support vector machine (QSVM) algorithms, and exponential degradation model (EDM) are used to predict the degradation of the endodontic file so that actions can be taken before actual failures happen. The EDM model accomplished the reliability and degradation characteristics of the endodontic instrument with sensory signals. Additionally, ensemble machine learning algorithms are utilized to evaluate the dimensions of the apical extent following preflaring with primary treatment and retreatment on human extracted teeth during endodontic treatment. In this manner, the thesis provides experimental and data-driven approaches for the health monitoring of endodontic instruments during RCT.

LIST OF PUBLICATIONS

List of Journal Publications:

1. **Thakur, V. S.**, Kankar, P. K., Parey, A., Jain, A., & Kumar Jain, P. (2022), Numerical analysis of WaveOne Gold and 2Shape endodontic files during root canal treatment. *Proceedings of the Institution of Mechanical Engineers, Part H: Journal of Engineering in Medicine*, 236(3), 329-340. https://doi.org/10.1177/09544119211068950.

2. **Thakur, V. S.**, Kankar, P. K., Parey, A., Jain, A., & Jain, P. K. (2022), Force and vibration analysis in biomechanical preparation of root canals using reciprocating endodontic file system: In vitro study. *Proceedings of the Institution of Mechanical Engineers, Part H: Journal of Engineering in Medicine*, 236(1), 121-133. https://doi.org/10.1177/09544119211044236.

3. **Thakur, V. S.**, Kankar, P. K., Parey, A., Jain, A., & Kumar Jain, P., (2022), Prediction of apical extent using ensemble machine learning technique in the root canal through biomechanical preparation: In-vitro Study, *Indian Journal of Pure & Applied Physics (IJPAP),* 60(973-981), 10.56042/ijpap.v60i12.67272.

4. **Thakur, V. S**., Kankar, P. K., Parey, A., Jain, A., & Kumar Jain, P., (2022) The implication of oversampling on the effectiveness of force signals in the fault diagnosis of endodontic instruments during R.C.T. *Proceedings of the Institution of Mechanical Engineers, Part H: Journal of Engineering in Medicine*, (Revision submitted).

5. **Thakur, V. S.**, Kankar, P. K., Parey, A., Jain, A., & Kumar Jain, P., (2022) Health prediction of reciprocating endodontic instrument based on the machine learning and exponential degradation models. *Proceedings of the Institution of Mechanical Engineers, Part H:*

Journal of Engineering in Medicine, (Under review).

List of Conference Proceedings:

1. **Thakur, V. S.**, Kankar, P. K., Parey, A., Jain, A., & Kumar Jain, P., Transfer learning-based approach for health monitoring of endodontic files using time-frequency transformation, *11th International Conference on "Advances in Metrology" AdMet - 2022*, August 24 - 26, 2022, CSIR - National Physical Laboratory, New Delhi, India.

TABLE OF CONTENTS

LIST OF FIGURES

xx

LIST OF TABLES

NOMENCLATURE

D_0	Diameter at the tip
D_0	Denote the diameter of the endodontic instrument at zero taper position
D_4	Denote the diameter of the endodontic instrument at 7% taper position
D_{12}	Indicate the diameter of the endodontic instrument at 6% taper position
D_{16}	Represent the diameter of the endodontic instrument at 3% (for WOG file), 4% (for TS1) and 6% (for TS2) taper position
R	Denotes the radius of the endodontic instrument
R_0	Represents the radius of the endodontic instrument at zero taper position
T	Indicates the taper of endodontic instruments
s	Indicates the distance from the endodontic head to the specific length along the instrument axis
ds	Denotes the root canal length at a particular position from the tip head along the axis of the instrument
β	Denotes the relative angle of the cross-section between two planes
α	Indicates the helical angle of the endodontic instrument
λ	Indicates the pitch of the active part of the endodontic instrument, and it is the distance between adjacent points in the cutting edge

k	Denotes the polar symmetry of the cross-section of the instrument ($k = 3$ for endodontic instrument with symmetry of 120°)
A	Denotes the cross-sectional area of the endodontic instrument
δ_x	Component denotes the deformation in the *x*-direction
δ_y	Component denotes the deformation in the *y*-direction
δ_z	Component denotes the deformation in the *z*-direction
R^2	Regression value
μ	Mean
σ	Standard deviation
$V_i,,$	Data value curve fitting model
V	Obtained from the function $P(F_i)$
X	Original datasets for SMOTE algorithm
N	Oversampling amount (i.e., $1 = 100\%$), N can be a vector with the same number of objects as the number of classes if the variable 'Class' is set
k	Consider the number of closest neighbors, k can be a vector with the same number of objects as the number of classes if the variable 'class' is set
C	Complete dataset classes
Xn	Observations after SMOTE
Cn	Classes of synthesized observation
$x_i \in R^n$	i[th] input vector for the training dataset,
$x_i \in R$	Target value for the ith training dataset,
n	Number of the training set

$G(x_i, x)$	Positive definite kernel function
b	Model parameter
ε	Epsilon margin
$H(t)$	Health indicator
α'	Intercept term considered as a constant
θ'	Random parameters for lognormal distributed
β'	Random parameters for Gaussian-distributed
ϵ'	Gaussian noise yielding
x_i	Observed value
x_i^*	Predicted value
n'	Number of samples

ACRONYMS

RCT	Root Canal Treatment
BME	Biomechanical Preparation
AAE	American Association of Endodontic
CT-Scan	Computed Tomography Scan
NiTi	Nickel Titanium
FEA	Finite Element Analysis
CAE	Computer Aided Engineering
CAD	Computer Aided Design
CAM	Computer Aided Manufacturing
GNB	Gaussian Naive Bayes
SVM	Support Vector Machine
LSVM	Linear Support Vector Machine
QSVM	Quadratic Support Vector Machine
KNN	K-Nearest Neighbor
FKNN	Fine K-Nearest Neighbor
EBT	Ensemble Bagged Tree
RUSBoosted	Random Under Sampling Boosted
SMA	Shape Memory Alloy
NiTiNOL	Nickel Titanium Naval Ordnance Laboratory
SME	Shape Memory Effect
M_s	Martensite start
M_f	Martensite Finish
A_s	Austenite Start

A_f	Austenite Finish
OTR	Optimum Torque Reverse
SAF	Self-Adjusting File
WOG	Wave One Gold
TS	Two Shape
TS1	Two Shape One
TS2	Two Shape Two
RMS	Root Mean Square
STD	Standard Deviation
AI	Artificial Intelligence
ML	Machine Learning
ANN	Artificial Neural Networks
CNN	Convolutional Neural Network
RF	Random Forest
GBM	Gradient Boosting Machine
CBCT	Cone Beam Computed Tomography
Ted4	Four Nodded Tetrahedrons
Hex8	Eight Nodded Hexahedron
H_2O_2	Hydrogen Peroxide
DAQ	Data Acquisition
ICP	Integrated Circuit Piezoelectric
SMOTE	Synthetic Minority Oversampling Technique
ADASYN	Adaptive Synthetic Sampling Approach
SMOM	Synthetic Minority Oversampling Technique for Multiclass

TN	True Positive
TN	True negative
FP	False Positive
FN	False Negative
CDAF	Case Difficulty Assessment Form
NIH	National Institution of Health
NLM	National Library of Medicine
SEM	Scanning Electron Microscope
FESEM	Field Emission Scanning Electron Microscopy
AFM	Atomic Force Microscopy
EDM	Exponential Degradation Model
PCA	Principal Component Analysis
DM	Diffusion Mapping
MVU	Maximum Variance Unfolding
SOM	Self-Organizing Mapping
ISOMAP	Isometric Feature Mapping
RMSE	Root Mean Square Error
MAE	Mean Absolute Error
CMOS	Complementary Metal–Oxide–Semiconductor
RVG	Radio-Visio-Graphy

Chapter 1

Introduction

═══════════════════════════════════════

A brief history of endodontics, root canal treatment (RCT), and its advancement throughout are presented in this chapter. The significance of root canal treatment, the essential measure for the biomechanical preparation of root canal, and the necessity of endodontic treatments are also discussed. Moreover, the crucial steps of the biomechanical preparation of the root canal and endodontic treatments are included in this chapter. Finally, the thesis's organizational structure is provided in the chapter.

═══════════════════════════════════════

1.1 Introduction: RCT and Endodontics

Root canal treatment and *Pathodontia* was the term used to describe *endodontics* in the 20th century [1]. The terminology "endodontics" was first used by a dentist and a famous professor from Georgia, Dr. Harry B. Johnston, in the early 20th century [2]. The meaning of endodontic is taken from the greek, which means **endo** for "inside" and **odont** for "tooth." After that, the term called endodontics deals with the inside of the tooth [2,3]. The clinical dentistry discipline of endodontics is related to pathosis treatment, diagnosis, and prevention of pulp from teeth and its effects. The primary objective of endodontic therapy includes saving and curing the tooth with infected and inflamed pulp. Endodontic therapy saves and cures teeth that have not healed before therapy [2,4]. Endodontics treatment has been described as a clinical dental specialty that combines art and science. It is so because even though endodontics is based on scientific facts, providing a perfect root canal therapy is still an art.

1

1.2 Origin of Endodontics

The field of endodontics has a long history. It started in the 17th century, and since then, there have been numerous advancements, improvements, and ongoing innovations [5]. This field has consistently progressed, especially following Pierre Fauchard (father of modern dentistry), who described the pulp in detail [4,5]. Another endodontics pioneer Dr. Grossman classified the field of history into periods, each covering 50 years, from 1776 onwards [6]. The periods were prior science, early modern periods, early middle age, middle age to modernity, and transformation/revolution age [6]. The progress of the endodontic treatment is presented in Fig. 1.1.

In *prior science (1776-1826)*, endodontic therapy focused on fundamental techniques, such as infections being cured using traditional remedies or leeches and pulps getting cauterized using warm tools [5,6].

In the *early modern period (1826-1876)*, Anaesthesia, obturation needles, piercing broaches, etc., were developed. Medicines were developed to cure the infected soft tissue, and obturation materials were identified that heal cavities [5,6].

In the *early middle ages (1876-1926)*, localized inflammation was the biggest problem. Thus, teeth removal was preferred over RCT despite the development of x-rays with common anaesthesia [5,6].

The treatments reached their heights in the *middle age to modernity era (1926-1976)*, when they became recognized as a technology and a therapeutic. It demonstrated the development of anaesthesia and radiography for improved therapeutic outcomes [5,6]. Additionally, the concept of localized inflammation started steadily declining, leading to an increase in the practice of endodontic treatment.

| Prior science 1776-1826 | Early modern period 1826-1876 | Early middle age 1876-1926 | Middle age to modernity 1926-1976 | Revolution age 1977- till date |

| In this age, therapy was focused on the primitive methods, cauterise pulps. | Anaesthesia, and barbed broaches were developed. The drugs were developed to treat dentinal lesions. | The use of general anaesthesia and X-rays because infection being the main concern at that time | In this era. it demonstrated how anaesthesia and radiography had improved for good clinical outcomes. | After 1977, improved biomechanical preparation technologies were established, reliable. |

Figure 1.1 History of endodontic treatment

Due to escalating attention in endodontics, the American Association of Endodontists (AAE) was established in 1943. The AAE aims to raise awareness and adherence to the most rigorous code of professional conduct for endodontics. The AAE encourages the best healthcare system levels and develops the science and art of endodontics.

From the *revolution age, 1977 to date,* the endodontics field has undergone significant improvements at a remarkably rapid speed starting since 1977 [5,6]. Improvements have been made to obturation, BMP methods, and perception so that the treatment becomes quicker, smoother, and more accurate.

1.3 Root canal treatment and alternative method

Root canal treatment is also known as endodontic treatment. It is a specialized area of dentistry [5] focused on treating disease and infection in the dental pulp area [7]. Endodontists are dental specialists with advanced training in root canal treatment. They hold expertise in saving natural teeth using the state of the art technology like a microscope, micro-CT scan, and other digital imaging to treat patients quickly and comfortably [8]. In modern RCT, a root canal is remarkably efficient and not too painful. The patient can smile right after treatment and bite and chew without difficulty [8]. A solid substance known as dentin within the tooth lies beneath the enamel, and spongy tissue known as pulp exists within the dentin. Pulp comprises tubes of nerves and blood vessels. It extends from the crown to the root of the tooth. If the pulp becomes inflamed or infected, the endodontic treatment help to remove it and relieve the patient from pain and discomfort [7,9].

Root canal treatment is usually advised when a tooth's pulp becomes infected or damaged in order to remove the damaged pulp and save the tooth. However, alternative treatments can be required in some circumstances. Before extracting a tooth, several alternative treatment preferences to root canal treatment (RCT) exist. The alternative treatment consists of medication, pulp capping, pulpectomy, partial pulpectomy, apexogenesis, apexification, regenerative endodontic,

extraction and replacement of teeth, etc.[10–15]. Each of the following treatments is discussed below.

Medication: Medications like antibiotics, painkillers, and anti-inflammatory drugs can sometimes be used to control the pain and infections associated with a loose tooth.

Pulp capping: This is a technique where a medicinal filling is placed over an exposed or nearly exposed pulp. It aims to encourage pulp tissue regeneration and healing.

Pulpectomy: In the partial root canal procedure, the pulp chamber and root canals deteriorated or contaminated pulp tissue are eliminated. After that, the canals are filled with temporary filling material, and the tooth is repaired with a permanent filling or crown.

Partial pulpotomy: This includes eliminating the infectious or inflammatory pulp while keeping the healthy pulp in place and giving a healing-promoting medication.

Apexogenesis: This treatment is utilized in cases where the pulp is exposed owing to trauma or disease, and the tooth is not yet fully matured. The tooth can form further because the dentist removes the unhealthy pulp and replaces it with a substance that encourages the development of healthier pulp.

Apexification: The apexification technique is used when the tooth is fully grown, but somehow the pulp is infected or injured. To stop subsequent infection, the dentists eliminate the damaged pulp and put a substance to promote the formation of a strong tissue barrier at the apex of the tooth.

Regenerative endodontics: This recent technique involves regenerating the injured pulp tissue and encouraging recovery using stem cells and growth recovery.

Extraction and replacement: If the tooth is significantly injured, cannot be saved by a root of the tooth, or the patient has other underlying

5

medical conditions that make a root canal dangerous, then extraction may be required. Then a dental implant, bridge, or denture can replace it in its place.

The patient's general health, the severity of tooth deterioration, and individual preferences would be considered when deciding which treatment to apply. An endodontist or dentist would examine the issue and then discuss each approach's positive and negative aspects with the patient. The cost of the treatment, how long it will take, the complications involved with each procedure, and any potential long-term impacts on the patient's oral health are all things to think about. To make an informed decision and select the best treatment course, patients consult carefully with their dentist or endodontist.

1.4 Biomechanical preparation (BMP)

Biomechanical preparation involves the controlled removal of root canal substances and dentin by carefully using the instruments and associated materials. The followings are the primary objective of the BMP procedure [5]:

- The prepared canal should stream with the contour of the existing canal
- The canal's dimension needs to be smaller at each apical point
- Tapers that gradually narrow out as they approach the access cavity
- Maintaining the initial position for the apical cavity
- Keep the apex space as minimal as possible

1.4.1 Access opening

An opening is made through the crown of the tooth and into the pulp chamber with the help of an airotor. The high-speed airotor help to make an initial ditch in the crown. Following ditching, the root canal path can be identified. A fluid is poured into the canal through the three-way syringe to flush bacteria and disinfect the canals. The ideal access cavity

produces a funnel-shaped straight entry into the canal orifices having line inclinations that descends gently into the canals. The removal of apical contacts reduces the accessibility of instruments to undesired unidirectional forces that may result in errors [16]. Access opening helps to debride the pulp area and increase the visibility to the apical portion, as shown in Fig. 1.2.

Decay
Infected Pulp
Gum
Abscess
Dentin
Blood vessels
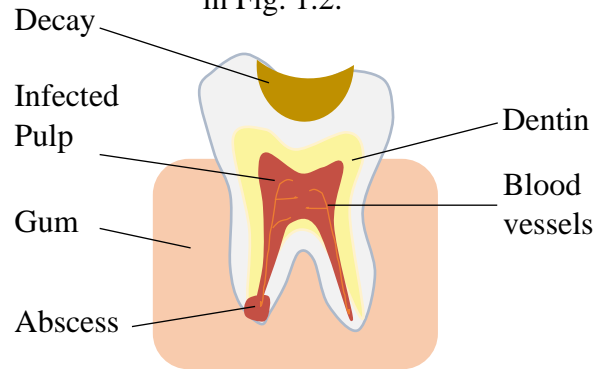
Figure 1.2 Schematic diagram of the access opening process

1.4.2 Cleaning and Shaping

It involves developing a logical cavity specific to each root's anatomy. Afterward, the pulp is removed using small instruments known as endodontic files, as shown in Fig. 1.3, to shape and clean the root canal. A tapering funnel should be formed during biomechanical preparation of the root canal, as shown in Fig. 1.4. It helps to establish the conception of "flow" by making preparations on several different levels [5]. Even as the canal is gradually and minutely enlarged while the location of the access cavity is preserved. The opening shape is kept as minimal as feasible to prevent the iatrogenic issues caused by the overlap cavity.

Airotor
Access opening
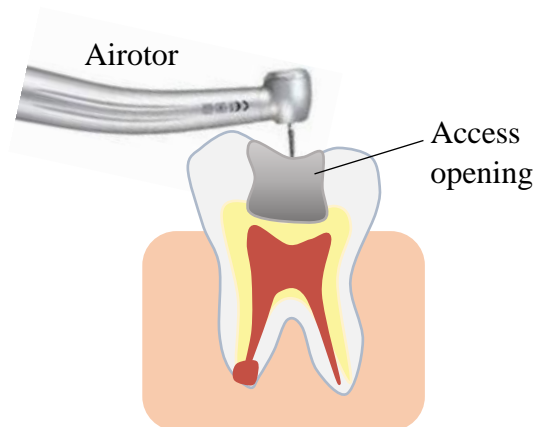
Figure 1.3 Schematic diagram of the shaping process
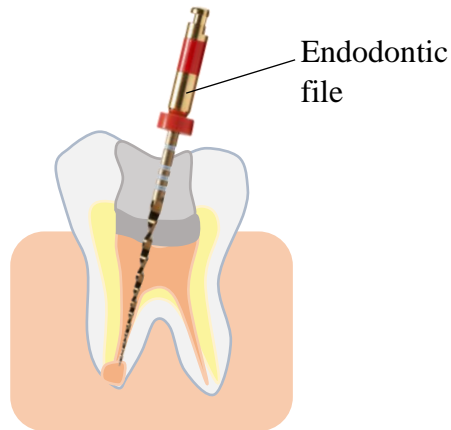
Figure 1.4 Schematic diagram of the cleaning process

1.4.3 Obturation

After the canal preparation, the practitioner fills with gutta-percha and seals the root canals. In most cases, the filling is temporary to close the opening until the practitioner seals the opening [5]. Obturation serves two primary goals: removing every potential point of dental cavity/nerve leaking and sealing the root canal. A correct therapy and evaluation approach is the foundation of successful RCT treatment. The shaping and cleaning procedure determines the level of cleanliness and potential to obturate the anterior area. Hence, it is a representation of shaping and cleansing. The obturating material needs to encapsulate RCT prepared region to restrict tissue fluids flowing into the cavity section [17]. Sealing the prepared space requires a diverse range of materials chosen for their inherent qualities and operating capabilities [18].
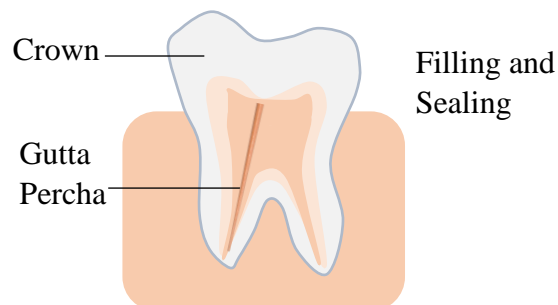
Figure 1.5 Schematic diagram of the obturation process

1.5 Necessity of endodontic treatment

Bacteria can enter the pulp if a tooth is fractured or has extensive cavities. When the pulp becomes inflamed or infected, it causes significant discomfort, and possibly an infection may form in the tooth. Therefore, endodontic treatment or root canal treatment is essential to eliminate the bacterial infection from the infected root canal for preventing the natural tooth.

Sometimes people may be afraid of getting a root canal because it hurts. However, local anaesthetics and dentistry techniques can mitigate pain in the treatment more widely. In fact, having a tooth in the mouth without a filling is more uncomfortable than getting RCT therapy.

1.6 Endodontic file system

An endodontic file is a surgical instrument that the dental practitioner uses for root canal treatment and therapy [19]. Endodontic files are among a large variety of instruments. Endodontic instruments are used to prepare and shape the root canals. These are considered for shaping and cleaning (hand-driven files and motor driven files) or mechanical preparation (reciprocating and rotary files) [20]. Endodontic instruments are manufactured from nickel-titanium alloys or stainless steel. These are effectively precisely twisted wires formed of one of the biocompatible metals or alloys [21]. Additionally, there is a variation in the cross-sectional geometry of files, which allows for a simple separation between them.

1.6.1 Hand-driven file system

Three types of hand files are called H-files, K-reamers, and K-files. The architecture of the cross-sectional shape and the number of threads is the crucial variation between these files. Their cross-section is shaped like a teardrop and manufactured from wire. These files are exclusively designed for reciprocation motion within the canal to obtain smooth canal surfaces. The colour of each hand file corresponds to the suitable dimensions of the instrument's tip because all hand files are colour

coded, as shown in Fig. 1.6. This information is necessary to determine the root canal's apex size before instrumentation.
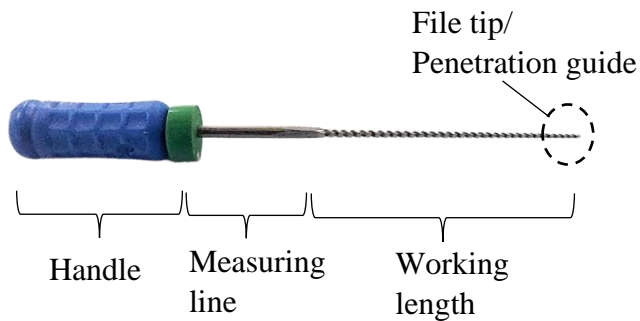
Figure 1.6 Illustrative figure of hand-driven file system

1.6.2 Motor-driven file system

The motor-driven NiTi (Nickel Titanium or Nitinol) endodontic instruments provide significant benefits primarily due to their excellent flexibility. Compared to traditional stainless steel, NiTi alloy has various benefits. Their enhanced flexural strength is advantageous for more efficient and secure treatment in curved and narrow canals. These files are entirely designed for insertion and retraction motion within the canal to obtain smooth canal surfaces, as shown in illustrative Fig. 1.7. Hence minimizing the possibility of an instrument's failure during RCT. At present, NiTi instruments are the primary choice for cleaning and shaping root canals.
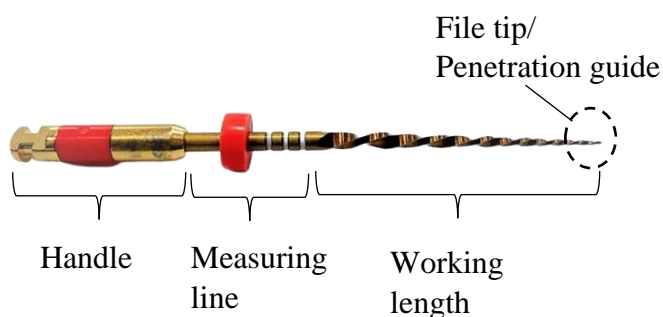
Figure 1.7 Illustrative figure of motor-driven file system

1.7 Multiple motor-driven file generations

Since the early days of contemporary endodontics, there have been several ideas, plans, and methods for canal preparation. Various instruments have been developed over the years for managing and designing canals. Despite the instrument design, a remarkable variety of methods recommended, and the quantity of equipment needed, endodontic therapy is often treated with hope for its possible accomplishment. Edward Maynard created the first file in the middle of the nineteenth century with pointed circular wires made of watch springs and then pianos wires [22]. These instruments had the ability to clean dental pulp and detritus.

The endodontic files were initially manufactured of carbon steel or stainless steel. The development of rotary files was recognized with nickel titanium files. This miracle metal demonstrated advantageous qualities, including super elasticity and shape memory effect [23]. Its characteristics enabled effective instrumentation of curved canals using rotational movement despite lowering the likelihood of catastrophes such as ledge generation or perforation [23]. The growth and development of the endodontic files is presented in Fig. 1.8.
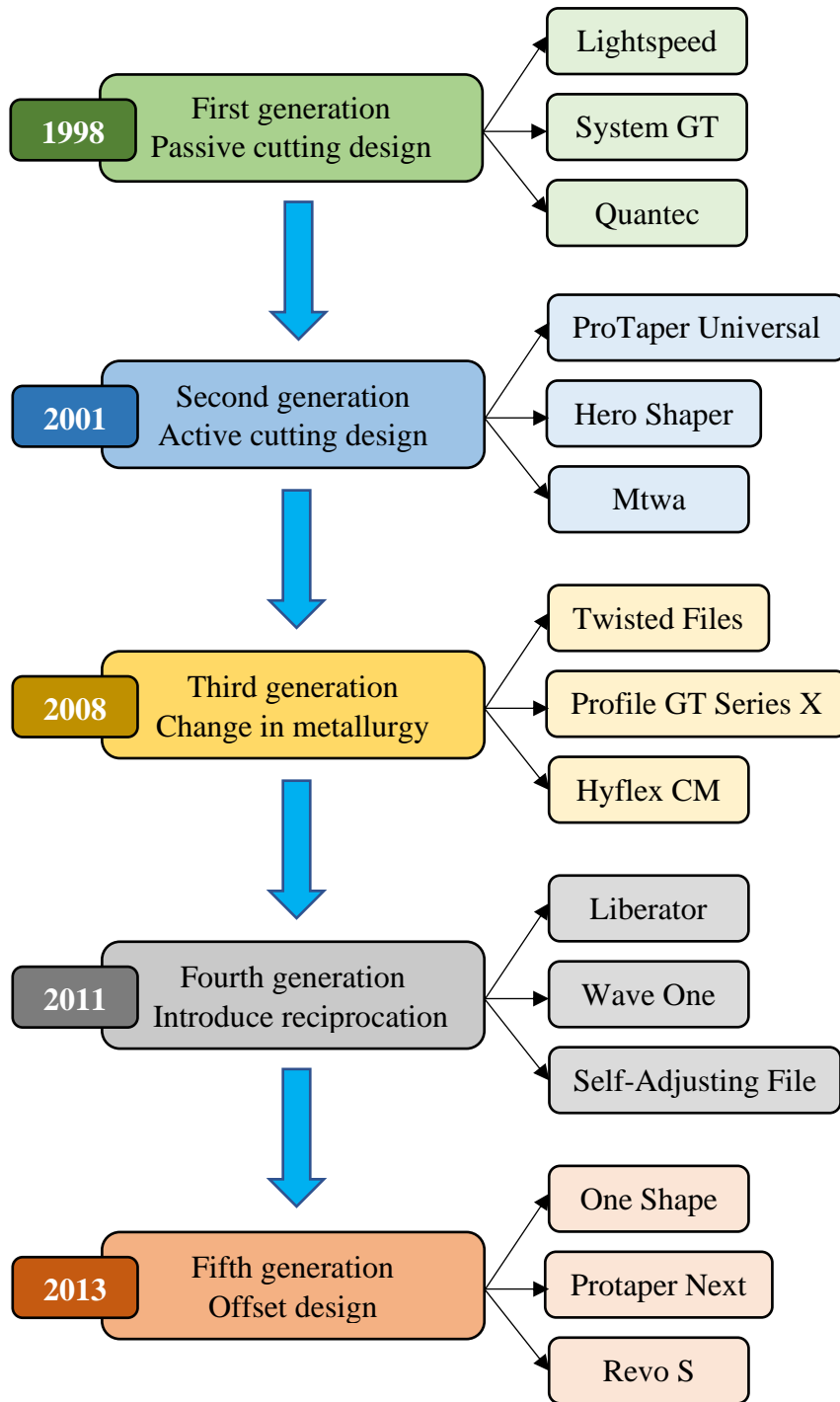
Figure 1.8 Successive generations of motor-driven files

1.8 Organization of Thesis

The thesis is organized into chapters in the following manner:

Chapter 1: Covered the introduction of root canal treatment (RCT), biomechanical preparation, development of endodontic file systems, and

their significance. The importance of root canal treatment, essential measures for the BMP of root canals, and the necessity of endodontic treatments are also included in this chapter. Moreover, the crucial steps of the BMP of the root canal and endodontic therapies are discussed in this chapter.

Chapter 2: Incorporates an overview of the earlier work done for treating root canals. The RCT instrument and mechanical characterization of the endodontic instrument are briefly explained. This chapter comprises the application of artificial intelligence and machine learning technique in endodontics, approaches to diagnostics, and prognostics in RCT. Additionally included the importance and the scope of the current research work.

Chapter 3: Investigates the FEA model of endodontic instruments and teeth during the BMP of the root canal. The nonlinear explicit dynamic analysis in the CAE package (ANSYS) is used to analyze the mechanical behaviour of endodontic instruments. Furthermore, the impact of total deformation, equivalent stress, and equivalent elastic strain on endodontic files during cleaning and shaping are evaluated.

Chapter 4: In-vitro study is carried out during biomechanical preparation of root canals. Actual human-extracted teeth are used in this work to analyze the real exposure of the endodontic therapy using the force and vibration signals. After that, A curve-fitting regression model investigates the interdependency between force and vibration signals.

Chapter 5: This chapter includes a machine learning and artificial intelligence-based method for determining the health condition of an endodontic instrument. This work offers an inventive methodology using force signals to diagnose endodontic instrument faults during endodontic therapy or root canal treatment. Additionally, using machine learning techniques for evaluating the model performance, such as Gaussian Naïve Bayes (GNB), quadratic support vector machine (QSVM), fine k-nearest neighbor (FKNN), and ensemble bagged tree (EBT).

Chapter 6: Presents the intelligent methodology for health prediction of the endodontic file during the RCT. This chapter includes the exponential degradation and machine learning models for assessing the endodontic instrument's state of health. This model is intended to forecast the degradation of the endodontic instrument so that measures can be implemented before actual failures occur.

Chapter 7: This chapter employs the ensemble machine learning approaches to predict the dimensions of the apical extent following preflaring with primary treatment and retreatment on human extracted teeth after endodontic treatment. The ensemble bagged, boosted, and RUSboosted tree classifiers are utilized in this investigation.

Chapter 8: Highlights the significant conclusions of the study and its future direction.

Chapter 2

Literature Review

═══════════════════════════════════════

This chapter briefly explains the RCT instrument for biomechanical preparation and its mechanical characteristics. The importance of endodontic treatment and the problem associated with canal preparation are discussed. Furthermore, the traditional biomechanical preparation techniques are also presented. This chapter comprises the application of artificial intelligence and machine learning in endodontics and approaches to diagnostics and prognostics in RCT. Towards the end, challenges and strategies of machine learning are also included in this chapter. Finally, the thesis's objectives and the present research work's scope are provided.

═══════════════════════════════════════

2.1 RCT instrument for biomechanical preparation

The endodontic file is an essential instrument for root canal cleaning and shaping. The endodontic file needs to be sharp enough to penetrate tissue, but it should also be flexible enough to twist around a complex root canal and access the apex portions of the canal. Initially, stainless steel was used for most of the endodontic files. The stainless-steel file offers excellent mechanical strength and excellent cutting ability. It has been shown to be a particularly efficient tool for straight root canal preparation. Nevertheless, it doesn't consistently or effectively produce excellent outcomes when applied to curved canals [24,25]. There may be unforeseen abnormalities like apical transportation, ledge growth, or perforations [26–30]. The graphical representation and stepwise flow chart of this chapter is presented for more comprehensive and effective

ways of conveying the technical description of the study is shown in the Fig. 2.1.
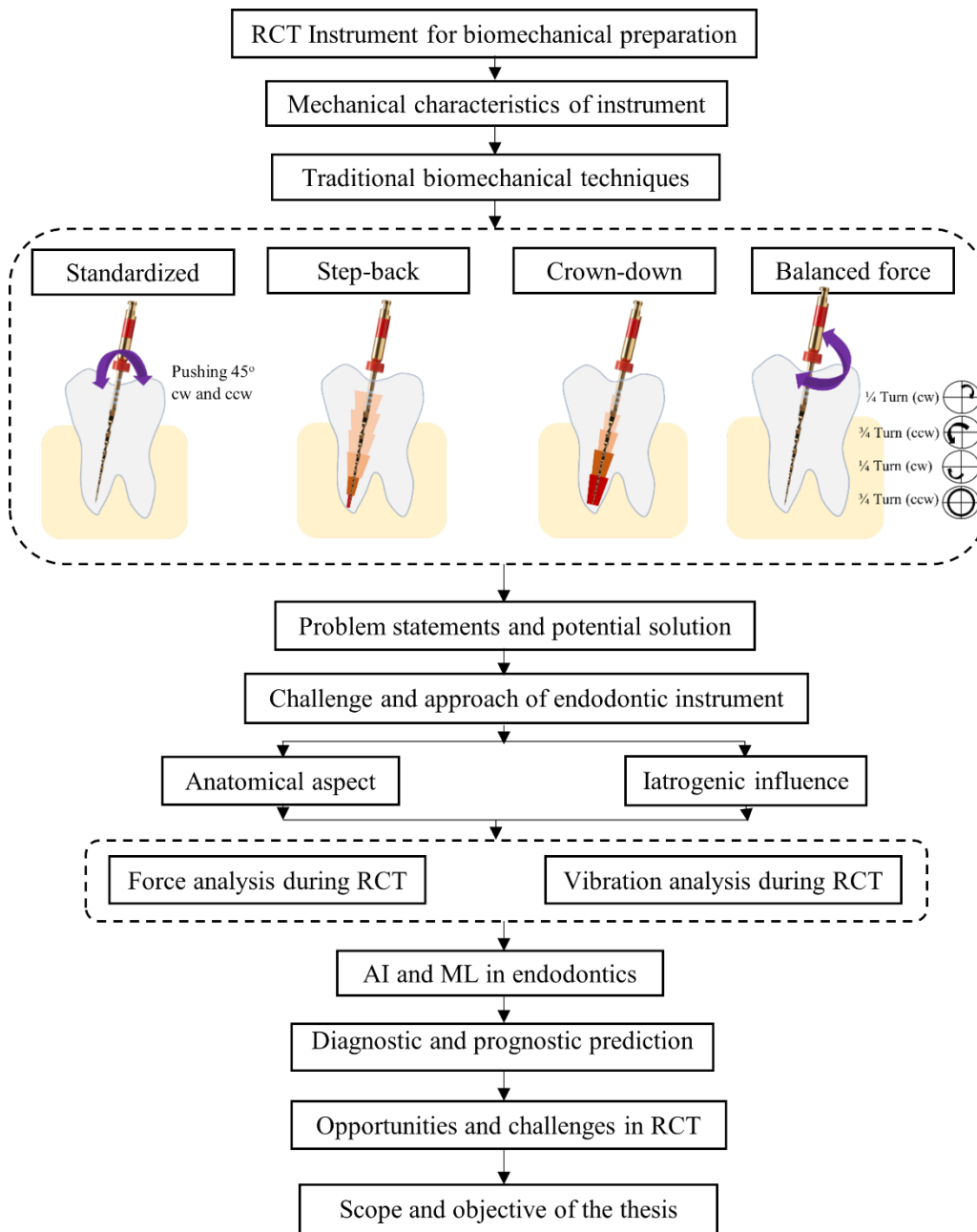
Figure 2.1 The graphical representation and stepwise flow chart of this chapter

2.2 Mechanical characteristics of endodontic instruments

Nickel-titanium (NiTi) or shape memory alloy (SMA) is used to make endodontic files. Endodontics has improved significantly since NiTi

instruments were introduced. The flexibility of NiTi instruments is considerably greater than that of stainless-steel ones [31,32]. This enhanced flexibility produces a considerable decrease in unfavourable variations in the morphology of root canals. An instrument's bending flexibility, torsional rigidity, and cutting effectiveness all characterize its mechanical performance [33]. The structural features of the instrument include bending flexibility and torsional stiffness, which have been the subject of numerous investigations. Additionally, because of this functionality, they can now be used as motor-driven files rather than hand-driven. Compared to the hand-driven file, the motor-driven has a higher cutting performance and considerably reduces the amount of time needed for canal preparation.

At the Naval Ordnance Laboratory, Buehler [34] discovered the NiTi alloy. This NiTi material's name, "NiTiNOL," was established in recognition of its discovery at the Naval Ordnance Laboratory (NOL) [32]. The distinctive properties of shape memory effect (SME) and superelasticity/pseudoelasticity are produced by combining quantities of Ni and Ti at a ratio of around 55 $wt.\%$ of Ni and 45 $wt.\%$ of Ti. The NiTi alloys are in a martensitic state (twinned martensitic state) at low temperatures. However, it transforms into a different condition whenever a load is imposed. The transforms condition referred to the deformed martensitic condition (twinned martensitic state). Martensite is changed into austenite when heated at austenite temperature, and subsequently, the NiTi alloys material returns to its original condition, as shown in the deformation mechanism curve of SMA in Fig. 2.2. Actually, the NiTi alloy goes through a complicated crystalline-to-solid phase transition from martensite to austenite throughout this process [35,36].
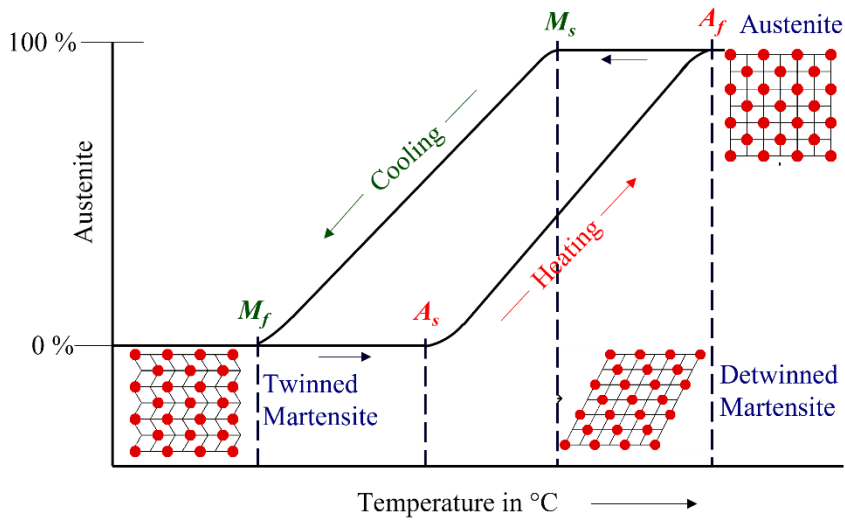
Figure 2.2 Deformation mechanism curve of NiTi shape memory alloy

NiTi's ability to be distorted far more than conventional metal alloys is referred to as superelasticity or pseudoelasticity. It regains normal shape after being unloaded without exhibiting any indications of long-term deformation. Fundamentally, this property is based on the properties of nitinol's stress-induced martensite development [35]. More particularly, at temperatures higher than martensite start temperature (M_s), the stress subjected to an external force causes the nitinol material to convert into martensite as shown in Fig. 2.2. The martensite returns to the austenite phase when the stress is released, and the alloy recovers its original form [36].

2.3 Traditional biomechanical preparation techniques

Few dentists might contest the necessity of cleaning root canal systems. However, there is wide variation in how clinicians describe the precise, feasible actions required to accomplish this purpose [7,37]. The instrumentation techniques have undergone numerous modifications, additions, and upgrades throughout time, and occasionally they have lost much of their original identity. The implementation of recent approaches is typically the result of the confluence of ideas from the past, including

existing methods and creative insights. The growth of taper formation and focus of the root canal can be preserved in varying degrees using each of the following canal preparation techniques.

2.3.1 Standardized technique

In the standardized technique, the geometry initially called for a round section with a small taper and a spherical portion with a slight taper [16]. The apical area of the structure showed a conicity variation of 14º to 75º typical of the endodontic instrument's tip. The endodontic instruments used in the root canal system are developed to a similar working length using the standard approach [16]. This strategy is also known as the "single-length technique." Subsequently, the introduction of NiTi instruments saw a surge in popularity.

2.3.2 Step-back technique

The working length gradually decreased as more extensive, more rigid instruments were utilized. This substantially reduces the frequency of errors committed during canal preparation, particularly with curved root canals [38]. The suggested preparation method has been updated to include cleaning and shaping the root canals [39]. It was in the form of an apical-coronal continual reduced tapered cone, with the chamber opening position having the greatest diameter and the coronal contraction position having the lowest diameter [40]. In order to widen the root canal without distorting it, a well-defined procedure follows the root canal's original shape. The procedure also demonstrates significant improvement in the elimination of debris in addition to preparation in almost parallel walls and provides greater space for their flush.

2.3.3 Crown down technique

Dr. Riitano was credited for developing the first mechanical system that allowed for a crown-down technique [41,42]. Appropriate root canal preparation consists of three steps: coronal, intermediate, and apical. Therefore, the crown-down technique is also known as the "three-time technique." Riitano recommends encouraging the insertion of

instruments into the apical third as straight as feasible [42]. In doing so, we can prevent disruptions from affecting the instrument's operating section. Pushing the tip against the dentinal walls increases the chance of iatrogenic mistakes (i.e., perforation, ledge, etc.). Fundamentally, the crown-down approach encourages a coronal apical advancement that removes the initial coronal disruptions that obstruct accessibility to the apex part.

2.3.4 Balanced force technique

In 1985, Roane & Sabala described using this technique [43,44]. Traditionally, this was connected to specifically designed endodontic instruments with modified tips that were arranged step down. A clockwise movement and apical progress are used to introduce instruments into the root canal, which are then rotated counter-clockwise with enough apical force [44]. The final removal stage is then carried out by rotating the file in a clockwise direction and removing it from the root canal [44]. Coronal preparations are advised for wider diameters than other manual approaches because the instrument doesn't cut along the entire length. The key benefits of the balanced force approaches were reasonable apical control of the file tip, excellent centering, and no need for pre-curving.

2.4 Problem statements and potential solution

Removing contaminated or diseased pulp inside a tooth as part of a root canal treatment helps reduce pain and prevent further damage. However, there are several problems with endodontic treatments that individuals and communities face at present.

- Root canal therapy can be expensive, rendering it unavailable to those who cannot afford it. Untreated tooth decay may arise, which may have major health consequences.
- RCT can be time-consuming and complicated, requiring several dental visits and specialized instruments. As a result, patients

may experience longer waiting periods and delayed treatment, resulting in more toothache and discomfort.

- The success rate of root canal treatment can vary, and some teeth may need to be extracted or retreated. It makes patients angry and unsatisfied, which could increase costs and health concerns.

Potential solutions for these issues include expanding access to relatively affordable dental care and raising capital to develop more efficient and effective treatment modalities, enhancing patient support and education to promote adequate oral hygiene and preventative care. Moreover, improvements in RCT technology and materials may increase success rates and decrease the need for retreatment or extraction.

2.5 Challenges and approaches of endodontic treatments

2.5.1 Anatomical aspects

Numerous anatomical and pathological investigations have shown the complexities of the RCT system's morphology [45]. Consisting of a wide range in the quantity, length, shape, and dimension of root canals, the complicated apical morphology with its extensions and additional canals, and connection with the lateral periodontal ligament and canal cavity region. One of the most challenging aspects of root canal therapy might be the complicated anatomy [46].

Tang et al. [47] observed anatomy's impact on the working length's accessibility during RCT. The anatomical risk factors comprised root canal curvature, calcification, tooth typology (position), and endodontic retreatment. Jain et al. [48] stated that the practitioner needs to overcome multiple obstacles during the cleansing or obturation of the canal because of the canal's complicated and irregular morphology. There is a wide association between the coronal and apical thirds of the canals in the c-shaped root canal system. The morphology of the canals deviates from the apical portion of the root [45,48].

2.5.2 Iatrogenic influence affected by preparing a root canal

A few studies [48–51] briefly mentioned the risk of iatrogenic consequences that might happen in roots while performing RCT using an endodontic file. Furthermore, they highlighted important distinctive preparation failures such as ledging, perforation, deterioration of the apical foramen, and apical blockage. Eleftheriadis and Lambrianidis [52] analyzed and identified the iatrogenic fault in dental healthcare. It was more frequently found that the health quality of the anterior teeth was appropriate, but the curving canals of molar teeth and ledges were observed more frequently [27].

Gorni et al. [53] investigated the patients and clinical features following RCT related to primary healing of iatrogenic perforations and variables influencing long-term prognosis and clinical response. Also, they presented convincing proof of the combined efficiency of skilled workers and the utilization of cutting-edge technologies [53]. Aidasani and Mulay [54] also said that the chance of the affected tooth failing after a root canal procedure increases if there are any perforations. The perforation's size, position, perforation configuration gap, and microbiological invasion of the endodontic system were impacting factors [54]. It is crucial to emphasize cleaning and sterilizing the cavity and affected region to perform successfully over time. If the right medical procedure is thought and carried out, nonsurgical care is feasible with a predictable outcome. Amza et al. [55] analyzed the causes and preventative measures concerning one of the most problematic endodontic treatments and file displacement during canal shaping. They avoided the instrument's severe curvature to accomplish an endodontic procedural approach and confirmed the root canals' accessibility along their full working extent [55]. Irrigation was used during the instrumentation, which was the efficient approach that provided the clearance of detritus along the entire root canal's length [18].

2.6 Force analysis during root canal preparation

Blum et al. [56] used the balanced forced approach to analyze the forces generated during root canal cleaning and shaping with the help of the force-analyzer device. Comparisons were made between the intentional failure of instruments which caused preparatory procedure. The endograph offers a new method for examining canal preparation since that emphasizes the connections between the preparation's factors. Gulabivala et al. [57] evaluated the effect of interfacial forces while RCT. The author used various interfacial forces specific to every individual with diverse file ranges. The utilization of mild or high forces did not affect physical perception [57]. It was indicated that the "manner of file modification" was still uncertain and seemed to be a key factor affecting the result of canal shaping. Peters et al. [58] performed the in-vitro study and evaluated the torque and force regarding canal morphology. While creating curved canals in maxillary molars, observe the physical characteristics of NiTi rotary files. There were significant positive associations between canal shape and physical characteristics [37,58,59]. Diop et al. [60] and Kim et al. [61] used the 3D FEA analysis to compare the force produced during the RCT. For different instrument configurations, there are differences in the position of the highest stress intensity, magnitude, and distribution of residual stresses. Boessler et al. [62] modified the NiTi instrument's surface through electropolishing to decrease the likelihood of fractures. However, this might change the instruments' mechanical behavior. Arias et al. [63] compared different instruments' peak torque and force when preparing distinctive root canals in extracted teeth. According to ProTaper Universal, ProTaper Next endodontic file exhibited more consistency in peak amplitude for distinctive canals. Tokita et al. [64] examined the concepts of continuous and reciprocal motion used to describe the development of apical force through NiTi instrumentation. Both continuous and reciprocal motions produced a substantially lower peak torque and may be advantageous in lowering stress development induced by screw-in forces. Kimura et al. [65] studied the optimum torque reverse (OTR) motion which affected torque and force minimization during RCT using the crown-down or single-length approach. The OTR motion could lower the incidence of

torsional fracture, especially in cases where coronal expansion is limited or specifically restricted. Nayak et al. [66,67] established a relationship between the forces and vibrations through root canal preparation. This work was utilized to anticipate self-adjusting file (SAF) breakage during RCT. They concluded that the vibration is closely related to the force on canals. Thus, the vibration characteristic showed a trend of force fluctuation [66]. Thu et al. [68] reviewed the thorough investigation of the development of torque and force during endodontic instrumentation. Endodontic instruments manufactured of conventional Ni-Ti alloys usually represented larger torque or apical forces than those manufactured of alloys that have undergone thermal treatment. Varying alloys with Varying heat treatments showed different parameter characteristics in instruments. Standardization of instruments is necessary to examine the complex metallurgical characteristics of many alloys.

2.7 Vibration analysis during root canal preparation

In 1996, Levy et al. [69] used the ultrasonically vibrated endodontic file in root canals, and the Nd-YAG laser was proposed for the RCT. They used sonically vibrated or ultrasonically vibrated files to characterize the pressure waves generated in the root canals. Lea et al. [70] performed the in-vitro study to analyze the fluctuation of the endodontic file during canal shaping. The study is based on driving a smaller instrument to oscillate easily inside the canal and triggering an irrigant fluid via biophysical forces like microstreaming. The oscillations characteristics of an instrument when operated in a fluid-filled environment, such as the canal root, were not well recognized. More significant generated outputs were provided to the instruments, which resulted in lower vibration displacement amplitudes [70]. This could minimize the existence of the biophysical forces required to enhance the productivity of the approach.

Verhaagen et al. [71] examined the endodontic instruments' vibration characteristics using the assessment of a numerical model. The vibration modes and probability of breakage of the endodontic file could be predicted using the numerical model of oscillation. Jeon et al. [72] introduced vibration features for distinct motions (conventional and reciprocating) of endodontic motors in dentistry. They used X-Smart (Dentsply, Switzerland), X-SMART PLUS (Dentsply, Switzerland), WaveOne Motor (Dentsply, Switzerland), and conventional motors in their study. Vibrational acceleration was recorded using an accelerometer sensor mounted to the motor's handpiece. Further, reciprocating motors outperformed traditional rotary motors in terms of average and highest vibrations. The standardization of endodontic vibration levels is required for dental health.

Choi et al. [73] compared the vibrations transmitted with two different motions (continuous and reciprocating) via numerous file systems. The vibration was monitored during the pecking action with the help of an accelerometer mounted to a specified location. There were noticeable differences in the mean vibration ranges generated by both motor and instrument systems. Later concluded that reciprocating file systems potentially produce more vibration than continuous file systems. The forces and vibrations produced by endodontic files with three distinct kinematics (rotary, reciprocating and transline motion) were compared by Nayak et al. [74]. The three endodontic files' RMS values regarding force and vibration showed considerable variations depending on their kinematics. The reciprocating file system produced more apical force and vibration than the other file systems. Nayak et al. [67] predicted the failure of the endodontic file using force and vibration signals to avoid iatrogenic mistakes [67]. Park et al. [75] studied the vibrational features in reference to file length and compared the traits across distinct file systems. When authors employed large-size files, a noticeably higher vibration acceleration was seen. Thus, vibrations might be minimized by selecting a file with the smallest size [75].

2.8 Artificial Intelligence (AI) and Machine Learning (ML) in endodontics

The use of AI and ML in endodontics and dentistry has made fantastic progress [76]. Boreak [77] reported the efficacy of AI programs developed for endodontic diagnosis, choice-making, and future forecasting. The RCT incorporated a variety of AI and ML applications. In terms of their neural frameworks, artificial neural networks (ANNs) and convolutional neural networks (CNNs) are mainly used. These AI models were utilized in identifying and classifying root canal failure, retreatment, periapical pathology estimations, and including evaluation of root morphology, as demonstrated in Fig 2.3. According to Boreak's study, neural networks outperformed skilled professionals in accuracy and precision, AI and ML technologies can be more helpful from an expert view [78].
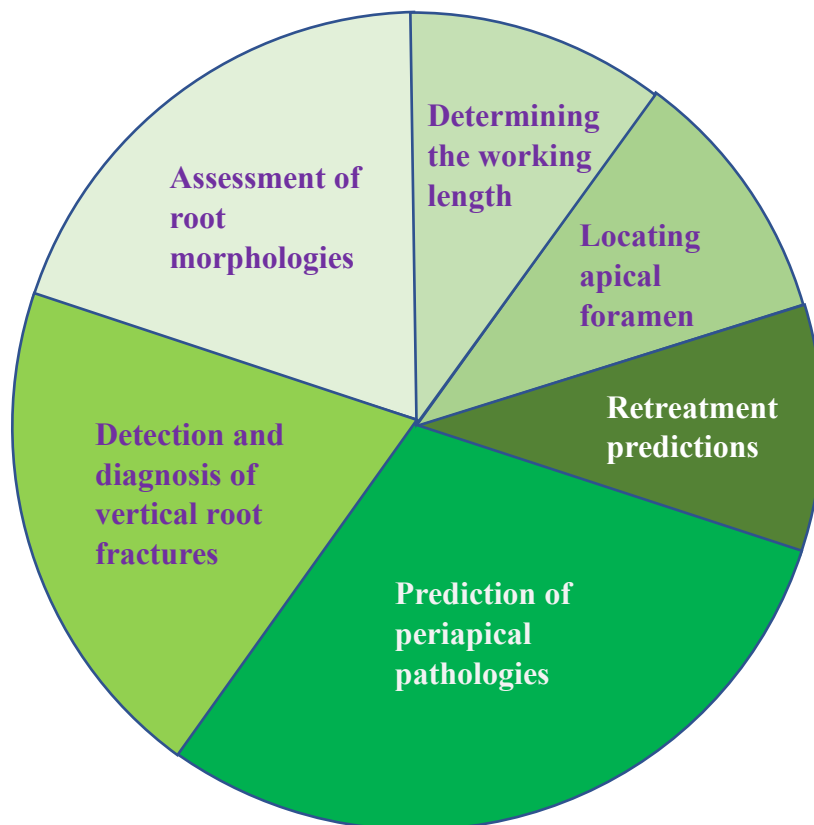
Figure 2.3 Systematic review of artificial intelligence and machine learning designs applications for endodontics in dentistry

2.9 Diagnostic and prognosis prediction of root canal treatment

In order to categorize the existence and lack of root caries and to assess the model performance, Hung et al. [79] used ML techniques in AI. The most prevalent issues with oral hygiene were dental caries [80,81]. AI was employed to create models identifying the chance of developing root infections and acquiring insightful knowledge. However, it wasn't used in dentistry. Making therapeutic approaches with appropriate root cavity identification may improve dental health results. The research was effective and can be used in healthcare situations by dentists, and other practitioners urged to utilize the algorithms for proactive diagnosis and treatment of dental caries. Qu et al. [82] established and validated the ML algorithms for prognostic predictions of RCT microsurgery, preventing therapeutic failures and enhancing clinical judgment. Qu et al. developed the models of random forest (RF) and gradient boosting machines (GBM). The algorithms are anticipated to increase medical decision-making effectiveness and facilitate healthcare professional interaction with patients [82,83]. Hwang et al. [84] employed AI in all spheres of society, including medicine and dentistry, to solve real-world problems. Their study aimed to discover further deep-learning applications in oral and maxillofacial radiography, and CNN was utilized as the primary network algorithm. For effective treatments in orthognathic surgery, diagnosis and treatment planning are the two essential aspects [85]. Therefore, Choi et al. developed and implemented a novel artificial intelligence framework for surgery and determined the type of extraction [85].

2.10 Opportunities and challenges of machine learning in endodontics

The part of artificial intelligence (AI) termed machine learning (ML) has arisen to deal with analyzing massive volumes of data. Dental care is now one of the several fields in which machine learning techniques have

found applications. Recent developments in this area anticipate advancements in clinical diagnosis and prognosis for infections affecting the teeth and dental structures in the future. AI has shown a strong impact and importance across a wide range of responsibilities and approaches in dentistry, and it has the potential to mimic human intelligence to conduct complicated predictions and decision-making in healthcare [86]. Rayes et al. [87] explained the conceptual background of the latest applications of ML to several dental sub-fields in order to identify common study algorithms. Furthermore, it highlights the difficulties involved and the application of these approaches in dental and medical care. Growing innovations' capability, which had started to exhibit successful outcomes in the diagnosis and prognosis of dental problems, could increase the accuracy of the potential treatments provided [87]. It is essential to recognize their complications and ensure that people experience better healthcare by utilizing the instruments efficiently in oral healthcare.

Primary characteristics of research reviewed utilizing machine learning algorithms in endodontics are discussed. Saghiri et al. [88,89] employed the x-ray feature extraction techniques for localizing the smaller apical cavity, followed by data processing using ANNs acting as a judgment mechanism. Through ANN image analysis, it was determined that radiography had a 93% performance level. Kositbowornchai et al. [90] developed an ANN algorithm, and Fukuda et al. [91] evaluated the CNN algorithms for detecting vertical root fractures (VRF) from the radiograph. Healthy and unhealthy vertical root failures were determined using a probabilistic network design. After training, the model obtained the highest sensitivity, specificity, and accuracy values, such as 98%, 90.5%, and 95.7%, respectively. This study has an excellent performance in serving as a framework for identifying vertical root failure. Hiraiwa et al. [92] utilized the CNN intelligence algorithm to evaluate the anatomy of a molar's root on a comprehensive radiograph using cone-beam CT (CBCT). A deep learning algorithm was used to segregate input images of the roots from radiographic images and

evaluate the diagnostic effectiveness in the root morphology classifications. The deep learning algorithm was accurately diagnosed with 86.9% model accuracy. Orhan et al. [93] used the AI approach-based deep CNNs algorithm in CBCT photographs to diagnose periodontal lesions.

This thesis presents a newly established root canal treatment setup involving a biomechanical and cleaning-shaping process. The biomechanical procedure consists of three components: micro-motor, three ways syringes, and an airotor. The endo-motor, endo-motor handpiece, endodontic instruments, and extracted teeth sample are included in the cleaning and shaping process. The established experimental apparatus is proficient in carrying out in-vitro RCT research work. This experimental setup and human-extracted tooth provide the endodontic treatment's actual exposure. The finite element modeling and machine learning approaches are defined the biomechanical behaviour and clinical implications during the RCT.

2.11 Scope and objective of the present research work

This thesis intends to propose a novel and innovative fault diagnosis and health monitoring approach for endodontics systems by obtaining force and vibration signals with the help of machine learning techniques. Additionally, the three-dimensional FEA model has been established to analyze the biomechanical behaviour through RCT. The following are the primary research objectives identified for this study.

- Development of experimental setup, collection of human extracted teeth, and biomechanical samples preparation
- Three-dimensional finite element analysis of endodontic files and tooth during root canal treatment
- Force and vibration analysis in biomechanical preparation of root canals using endodontic file system: In vitro study

- The implication of oversampling and fault diagnosis of endodontic instruments during RCT
- Health prediction of the endodontic instrument based on machine learning and exponential degradation models
- Prediction of apical extent using ensemble machine learning technique

Chapter 3

Numerical analysis of the endodontic files during root canal treatment

===========

Finite element models of the nickel-titanium (NiTi) endodontic instrument used in root canal treatment (RCT) are developed and investigated in this chapter. Three-dimensional models of the tooth and the endodontic tool have been created individually using computer-aided design (CAD) software. These two models are combined to make tooth-endodontic file assembly. The endodontic instrument's mechanical behaviour is investigated by employing the nonlinear explicit dynamic analysis in the CAE package. Total deformation, equivalent elastic strain, and equivalent stress during canal preparation have been evaluated for mechanical behaviour analysis. The three NiTi alloy endodontic instruments available commercially, namely WaveOne Gold (WOG), TwoShape One (TS1), and TwoShape Two (TS2) files, are used for numerical analysis using the FEA. The impact of total deformation, equivalent stress, and equivalent elastic strain on endodontic files during cleaning and shaping are evaluated. The results demonstrate that the TS1 endodontic file exhibits the maximum deformation and equivalent elastic strain compared to TS2 and WOG files.

===========

3.1 Introduction

Root canal treatment is required to prevent infection of the tooth. The infected or inflamed pulps are removed, cleaned or disinfected using the endodontic file. The dental pulp is a structure that lies within the root canal and contains nerves. When the pulp becomes inflamed or infected with the roots of the tooth, it causes pain and toothache. Deterioration in the tooth results in severe decaying, which cannot be treated, and left

with no choice except replacement of the tooth. To prevent the natural tooth from being lost, this procedure is used to get rid of bacterial infection from the infected root canal [94].

In the past, few approaches were used for analyzing the finite element and 3D modelling in cleaning and shaping. Most of the literature discussed the FEA modelling of either an endodontic file or a separate tooth and crown. Kim et al. [61] and Ismail et al. [95] used the WaveOne gold endodontic file for performing the finite element analysis subjected to residual stress, bending, and torsional load, respectively. Özyürek et al. [96] employed the WaveOne gold and TwoShape NiTi endodontic file in the different artificial canals. They statistically analyzed the cyclic fatigue resistance in the artificial canal and compared the scanning electron microscopic analysis between files. Ausiello et al. [97] investigated the mechanical behaviour of the restored model in terms of displacement distribution and stress distribution. Subsequently, the analysis evidenced that the resin slightly affected the stress level of the restored teeth. Tribst et al. [98] developed the implant-supported full-arch dental prosthetic using FEA modelling software. Experimental prosthetic and conventional casted frameworks they were modelled. Afterwards, experimental framework results were analyzed regarding the microstrains, displacement, and von-Mises stress [98]. Borges et al. [99] compared the effect of crown fracture load and stress distribution of occlusal anatomy with the help of FEA modelling. They concluded that the acrylic resin CAD/CAM modelled crown reduces the fracture load and increases the stress concentration. Martorelli et al. [100] proposed a novel approach to evaluate the simplified 3D tooth reconstruction using the finite element method. This approach acquired model data from non-contact laser systems and implemented them for dental and biomechanical applications. Jin et al. [101] investigated the influence of micro-thread in peri-implant bone on stress distribution. Dinc et al. [102] investigated the influence of distinct dental implants on the implant-abutment complex and mandibular crestal bone using the 3D FEA method. Subsequently, it significantly evaluated the

mechanical behaviour of the implant-abutment complex and peri-implant bone.

Recently, Nickel-Titanium (NiTi) endodontic file system has been used in root canal preparation, which includes approximately 55 wt % Ni and 45 wt % Ti [103,104]. The NiTi endodontic instruments are much more flexible than traditional stainless-steel instruments [105,106]. These instruments are used to improve the effectiveness and speed of RCT preparation, even in curved root canals [37]. This research work uses WOG (Dentsply Maillefer, Ballaigues, Switzerland) and TS (Micro-Mega, Besancon Cedex, France) endodontic files. These endodontic files are made up of the M-wire and conventional techniques [104,107,108]. The endodontic file holds superelastic behaviour subjected to highly influenced by the thermal treatment [32]. Based on the temperature provided during heat treatment, the crystallographic structures of endodontic NiTi instruments were categorized as martensitic, austenitic, and R-phased structures [32,103,109]. The NiTi alloys instrument had more flexibility and gave a longer instrument life than other alloys materials [32].

The endodontic files play a significant role in cleaning and treating the entire root canal system. Root canal treatment is an intricate procedure handled frequently by dentists. A crack could be formed during the canal preparation time, and there might be a chance of file failure [21–23]. The file becomes stuck between the root canals in this situation, leading to ledge formation [27]. To prevent this, a recent development that enhanced usages of instrumentation and robotics for a minimally invasive treatment was encouraged [110,111]. One of the best possible ways to prevent the failure of endodontic files is to analyze the maximum working stress and strain in the endodontic file simulation [95,112–114].

In this chapter, a tooth-file assembly has been modelled with the help of a micro-drilling approach to simulate the real-life condition of root preparation during RCT. Simulations have been carried out in the

computer-aided engineering package ANSYS for three different endodontic files: TwoShape (TS1 and TS2) and WaveOne Gold (WOG). The results obtained from the FEA modelling facilitate the accurate knowledge simulation and their respective contours. The outcomes revealed a significant difference in the deformation, equivalent elastic strain, equivalent stress of endodontic files, and tooth assembly. The analysis suggested that the maximum permissible amount of stress within the safe limit avoids mechanical failures in the endodontic files and tooth assembly. The methodology adopted in this study is shown in Fig. 3.1.

3.2 Material and methods

In this work, three different kinds of NiTi endodontic files have been used, namely WaveOne Gold (WOG), TwoShape One (TS1), and TwoShape Two (TS2). The endodontic files were 25 mm long with a standard working length of 16 mm and the tip of the files 0.25 mm [115]. The WaveOne Gold file had a three-variable taper of 7%, 6%, and 3%, respectively, across the file length, whereas TS1 and TS2 had 4% and 6% taper across their length, respectively. Subsequently, these modelled files in CAD package were simulated to real-life usage conditions using the computer-aided engineering (CAE) package ANSYS. For investigating the mechanical behaviour of these three endodontic files, dimensions for the WOG file have been considered as per Dentsply Maillefer, Ballaigues, Switzerland. Whereas, for TS1 and TS2, dimensions used by Micro Mega, Besancon Cedex, France, have been considered. A few endodontic files possess austenitic behaviour, whereas some exhibit martensitic behaviour [104,107]. Thus, two different values of young's modulus are used for the austenite and martensite material.

```
        ┌─────────────────────────────────────────────┐
        │      Create geometric objects (CAD model)    │
        └─────────────────────────────────────────────┘
                            │
                            ▼
        ┌─────────────────────────────────────────────┐
        │       Assemble the geometries (CAD model)    │
        └─────────────────────────────────────────────┘
                            │
                            ▼
        ┌─────────────────────────────────────────────┐
        │         Analysis system model (ANSYS)        │
        └─────────────────────────────────────────────┘
                            │
                            ▼
        ┌─────────────────────────────────────────────┐
        │          Specify the material properties     │
        └─────────────────────────────────────────────┘
                            │
                            ▼
        ┌─────────────────────────────────────────────┐
        │   Edit mechanical (ANSYS mechanical enterprise) │
        └─────────────────────────────────────────────┘
                            │
                            ▼
        ┌─────────────────────────────────────────────┐
        │    Assign the given properties to file and tooth │
        └─────────────────────────────────────────────┘
                            │
                            ▼
        ┌─────────────────────────────────────────────┐
        │         Set the coordinate system setting    │
        └─────────────────────────────────────────────┘
                            │
                            ▼
        ┌─────────────────────────────────────────────┐
        │          Connection and body interaction     │
        └─────────────────────────────────────────────┘
                            │
                            ▼
        ┌─────────────────────────────────────────────┐
        │                Create the mesh               │
        └─────────────────────────────────────────────┘
                            │
                            ▼
        ┌─────────────────────────────────────────────┐
        │             Analysis model setting           │
        └─────────────────────────────────────────────┘
                            │
                            ▼
        ┌─────────────────────────────────────────────┐
        │           Define the boundary conditions     │
        └─────────────────────────────────────────────┘
                            │
                            ▼
        ┌─────────────────────────────────────────────┐
        │              Solve (run simulation)          │
        └─────────────────────────────────────────────┘
                            │
                            ▼
        ┌─────────────────────────────────────────────┐
        │        Solution (post-processing results)    │
        └─────────────────────────────────────────────┘
```

Figure 3.1 Simulation workflow chart of FEA modelling

The parameters of the NiTi superelastic endodontic instruments used to describe the FEA model are shown in Table 3.1. The properties of the dental enamel and dentin considered for the modelling are mentioned in Table 3.2. Enamel is the hard calcified tissue covering the dentin in the tooth's crown. Dentin is the part of the tooth beneath the enamel. The CAD models of three different endodontic files with dimensions are

demonstrated in Fig. 3.2. The geometric parameter used to describe the endodontic file and tooth assembly details are mentioned in Table 3.3.

Table 3.1 Parameters used to describe the properties of the NiTi endodontic file [116,117]

Parameter	Description	Value
E_A	Young's modulus (Austenite)	42.530 GPa
E_M	Young's modulus (Martensite)	12.828 GPa
μ_F	Poisson's ratio	0.33
ρ_F	Density of the NiTi instruments	6450 kg/m^3
G_A	Shear modulus (Austenite)	15.98 GPa
G_M	Shear modulus (Martensite)	4.82 GPa

Table 3.2 Parameters used to describe the properties of dental enamel and dentin [113,118,119]

Parameter	Description	Value
E_E	Young's modulus of enamel	84.1 GPa
E_D	Young's modulus of dentin	18.6 GPa
μ_E	Poisson's ratio of enamel	0.33
μ_D	Poisson's ratio of dentin	0.31
ρ_E	Density of enamel	2970 kg/m^3
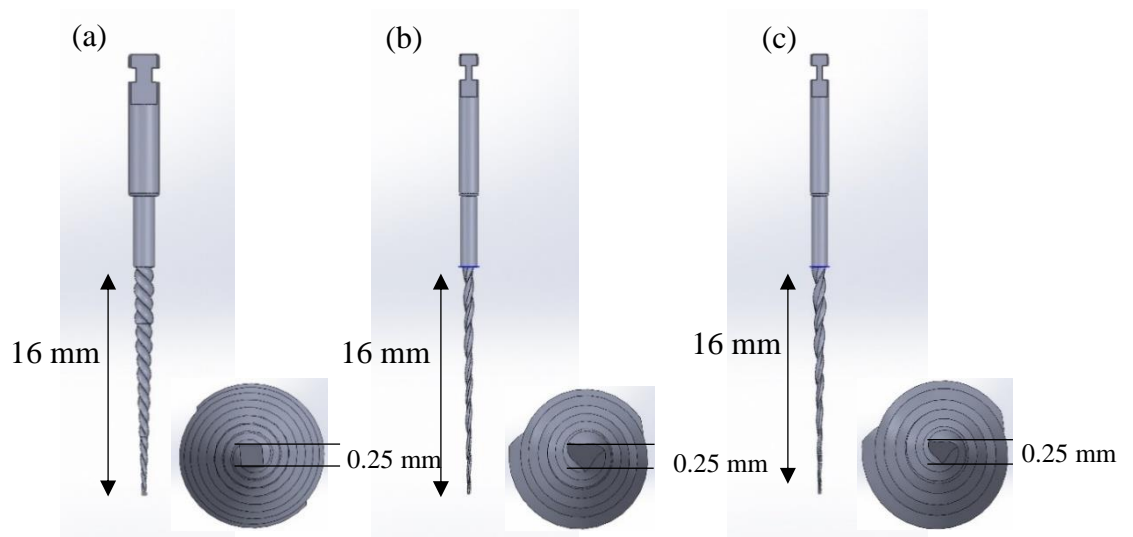
Figure 3.2 CAD model of the (a)WaveOne Gold (WOG) (7%, 6% and 3% taper), (b) TwoShape One (TS1) (4% taper), and (c) TwoShape Two (TS2) (6% taper)

Table 3.3 Geometric parameters used to describe the endodontic file and tooth details

Parameters	values
Length of the endodontic file	25 mm
Working length of the endodontic file	16 mm
Tip diameter	0.25 mm
Taper	WaveOne Gold: 7%, 6% and 3%
	TwoShape One: 4%
	TwoShape Two: 6%
Length of root	14 mm
Length of crown	9 mm
Diameter of crown	7 mm

3.3 Mechanical characteristics of NiTi alloy

The NiTi alloys exist in two different temperature-dependent crystal structures named austenite and martensite phases [31]. Austenite has a high-temperature phase with a cubic B2 crystal structure, and martensite

37

has a low-temperature phase with a monoclinic B19' crystal structure [107]. The super elasticity of the NiTi alloy is associated with transforming austenite to martensite [31,104]. According to Shim et al. [104] and Zupanc et al. [107], the WOG file has the austenite phase with superelastic properties. In contrast, the TS file has the austenitic with small amounts of R-phase and martensite phase with superelastic and two-stage stress-induced transformation properties. Based on the phases, the properties of the endodontic instruments are assigned in the simulation.

3.4 Geometric parameters of the endodontic instruments

The geometric parameters are required for the mathematical model to simulate the endodontic instrument model in computer-aided engineering software. These parameters include the endodontic file's taper, radius, helical angle, relative angle, etc. The simplified geometry of the instrument is discussed in this section. Diameters of the WaveOne Gold file at various locations shown in Fig. 3.3, are calculated using Eq. 3.1 to Eq. 3.3.
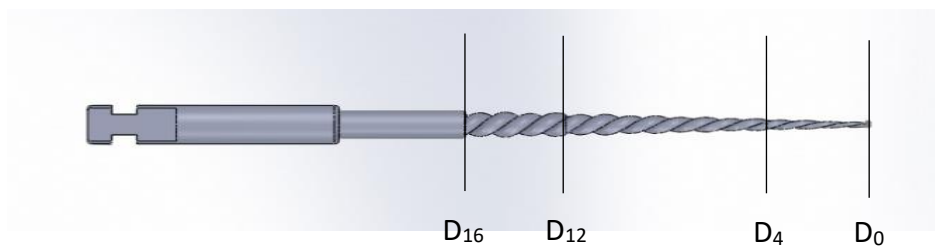
Figure 3.3 Schematic diagram of the WaveOne Gold (WOG) file

Now, calculating diameter according to the design taper section of the endodontic files

Diameter at the tip, $D_0 = 0.25 \ mm$

Thus, at $D_4 = D_0 + (0.07 * 4) = 0.25 + 0.28 = 0.53 \ mm$ (3.1)

Now at

$$D_{12} = D_0 + (0.07 * 4) + (0.06 * 8) = 0.25 + 0.28 +$$
$$0.48 = 1.01 \, mm \tag{3.2}$$

$$D_{16} = D_0 + (0.07 * 4) + (0.06 * 8) + (0.03 \, x \, 4)$$
$$= 0.25 + 0.28 + 0.48 + 0.12 = 1.13 \, mm \tag{3.3}$$

where, D_0 denote the diameter of the endodontic instrument at zero taper position,

D_4 denote the diameter of the endodontic instrument at 7% taper position,

D_{12} indicate the diameter of the endodontic instrument at 6% taper position,

D_{16} represent the diameter of the endodontic instrument at 3% taper position,

Similarly, diameters for TwoShape (TS) files (as shown in Fig. 3.4) can be derived using Eq. 3.4 and Eq. 3.5.
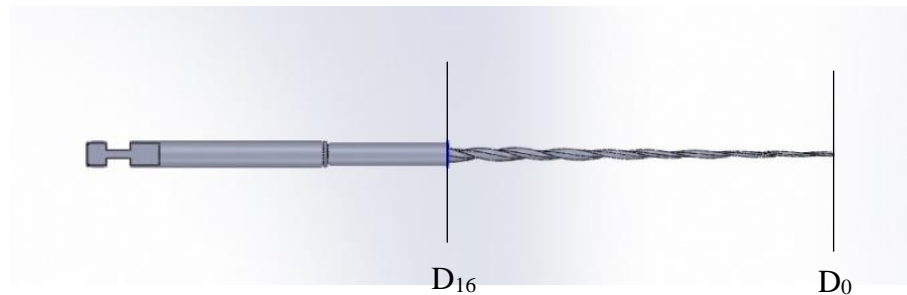
D₁₆   D₀

Figure 3.4 Schematic diagram of the TwoShape (TS) file

Now, calculating the diameter of TwoShape One

$$D_0 = 0.25 \, mm$$

Thus, $D_{16} = D_0 + (0.04 * 16) = 0.25 + 0.64 = 0.89 \, mm \tag{3.4}$

where, D_0 is the diameter of an endodontic instrument at zero taper position,

D_{16} is the diameter of an endodontic instrument at 4% taper position,

Now, for TwoShape Two

$$D_0 = 0.25mm$$

Thus, $D_{16} = D_0 + (0.06 * 16) = 0.25 + 0.96 = 1.21\ mm$ (3.5)

> where, D_0 denote the diameter of an endodontic instrument at zero taper position,
>
> D_{16} denote the diameter of an endodontic instrument at 6% taper position,

The endodontic instruments geometry is shown in illustrative Fig. 3.5. The geometry shows the longitudinal view of the cross-section, and this geometry has been made with the *x-y* plane as a reference coordinate along the *z*-axis.

The radius 'R' of a specific cross-section of the endodontic instrument is a function of distance from the endodontic head 's' and the taper T such that [120]:

$$R(s) = R_0 + \frac{1}{2}\int_0^s T\,ds \tag{3.6}$$

where, R denotes the radius of the endodontic instrument,

> R_0 represents the radius of the endodontic instrument at zero taper position,
>
> T indicates the taper of endodontic instruments,
>
> s indicates the distance from the endodontic head to the specific length along the instrument axis,
>
> ds denotes the root canal length at a particular position from the tip head along the axis of the instrument,

The relative angle of the cross-section of the endodontic instrument between the planes for the orientation may be written as [120]:

$$\beta(s) = \int_0^s \frac{\tan(\alpha(s))}{R(s)}\,ds \tag{3.7}$$
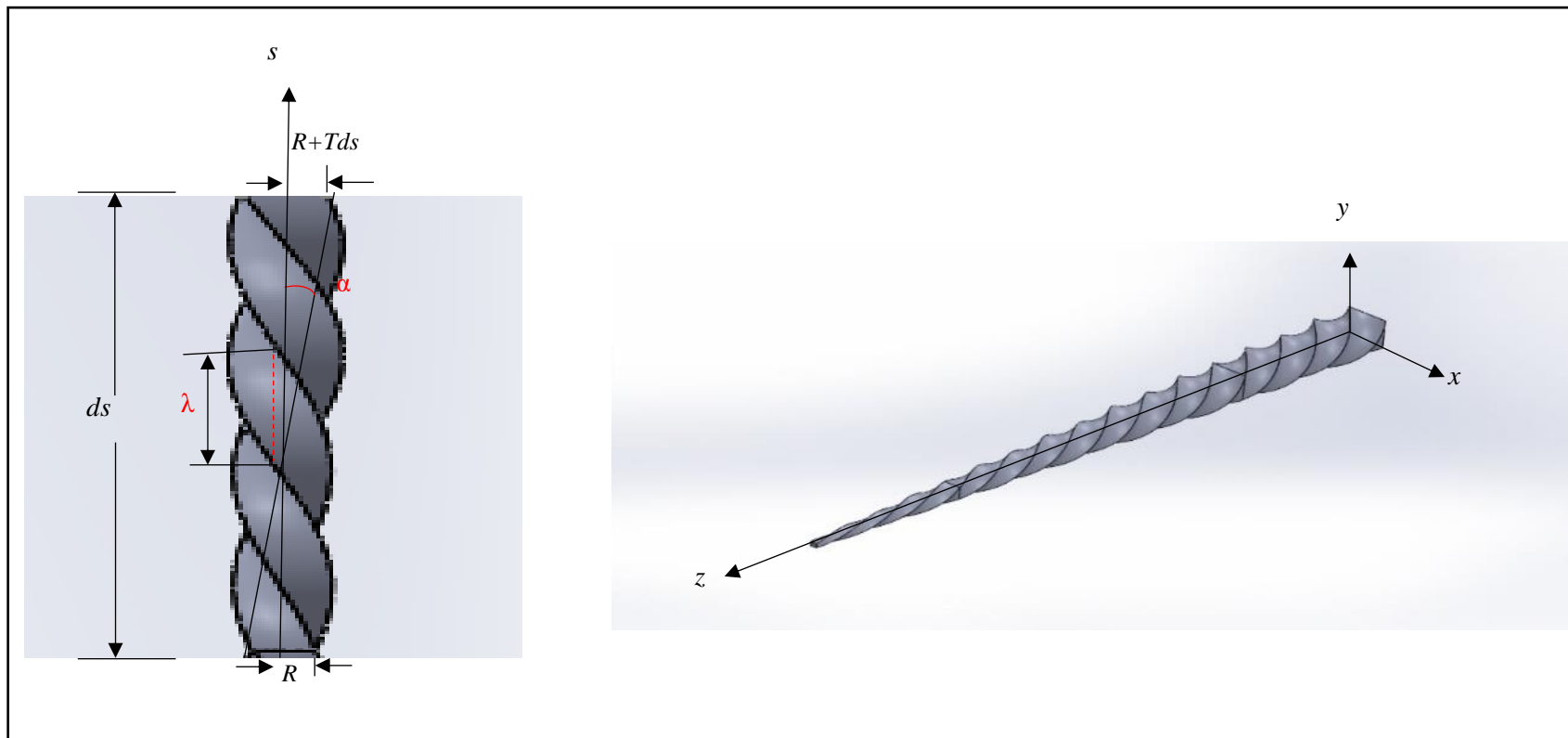
Figure 3.5 Schematic diagram illustrates the geometric parameter for the endodontic instrument for the small section

In terms of endodontic file pitch and polar symmetry, the following relation is obtained,

$$\beta\big(s + \lambda(s)\big) - \beta(s) = \frac{2\pi}{k} \tag{3.8}$$

where β denotes the relative angle of the cross-section between two planes,

α indicates the helical angle of the endodontic instrument,

λ indicates the pitch of the active part of the endodontic instrument, and it is the distance between adjacent points in the cutting edge,

k denotes the polar symmetry of the cross-section of the instrument ($k = 3$ for endodontic instrument (Dentsply Maillefer, Ballaigues, Switzerland) and instrument (Micro-Mega, Besancon Cedex, France) with symmetry of 120º) [120],

when T and $\alpha(s)$ are constant, that means for the endodontic file with the taper.

Now, from Eq. 3.6, 3.7 and 3.8, after substituting the constant value for these equations, can be written as [108]:

$$R(s) = R_o + \frac{1}{2}\,Ts \tag{3.9}$$

$$\beta(s) = \frac{2\tan{(\alpha)}}{T}\ln{\left(1 + \frac{T}{2R_o}s\right)} \tag{3.10}$$

$$\lambda(s) = \left(e^{\frac{\pi T}{k\tan(\alpha)}} - 1\right)s + \frac{2R_o}{T}\left(e^{\frac{\pi T}{k\tan(\alpha)}} - 1\right) \tag{3.11}$$

Meanwhile, all the parameters of the endodontic instrument cross-section vary with the distance 's'. The parameter, such as the cross-sectional area of the endodontic instrument, can be written concerning the function of s in the following way:

$$A = \int_{A(s)} dA \tag{3.12}$$

where A denotes the cross-sectional area of the endodontic instrument.

3.5 Finite element analysis

The finite element analysis of the tooth and the endodontic instrument has been performed in this study. The mechanical behaviour of endodontic instruments during RCT has been analyzed numerically in CAE to simulate using explicit dynamics. The explicit dynamics facilitate the evaluation of total deformation, equivalent elastic strain, and equivalent elastic stress (von-Mises stress). This analysis is a computationally efficient method for studying the model with relatively short dynamic response times. The explicit dynamics analysis responds by the central difference algorithm [121] to integrate the equation of motion. The endodontic files and tooth assembly modelling has been carried out in SolidWorks software (Dassault Systèmes) and later imported to the ANSYS software. Subsequently, material properties have been assigned to the imported model. The NiTi instruments material is deemed nonlinear and isotropic to mimic the actual behaviour of NiTi alloys under stress and strain [95,112,121,122]. Before beginning the simulation, the connection and contact between the two components endodontic file and the tooth are established. Contact designation is necessary to accomplish the appropriate behaviour of numerical accuracy in the explicit dynamic analysis. The adequate selection of the contact and target side depends on the model's geometry. Contact side and target side elements are assigned to both surfaces to enable interaction. The interaction part provides the asymmetric contact behaviour between the contact side and the target side in the body.

Before initiating the simulation, meshing was performed in the last step by discretizing the model. The adaptive meshing technique has been employed to generate the mesh. This technique combines the feature of the ALE (Arbitrary Lagrangian and Eulerian) approach for the meshing. Two different mesh elements have been used for meshing the tooth and file assembly model, namely four-nodded tetrahedrons (Tet4) and eight-nodded hexahedrons (Hex8). Tetrahedron elements are mostly in the region of the endodontic file, and hexahedron elements are in the tooth

region. Details of the meshing elements and nodes for the tooth-file assembly are given in Table 3.4.

The mesh convergence analysis and refinement are carried out to get the appropriate parameter of the mesh. The investigation has been optimized between time (hour), mesh size (mm), and the deformation/displacement (mm) of the model. In this analysis, time and deformation of the model have been obtained while employing the mesh size. The most crucial parameter in the meshing is the selection of optimal mesh size. If the mesh size is too small, it will increase the computational cost, and incorrect results would be reported for a relatively larger value of mesh size. Based on the mesh convergence, an appropriate meshing parameter is selected, and the mesh has been generated on the model, as shown in Fig. 3.6.

The initial and boundary condition of the endodontic instrument and tooth assembly are imposed to simulate the behaviour of the RCT. According to the coordinate system in the explicit dynamics model, displacement is allowed in z-component for penetration of the file inside the tooth, as shown in Fig. 3.7. The rotational movement is provided to the y-component where the endodontic file can rotate inside the root canal. The endodontic file speed is kept constant for specific file. For each type of endodontic file, the speed of the motor is selected based on the manufacturer's specifications. In contrast, the x-component kept fixed, respectively, as summarized in Fig. 3.7. For the tooth, fixed support is provided to the crown and root surface (blue colour in Fig. 3.7) to avoid movement during the root canal preparation.

Table 3.4 Details of the meshing element and nodes

Endodontic files	Number of nodes	Number of elements
WaveOne Gold (WOG)	6893	11384
TwoShape One (TS1)	6241	9026
TwoShape Two (TS2)	6398	9135
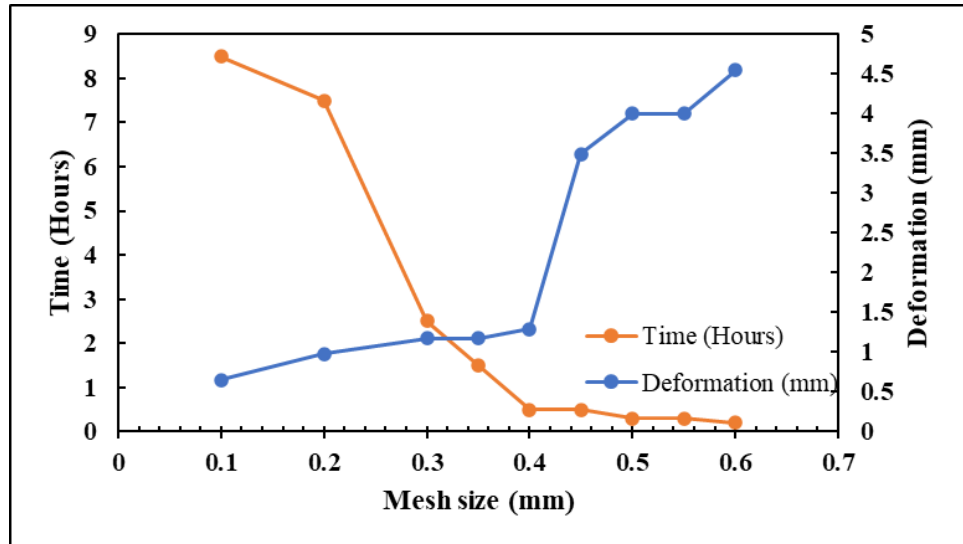
Figure 3.6 Mesh convergence analysis of the tooth-file assembly
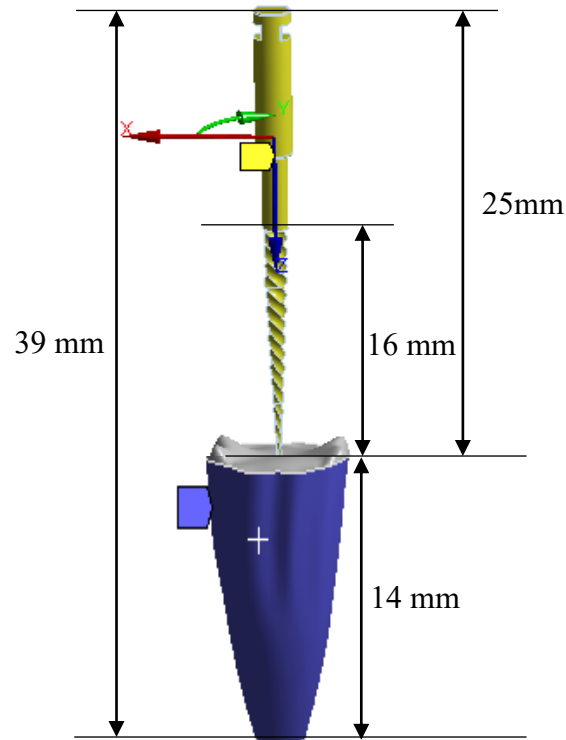
Figure 3.7 Boundary condition of the tooth-file assembly, the yellow colour endodontic file indicates the contact body, whereas the blue and grey colour body indicate the target body

3.6 Results

In this section, the mechanical behaviour of three different endodontic files is obtained in terms of the total deformation of the file under the

applied load during the root canal. Further, the analysis of equivalent strain and stress is carried out. This section also visualizes the tooth-endodontic files combined geometry, deformation, equivalent strain, and stress contour in the tooth-file assembly. Towards the end of this section, results are presented in a comparative table enlisting total deformation, equivalent elastic stress, and strain for tooth, file and assembly for all three endodontic files.

3.6.1 Total deformation

Using the FEA simulation of the tooth-file assembly, the deformation contours are obtained for WOG, TS1, and TS2 endodontic files. A maximum of 1.29 mm deformation is observed in the WOG file, as shown in Fig. 3.8 (a). The maximum deformation amplitude for both TS1 and TS2 files is found to be 3.0 mm and 1.82 mm, respectively. In both TS1 and TS2 files, maximum deformations are obtained at the endodontic's initial shank position and upper section, as shown in Fig. 3.8 (b) and Fig. 3.8 (c), respectively. Out of the three endodontic files considered, WOG suffers 1.29 mm deflection, which is the lowest among all file systems considered in this study. It is because WOG has three different tapers along with the endodontic file, while TS1 and TS2 had a single individual taper along with the file. On the other hand, maximum deformation is observed in the TS1 file. The magnitude of the total deformation (directional deformation in the *x*, *y*, and *z* plane) of the tooth and file assembly is computed numerically in this study using Eq. 3.13 [123,124].

$$\delta_{Total\ deformation} = \sqrt{(\delta_x^2 + \delta_y^2 + \delta_z^2)} \qquad (3.13)$$

where δ_x component denotes the deformation in the *x*-direction, δ_y component denotes the deformation in the *y*-direction, δ_z component denotes the deformation in the *z*-direction.
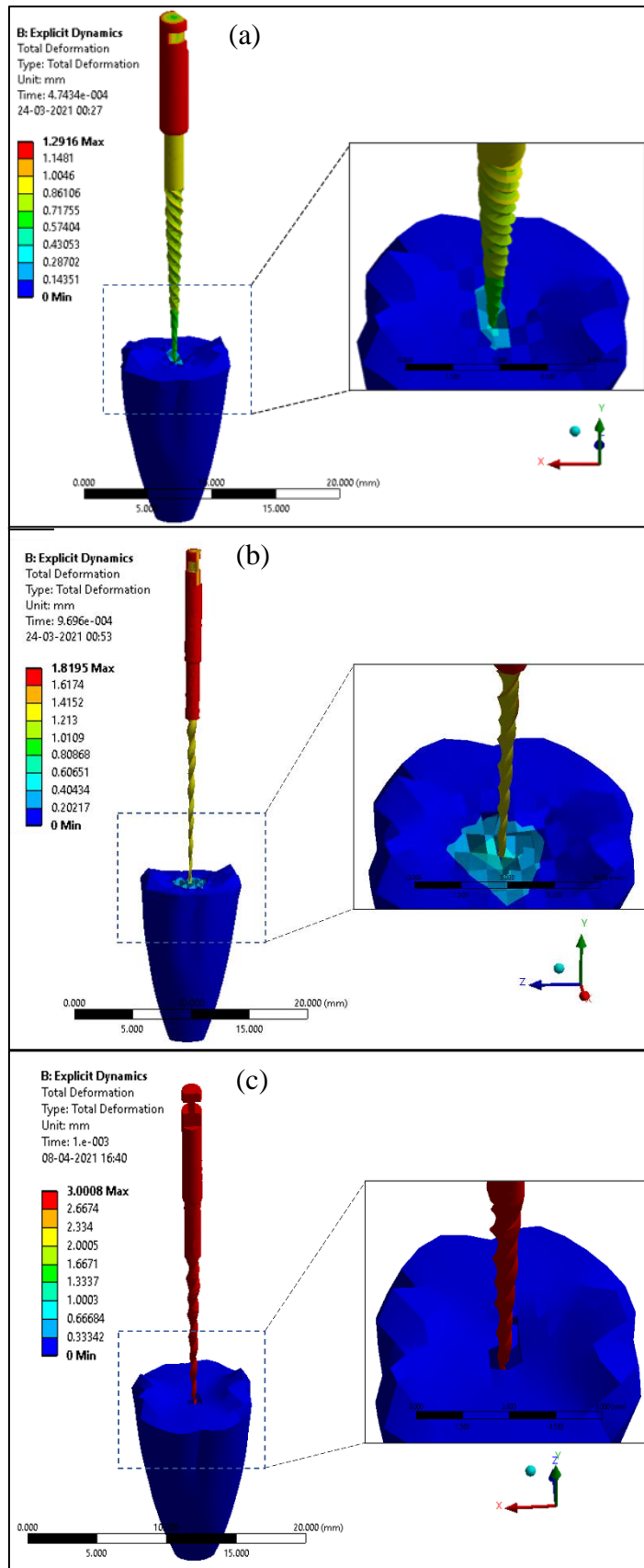
Figure 3.8 Total deformation of the tooth-file assembly (a) Wave one Gold (WOG), (b) 2Shape one (TS1) and (c) TwoShape Two (TS2)

3.6.2 Equivalent elastic strain

The equivalent elastic strain gives the strain value up to which the object will rebound and return to its original position after the load removal. The equivalent elastic strain of tooth-file assembly has been obtained. The simulation is executed to observe the strain distribution over the tooth and file assembly. By comparing the results in Fig. 3.9, it is observed that the tooth is subjected to the maximum amount of strain for all three different file systems. While using the WOG file, the maximum equivalent elastic strain of 0.12 is observed on the tooth as the file penetrated inside the root canal. The maximum equivalent elastic strain using TS1 and TS2 are observed as 0.15 and 0.11, respectively, as shown in Fig. 3.9 (b) and Fig. 3.9 (c). The TS2 developed a less elastic strain in this analysis than the other two endodontic files.

3.6.3 Equivalent stress

The equivalent stress (von-Mises) is one of the criteria that state the maximum distortion energy of the stressed body that attributes to yielding. The von-Mises stress criteria are generally used for a ductile material. The von-Mises stress analysis is carried out for WOG, TS1 and TS2 file systems to get the equivalent stress distribution on the file system, as evident in Fig. 3.10. The maximum von-Mises stress in WOG endodontic file appeared as 1012.5 MPa at the point of contact during the RCT and tip head of the endodontic file, as shown in Fig. 3.10 (a). The maximum values of von-Mises stress for the TS1 and TS2 have been obtained at the same position as observed for the WOG file, as shown in Fig. 3.10 (b) and Fig. 3.10 (c), respectively. The maximum equivalent stress for the TS1 and TS2 endodontic file assembly is 1370.2 MPa and 700.7 MPa, respectively. In the equivalent (von-Mises) stress distribution, the maximum stress is observed in the TS1 file as compared to WOG and TS2 files. Because of the smaller core volume, smaller taper and reduced diameter in the apical length of the TS1 file. Therefore, WOG and TS2 endodontic files have lower stress values than the TS1 endodontic file.
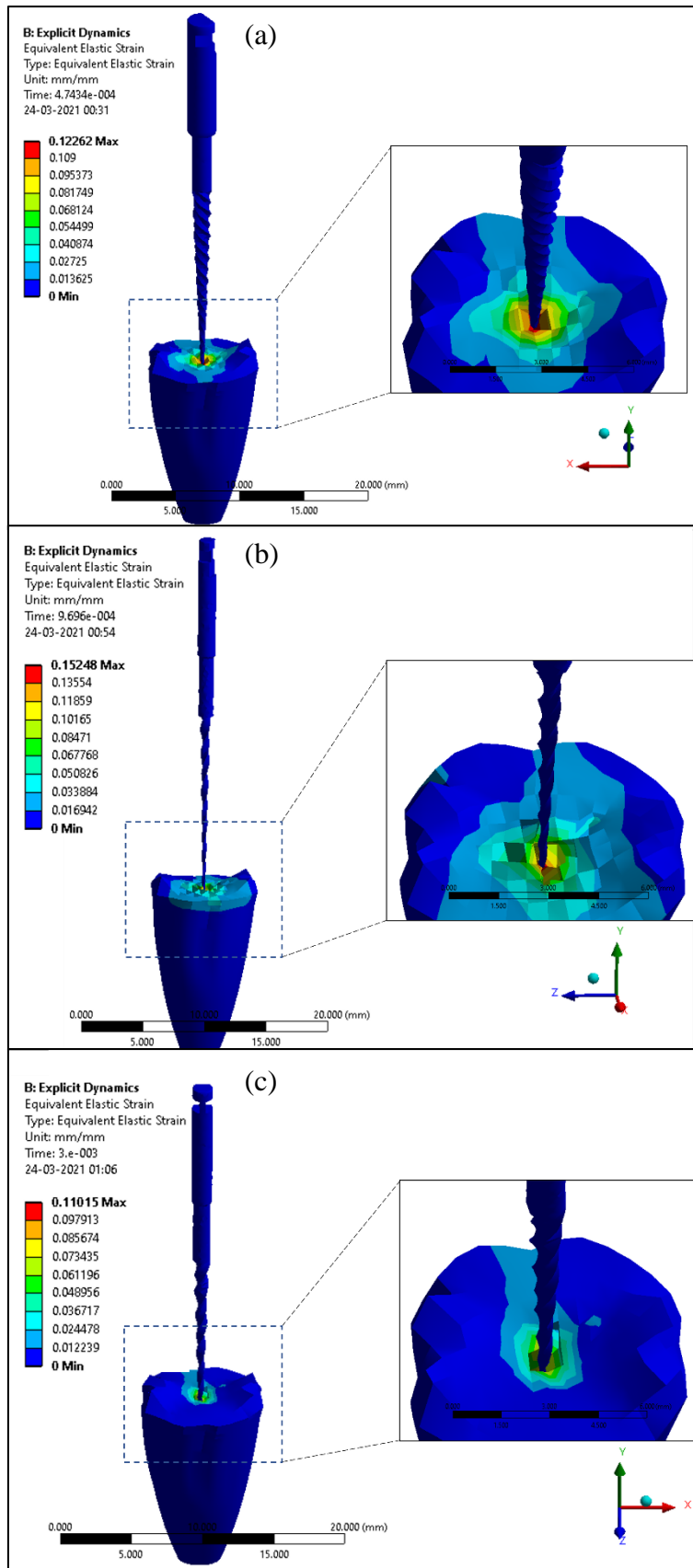
Figure 3.9 Equivalent elastic-strain distribution of the tooth-file assembly (a) Wave one Gold (WOG), (b) TwoShape One (TS1) and (c) TwoShape Two (TS2)
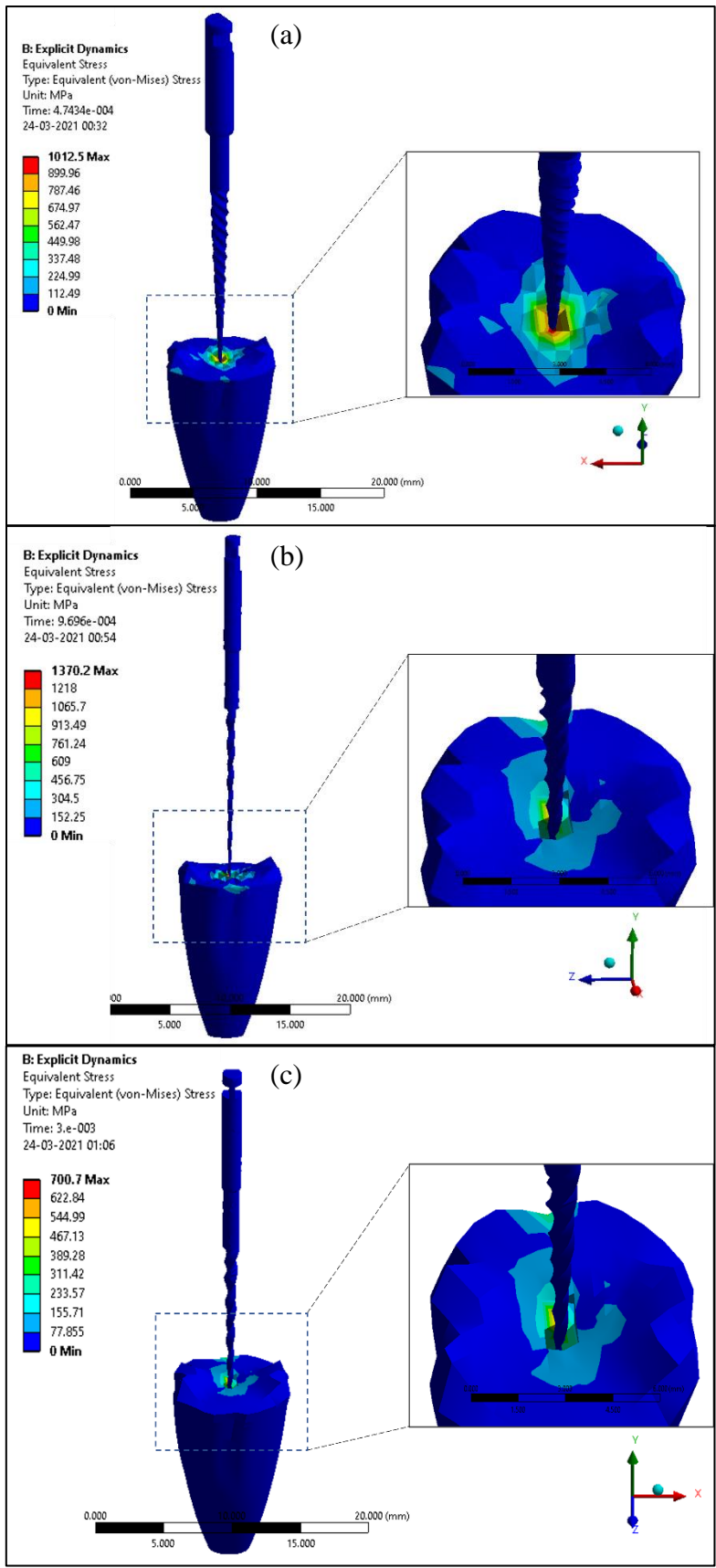
Figure 3.10 Equivalent stress (von-Mises) stress distribution of tooth-file assembly (a) Wave one Gold (WOG), (b) TwoShape One (TS1) and (c) TwoShape Two (TS2)

The results observed that the total deformation, equivalent elastic strain, and equivalent stress dissemination models were affected by the tooth and endodontic file properties of the material and cross-sectional geometry. The simulation results of the endodontic file and tooth assembly categories are mentioned in Table 3.5.

Table 3.5 FEA model analysis result of tooth-file assembly)

		WOG	TS1	TS2
		Maximum	Maximum	Maximum
Tooth-file assembly	Total deformation (mm)	1.29	3.0	1.82
	Equivalent elastic strain (mm/mm)	0.12	0.15	0.11
	Equivalent stress (MPa)	1012.5	1370.2	700.7
File	Total deformation (mm)	1.29	3.0	1.82
	Equivalent elastic strain (mm/mm)	0.001	0.0005	0.0003
	Equivalent stress (MPa)	12.28	2.24	2.64
Tooth	Total deformation (mm)	0.39	0.79	0.27
	Equivalent elastic strain (mm/mm)	0.12	0.15	0.11
	Equivalent stress (MPa)	1012.5	1370.2	700.7

3.7 Discussion

The current study analyzed the mechanical behaviour of the NiTi endodontic files during root canal cleaning and shaping. The total deformation, equivalent elastic strain, and von-Mises stress are obtained for endodontic files and tooth assembly with the help of the FEA. The CAD models used in this study are characterized by a specific design for endodontic files and teeth. The maximum total deformation of the root canal model has been observed when employing the TS1 endodontic file. The maximum deformation amplitude obtained in this analysis is 3.0 mm, as shown in Fig. 3.8 (b). The maximum deformation obtained at the shank region, narrow and wider-mid lands region of the

endodontic file. The TS1 endodontic file's reduced size and the tapered region produced more displacement when the instrument rotated inside the root canal. As a response, the TS2 and WOG endodontic files had increased possibilities of deformation. In this study, the maximum equivalent elastic strain is observed when the TS1 file is employed in the root canal model, as shown in Fig. 3.9 (b). The equivalent elastic strain is observed at the tip of the endodontic file, where the sharp cutting edge is employed for removing debris during canal preparation. The maximum von-Mises stress is obtained in the TS1, as shown in Fig. 3.10 (b). The maximum von-Mises stress is observed when the endodontic file penetrates inside the root canal, which might be the reason for the complex anatomy of the root canal [125–127]. The WOG endodontic file reduces the torsional stress because reciprocating movement engages the dentin at the instrument tip portion during the anticlockwise movement. Whereas the disengages instrument in a clockwise movement immediately afterward [122,128]. In TwoShape, the rotary movement increases the internal resistance in the canal and torsional stress during the canal cleaning and shaping [129,130]. Thus, TS1 endodontic instrument has observed the maximum von-Mises stress. Rundquist and Versluis [125] also showed that the smaller taper's endodontic files are more likely to generate higher stresses. According to the American Dental Association, numerous scientific studies indicated that oral health was associated with other general health conditions such as muscle of the head, neck area, and nervous system health [131,132]. The area of care of dentists includes not only the patient oral health condition but also the overall health condition [133]. This work is dedicated to the study of mechanical behaviour in the tooth-file assembly during the preparation of root canal. A finite element-based approach proposed in this study facilitates the equivalent stress (von-Mises) contours. It can indicate the critical components and the location of high-stress concentration in root canal components, i.e., tooth and file. In addition, the total deformation obtained in this study can help the practitioner to select the suitable file for a designated task.

Table 3.6 Comparative study between the present work and some previous research works

	References			
	Zanza et al. [134]	*Kim et al.* [112]	*Prados-Privado et al.* [117]	*Present work*
Aim and Objective	Mass and polar moment of inertia, torsional failure	Stress distribution in the simulated canal	Bending and torsional properties	Develop and analyze the FEM model
Endodontic instrument	Ni-Ti Rotary instrument	Ni-Ti rotary instrument	Ni-Ti reciprocating file	NiTi rotary and reciprocating instrument
Kind of endodontic instrument	NA	Profile, Protaper, Protaper universal	WaveOne, WaveOne Gold, Reciproc, Reciproc Blue	WaveOne Gold, TwoShape One TwoShaoe Two
Chapter considered	Torsional resistance on the endodontic instrument	Residual stress on the endodontic instrument	Mechanical properties on the endodontic instrument	Mechanical behaviour (through explicit dynamics analysis) on endodontic instruments and tooth
CAD software	SolidWorks	Scanned Micro-CT images	SolidWorks	SolidWorks
Simulation Software	SolidWorks	ABAQUS	ANSYS	ANSYS
Outcomes	Von-mises stress and torsional fracture	Force acting on the instrument and acting torque	Stress distribution, thermal analysis	Total deformation, equivalent elastic strain and equivalent stress

The comparison between previously published research and current research work has been shown in Table 3.6. In this table, the compressive study has been made based on the aim and objective, endodontic instrument, kind of endodontic instrument, the chapter considered, CAD and simulation software, and outcomes of each study.

3.8 Conclusions

In this study, a three-dimensional finite element analysis modelling of the endodontic file during RCT has been performed. The simulation results are investigated in terms of total deformation, equivalent elastic strain, and equivalent stress. The following conclusions are drawn from the study:

- The simulation outcomes evidently show the value of total deformation in the TS1 endodontic file led to the maximum at the narrow lands of the tip region, wider mid-file lands, and shank region among all three endodontic files due to the flared root canal.

- The NiTi alloy-based endodontic instrument possesses superelastic behaviour. Because of the superelastic behaviour, the maximum equivalent elastic strain was obtained in the TS1 endodontic file at the narrow tip region and in the internal canal surface. It is observed when the endodontic file penetrates during the root canal preparation.

- The minimum von-Mises stress in WOG endodontic file is observed on the shank region and the point of contact during RCT. The equivalent stress of TS1 in the assembly of file and tooth having maximum von-Mises stresses distribution compared to WOG and TS2 endodontic files. Thus, the root canal using TS2, and WOG endodontic files is more suitable in RCT than the TS1 endodontic file.

This chapter describes the properties of the NiTi endodontic file, tooth, and a geometric parameter that gives the endodontic file and tooth

54

assembly details. The WOG and TwoShape files geometry has been analyzed for the model preparation using mathematical formulations. Finite element analysis of tooth-file assembly was performed in this chapter. The results of the FEA modelling were covered, which allows for precise knowledge simulation as well as the corresponding contours.

The next chapter provides insight into the experimental analysis of endodontic treatment using real human extracted teeth. Furthermore, an investigation of force and vibration has been carried out for biomechanical preparation using an endodontic file during the root canal treatment.

Chapter 4

Force and vibration analysis during biomechanical preparation of the root canal

The cleaning and shaping of the root canals are essential in root canal treatment (RCT). Excessive forces and vibrations during the process may affect the endodontic file and result in the failure of the file. This chapter investigates force and vibration signals during the root canal's biomechanical preparation. The WaveOne Gold (WOG) and TwoShape (TS) endodontic files have been utilized for root canal preparation. An accelerometer and dynamometer have acquired the vibration and force signals, respectively. The signals are denoised employing db4 (SWT denoising 1-D) wavelet. After that, the statistical features are extracted from the raw and denoised signals. The denoised signals are utilized for the post-processing work. During RCT, the endodontic file severity levels are visualized through the FESEM analysis. Most often, failures are occurred by inadequate root canal instrumentation. The proper instrumentation and the optimal force have been utilized to prevent file failure. A curve-fitting regression model investigates the interdependency between force and vibration. A higher magnitude of vibration and force is generated during canal preparation due to overloading in the uneven morphology of the root canal. These vibrations and forces may initiate the fault in the endodontic file.

4.1 Introduction

One of the crucial steps in RCT is preparing the root canal structure [37]. The circumferential pressure of the canal facilitates the endodontic file to progressively remove the pulp and hard tissue from the root canal surface [7,135]. This circumferential pressure allows the abrasive

57

surface of the endodontic file to uniformly remove the layer of hard tissue from the entire root canal surface [136–138]. Thus, the designated root canal preparation method allows the tooth to reach the centre portion of the pulp with the help of an endodontic instrument to remove infected and decaying tissue [5]. Endodontic instruments play a significant role in root canal preparation [6]. These instruments are made up of nickel-titanium (NiTi) shape memory alloys that are flexible and possess super-elastic behaviour [104,105,107]. At the same time, a major limitation is the failure of endodontic files through cleaning and shaping. The endodontic file sometimes fractures, usually without any visual signal of degradation [139]. The fractured instrument develops the fragment in the canal, creating another task to remove this fragment. The consequences of these fractured instrument fragments influence the success rate of root canal treatment [140]. Thus, there is a need for early detection of such degradation during the initial phase of failure development.

In the past, some approaches are used to predict the failure or fracture during root canal treatment. Most of the literature discussed fractographic analysis, optical micrographs, scanning electron microscopic images, etc., to figure out the failure initiation and cause in endodontic files. McGuigan et al. [141] reviewed the incidence and aetiology of endodontic file failure and analyzed the suggested prevention protocol. They also reported that endodontic files get fractured by torsional overload and flexural fatigue, generally occurring in the apical third of the root canal or with inappropriate use. Gerek et al. [142] evaluated the force required to remove fractured endodontic instruments from the vertical root using the ultrasonic tip. They compared the force with two groups, namely the control and experimental groups. They later reported that the control group had higher significance than the experimental group. Hof et al. [143] explored the properties of the endodontic files and their application in the root canal. The authors also discussed that the vibration of the endodontic file and peripheral force allow hard tissue removal. They

concluded that repetitive use of endodontic files reduces their working efficiency, and efficient removal of pulp is not achieved. Tokita et al. [64] compared the two modes of reciprocating rotation with the continuous revolution in terms of apical force and torque during root canal preparation. Two different modes of reciprocating motion were, namely, time-dependent reciprocating rotation and torque-sensitive reciprocating rotation. They concluded that the reciprocating rational modes reduce stress and torsional fatigue [64]. Burklein et al. [144] prepared the straight root canal with the help of three different endodontic motors and handpieces. Subsequently, they evaluated the axial force and real-time dynamics torque during root canal treatment. They emphasized that rotatory endodontic motors do not provide significant results in clockwise and counter-clockwise peaks. However, manual preparation relatively showed significant peaks compared to rotatory instruments [144]. Nayak et al. [67] acquired the force and vibration signal experienced by endodontic files in the root canal treatment process. They predicted the fracture of the self-adjusting file by statistical analysis of force and vibration signals.

Nickel-titanium (NiTi) endodontic instruments have significantly impacted root canal preparation [145,146]. These instruments have the potential to overcome the chances of failure and avoid fracture during canal preparation [140]. Mirceska and Popovsk [147] compared the various endodontic file systems to examine the accomplishment of endodontic treatment-retreatment. They concluded that the NiTi endodontic systems are better in terms of preservation of the form of the root canals [147]. At present, real-time measurement of the mechanical signals in the in-vitro operation has focused signal characteristics upon simulated model [73], endo turbine with handpiece [148], endodontic motor and handpiece [144] and endo motors with different motions [72]. A few of the literature deals with the force and vibration analysis in the simulated root canal with endo-training blocks [66,74], plastic blocks with curved canals [149], and simulated resin blocks [150] for obtaining uniform root canal geometry and uniform surface. These studies utilized

the simulated root canal with the help of endodontic blocks, which is not real-world practice. For more accurate and practical results, we conducted the root canal preparation on teeth extracted from human beings using the WaveOne Gold (WOG) and TwoShape (TS) files. Every human being has a different tooth structure; thus, root canaling also varies. This effect cannot be noticed in simulated root canal preparation.

4.2 Material and methods

4.2.1 Sample selection and preparation

The human extracted teeth (30 samples) were provided by the College of Dental Science and Hospital Rau, Indore. Each of these extracted teeth had a different kind of root canal. For the selection and preparation of the teeth, the sample preparation process was followed, as shown in Fig 4.1. After receiving the human extracted teeth, then cleaned with the help of hydrogen peroxide (H_2O_2) solution. Followed by a mounting process in a specially designed mould prepared using cold setting material (a mixture of powder and liquid) as shown in Fig. 4.1. The tooth, once embedded into the mould was allowed to cool down to solidify so that the mould gains enough strength. After getting the moulded teeth samples, the biomechanical preparation was carried out.

4.2.2 Root canal preparation

Root canal preparation begins with the creation of an initial ditch using a round burr (Prime Dental Products Pvt Ltd.) in a high-speed airotor handpiece. Afterwards, root canal cavities are made through a straight burr (Prime Dental Products Pvt Ltd.). Subsequently, water irrigation was provided at regular intervals during root canal preparation [5], as shown in Fig. 4.2 (a).
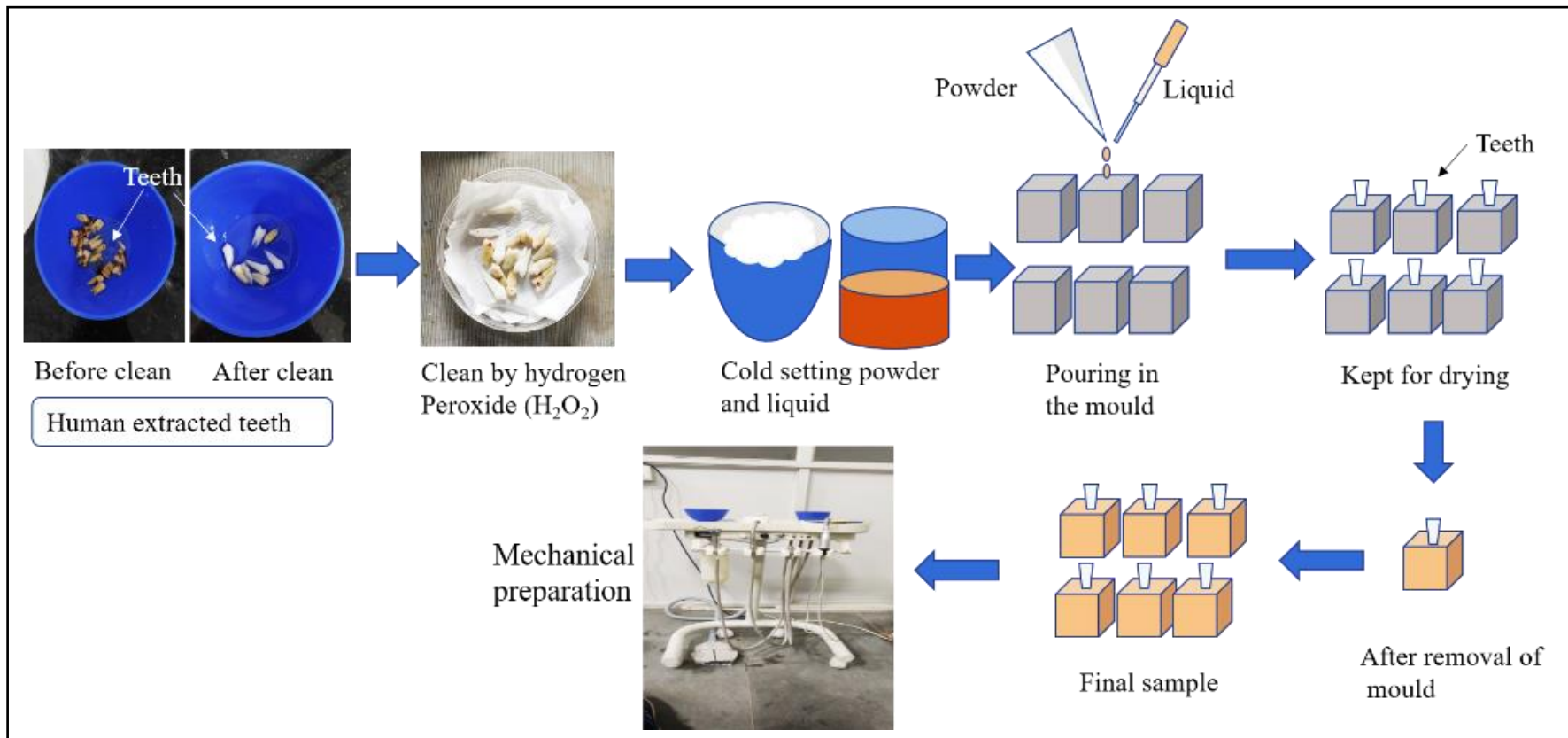
Figure 4.1 Process flow diagram of the sample preparation

Irrigation is a significant part of canal preparation, which assists in removing the necrotic tissue and helps in the debridement of the root canal system [5,111,151,152]. The WaveOne Gold (WOG) and TwoShape (TS) endodontic files remove the smear layer and debris from the interior surface of the root canal dentin. The WOG and TS endodontic files are reciprocating and rotatory files, respectively. The WOG and TS endodontic file systems are manufactured by Dentsply (Dentsply Maillefer, Switzerland) and MicroMega (Besancon Cedex, France), respectively. The reciprocating WOG #25.07 file revolves at a speed of 300 rpm and torque of 5 N-cm, whereas the rotatory TS #25.04 file which rotates at a speed of 250-400 rpm and torque of 2 N-cm. The endodontic file was coupled with the endo-motor X-SMART PLUS (Dentsply Maillefer, Switzerland, imported & marketed by Dentsply India Pvt. Ltd). The endodontic file systems were used with reciprocating and rotary motion as per the user manual.

4.3 Experimental setup and data acquisition

After the biomechanical preparation of the root canal, the experimental setup, as shown in Fig. 4.2, was used to acquire the force and vibration signals. Initially, the prepared tooth sample was gripped in an alloy vice which was mounted over the Kistler dynamometer (Kistler Group, Winterthur, Switzerland). The vice provided rigid support during the experimentation process to prevent the sample's movement, as shown in Fig. 4.2. A tri-axial accelerometer (PCB Piezotronics Inc., Depew, New York) was used for the vibration acquisition. The accelerometer was placed adjacent to the mounted tooth sample on the vice, as shown in Fig. 4.2 (a) and 4.2 (b). The sensitivity of the highly sensitive ceramic shear ICP® accelerometer is ($\pm$10%) 100 mV/g or (10.2 mV/(m/s²)) and the measurement range is $\pm$ 50 g pk ($\pm$490 m/s² pk). The dynamometer measures the force up to 10 kN and sensitivity: $\approx$ -7.5 pC/N (F_x, F_y) and $\approx$ -3.5 pC/N (F_z). The accelerometer and dynamometer were directly connected to the data acquisition (DAQ) system (OROS SA, Grenoble, France). Force signals were sampled at 7.1 kHz, and vibration signals at

51.2 kHz [67,74]. The accelerometer and dynamometer were connected to the data acquisition system. DAQ system was connected to the desktop and laptop for transferring the data. The signals were visualized and processed in MATLAB software (MathWorks, MA, USA). The reciprocating and rotary file system used WaveOne Gold (WOG) and TwoShape (TS) endodontic files for the RCT. A highly experienced practitioner has prepared the root canal. This study used a new WOG and TS file for each tooth sample and distilled water for irrigation during this process.
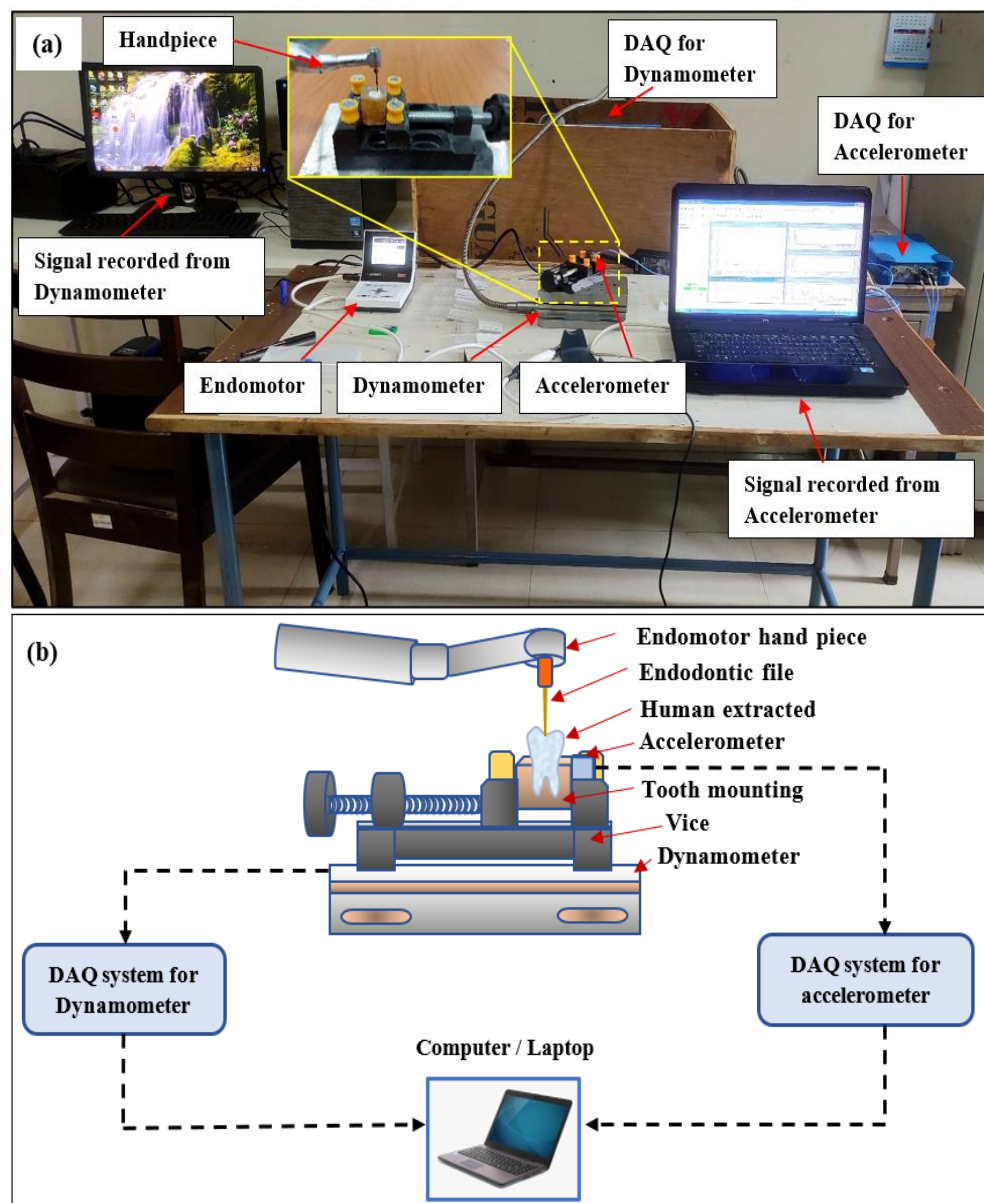
Figure 4.2 (a) Experimental setup for root canal cleaning and shaping
(b) Schematic diagram for root canal cleaning and shaping

Initially, a glide path is prepared using #10 and #15 endodontic hand-driven K-files [153,154] to establish the length of the canal, followed by verifying the glide path [153]. The WOG and TS files cleaned and shaped the canal based on the manufacturer's instructions.

4.4 Components and accessories used in RCT experimental setup

The experimental root canal system comprises a Dentsply endo-motor for providing the source for utilizing the endodontic instruments. It was a suitable power-driving device for delivering the input energy as the RCT system's output. A dynamometer and triaxial accelerometer were used throughout the RCT to capture the force and vibration signals. The DAQ is employed to acquire the signals. Following are the main components and accessories which are used for RCT experimental works are discussed below.

4.4.1 Endo-motor and control unit

The X-SMART Plus endo-motor is an endodontic micromotor used to drive NiTi motor-driven instruments, as shown in Fig. 4.3. Experienced dental professionals who are doing endodontic or RCT procedures utilize this motor. The endo-motor maintains classic features like the compact contra-angle head and the on/off switch on the motorized handpiece while enhancing the user interface. The endo motor control unit works as rated input direct current $18V, 0.5A$, torque range between $0.6 - 4\ Ncm$, and a speed range between $250 - 1200\ rpm$. The motor is capable of both reciprocating and continuous action. It features a few free programs for customized configurations in addition to pre-programmed settings for different endodontic files system.

Control unit

Motor hand piece with cable and connector

Contra-angle

Stand

Endodontic file
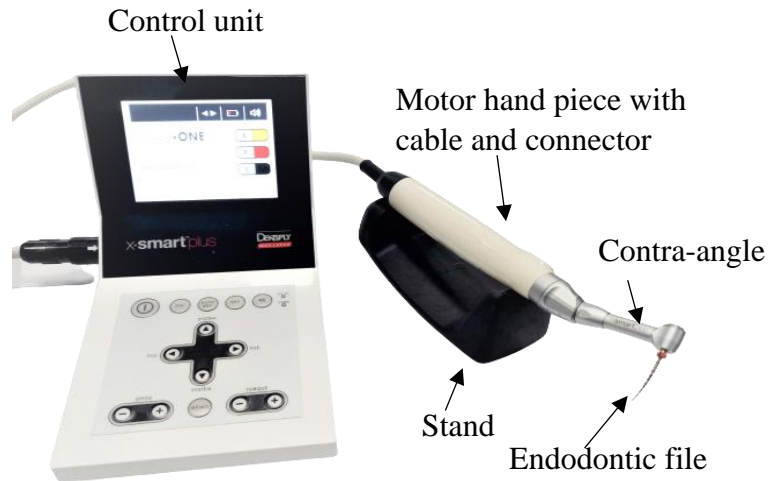
Figure 4.3 Illustrative diagram of RCT endo motor with control unit

4.4.2 Dynamometer unit

A three-component force measurement device known as a dynamometer is used to measure the force. This sensor unit consists of a dynamometer (type 9257B), charge amplifier (type 5080A), and DAQ system (type 5697A1), respectively. The Kistler produces the whole component setup, as shown in Fig. 4.4. The tooth mounted RCT setup is placed over the dynamometer. The dynamometer is connected through the charge amplifier, which is directly attached to the DAQ system. This sensor is stable and reliable and has excellent rigidity, consequently, higher natural frequency. Due to its good resolution, it is possible to measure even minor dynamic changes in force signals.

Dynamometer
Type 9257B

DAQ System
Type 5697A1

Figure 4.4 Major components and accessories of the dynamometer

4.4.3 Accelerometer unit

A piezoelectric ICP-based tri-axial accelerometer (Model 356A26) is used in this research work, as shown in Fig. 4.5. The accelerometer is manufactured by PCB Piezotronics Inc., Depew, New York. A highly sensitive sensor termed an ICP accelerometer produces an electrical output in proportion to an applied acceleration. It can be used for a wide range of applications to monitor vibration and shock. The sensor is connected to the DAQ system to record the signals.

Accelerometer
Model 356A26

DAQ System
(OROS)

Figure 4.5 Major components and accessories of the accelerometer

4.5 Field-emission scanning electron microscopy (FESEM) analysis

The failure surface of the reciprocating endodontic file system was investigated under field-emission scanning electron microscopy (FESEM) (JOEL, JOEL Ltd. Musashino, Akishima, Tokyo, JAPAN). The tip of the healthy endodontic file was clean and sharp during the initial process of the root canal preparation, as shown in Fig. 4.6 (a). After that, wear edges and irregularities were observed in the endodontic file. Some debris and smear substances remain on the cutting edge of the endodontic file that was visible on the endodontic file surface, as shown in Fig. 4.6 (b) [155,156].

The failure initiation and overload fast failure zone on the surface has been observed in Fig. 4.6 (c), and from the tip of the endodontic file, the thin surface film has been chipping out, as shown in Fig. 4.6 (c) [106,157,158]. After the canal preparation, the file was blunt, and the edge was disrupted. A crack along the grooves on the surface of the

endodontic instruments is initiated, as shown in Fig. 4.6 (d) [137]. FESEM analysis was employed to observe the levels of severity of endodontic files during the root canal preparation, as shown in Fig. 4.6. FESEM was used for the high-resolution imaging of endodontic files before and after the root canal cleaning and shaping. The FESEM uses the electron source for imaging, even though an optical microscope uses a visible light source. The advantages of FESEM over optical microscopy include much higher magnification, depth of focus, and greater depth of field up to 100 times that of an optical microscope [158–160].
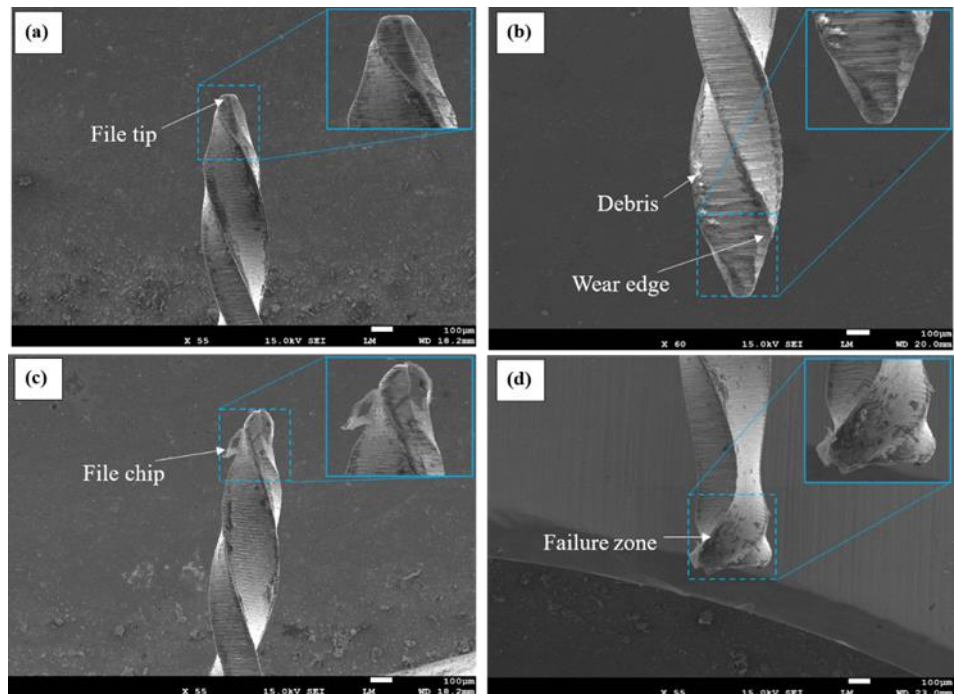
Figure 4.6 FESEM micrograph of endodontic files according to the conditions of their severity (a) healthy file, (c) incipient, (b) moderate, and (d) severe condition

4.6 Force and vibration signal of endodontic files system

Force and vibration data were represented as time responses. The amplitude of both force and vibration generated in root canaling by the endomotor using primary reciprocating and rotary endodontic instruments are shown in Fig. 4.7, and 4.8. The tri-axial accelerometer and dynamometer utilized to acquire the signal from x, y, and z-direction. The z-direction signal was used to carry out the works, which corresponds to the vertical movement that would be significant for this study. The z-direction signal was the most important or informative when considering all three directions of signals. Signal denoising was used to remove unwanted noise from the acquired signal. In this proposed study, a wavelet-based approach has been used to denoise the force and vibration signals. Stationary wavelet transform (SWT) denoising with the db4 mother wavelet method was employed. The denoised vibration and force data were presented in Fig. 4.9 and 4.10. It is well noted that the endodontic signals contain useful information in low-frequency regions and thus, there is a requirement to filter out the high-frequency noise from the signal. Stationary Wavelet Transform (SWT) can characterise local time-frequency with multi-resolution analysis. Thus, SWT is suited for denoising endodontic signals as it separates the noise in the high-level frequency components while keeping the signal information in the low-level frequency components. Additionally, SWT prevents distortion or shifting of the signal during denoising. Compared to conventional denoising methods like Fourier transform (FT), empirical mode decomposition (EMD), wavelet packet transforms (WPT) etc., stationary wavelet transform denoising is a powerful method for removing noise from signals, as it is adaptive, efficient, and can retain important signal features. It was evident from the responses that as the force increases, the maximum amplitude of the vibration also increases. Some of the previous authors [66,67,74,161] have reported the same observation as observed in this study.
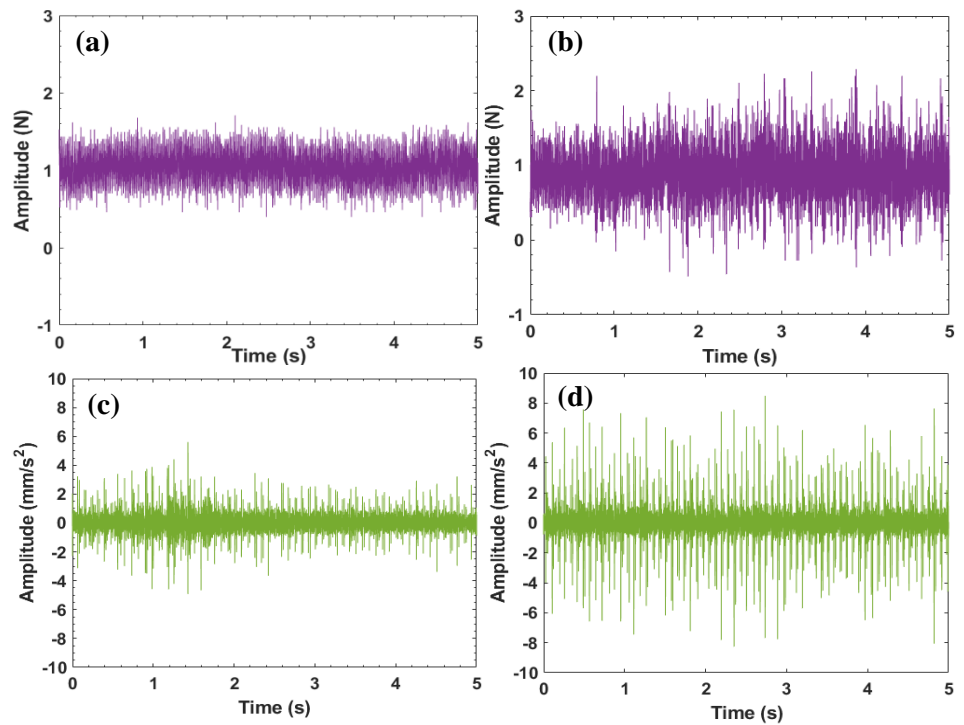
Figure 4.7 (a) Force signal of the WOG healthy file, (b) Force signal of the WOG unhealthy file, (c) Vibration signal of the WOG healthy file, (d) Vibration signal of the WOG unhealthy file
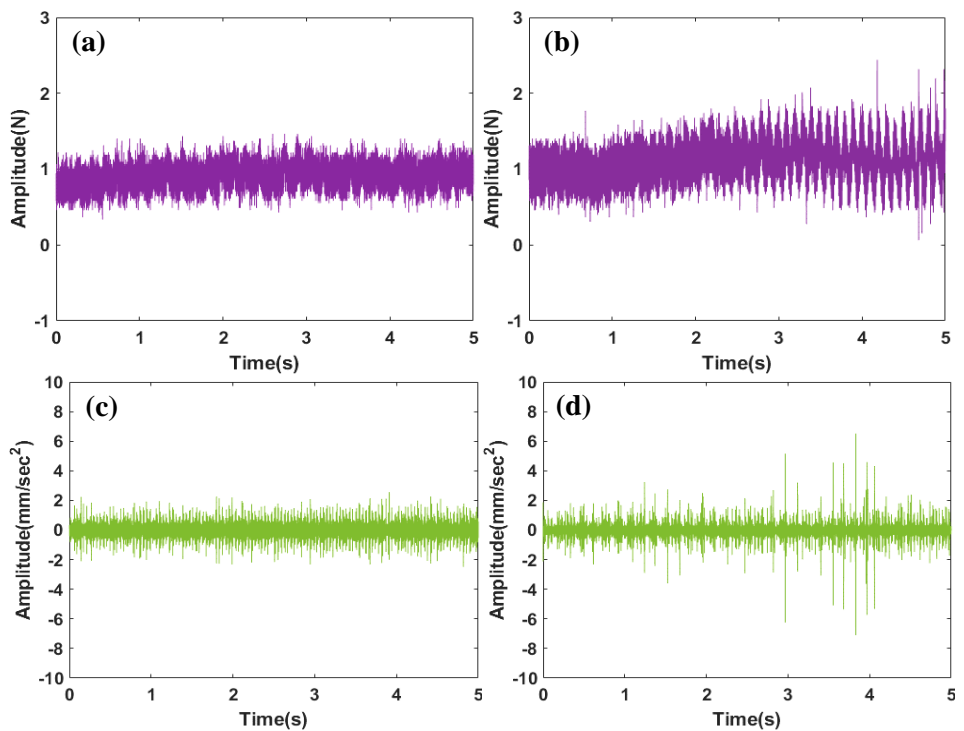
Figure 4.8 (a) Force signal of the TS healthy file, (b) Force signal of the TS unhealthy file, (c) Vibration signal of the TS healthy file, (d) Vibration signal of the TS unhealthy file
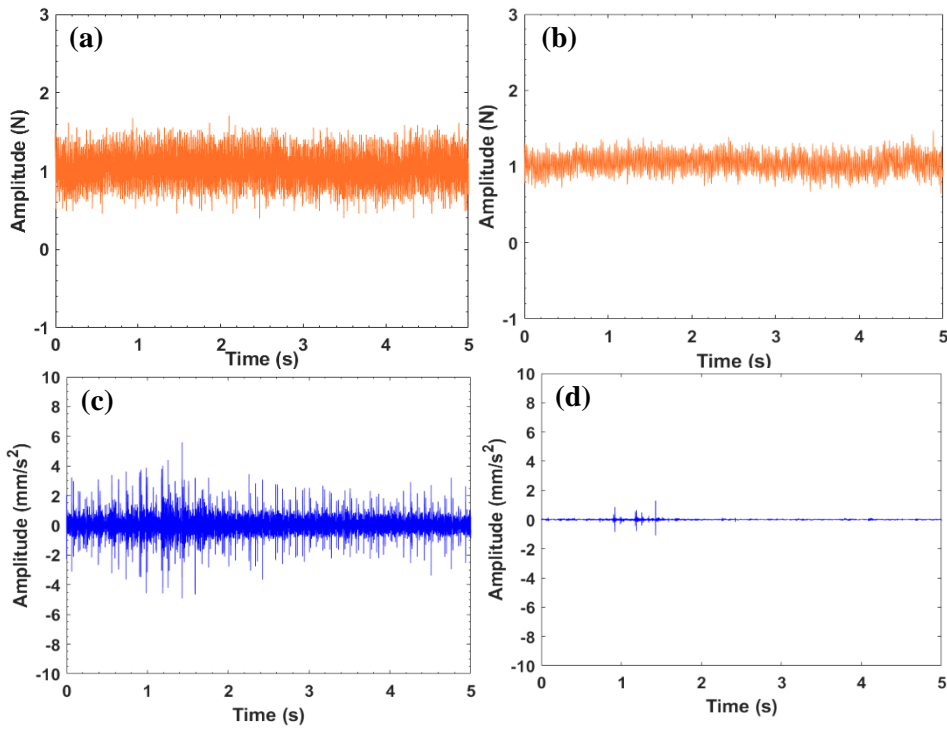
Figure 4.9 (a) Force signal of WOG file (raw signal), (b) Force signal of WOG file (denoised signal), (c) Vibration signal of WOG file (raw signal), (d) Vibration signal of WOG file (denoised signal)
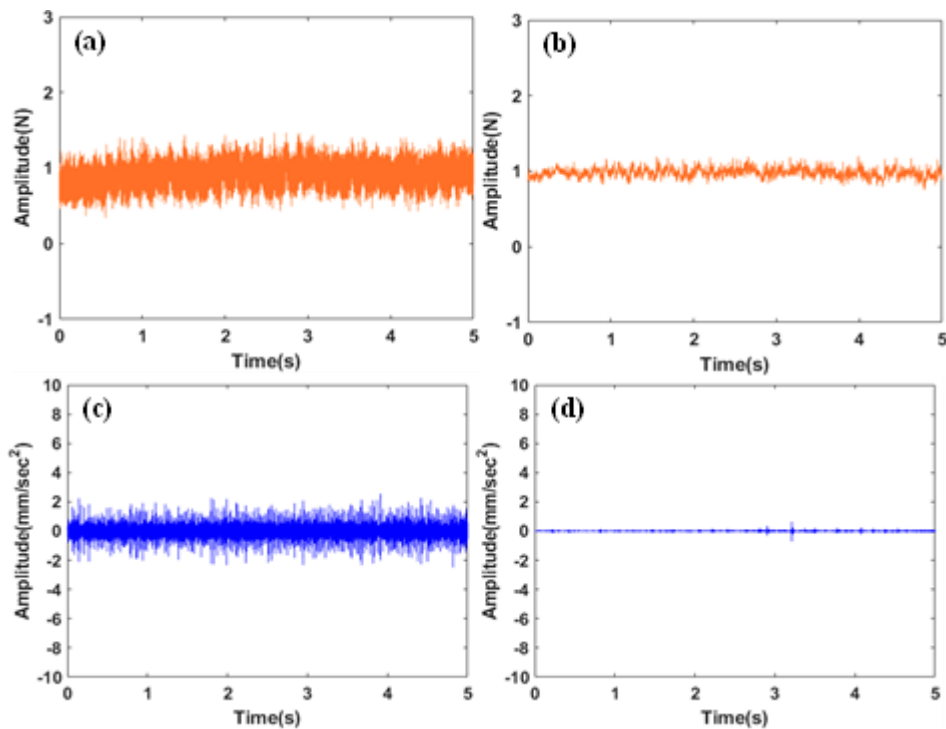
Figure 4.10 (a) Force signal of TS file (raw signal), (b) Force signal of TS file (denoised signal), (c) Vibration signal of TS file (raw signal), (d) Vibration signal of TS file (denoised signal)

4.6.1 Statistical feature extraction

Some well known statistical features like mean, standard deviation, root mean square, kurtosis, skewness, crest factor, clearance indicator, shape indicator, impulse indicator, etc., were used in literature to correlate the force and vibration signals [162–164]. In the present study, features like root mean square, kurtosis, maximum and minimum value of signals have been extracted from the raw signal and denoised signals.

(i) Maximum amplitude: It is the maximum value attained by any signal.

(ii) Minimum amplitude: It is the minimum value attained by any signal.

(iii) Root Mean Square (RMS): RMS is the square root of the arithmetic mean of the squares of the signal.

$$RMS = \sqrt{\frac{1}{n}(x_1^2 + x_2^2 + \cdots + x_n^2)} \qquad (4.1)$$

(iv) Kurtosis: Kurtosis, the word coming from the greek word 'kurtosis', means 'curve'. It measures the flatness of the curve with respect to the normal distribution.

$$Kurtosis = \frac{\sum_{i=0}^{n} x_i}{\sigma^4} \qquad (4.2)$$

4.6.2 Curve fitting model

In curve fitting, the least squares method is used when fitting the data. This requires a parametric model that relates the predictor data from the response data with one or more coefficients. The outcome of the curve-fitting model is an estimate of the model coefficients [165,166]. A MATLAB-based curve-fitting regression model was employed for raw and denoised signals to analyze the relationship between force and vibration signals during root canal preparation. This model used the robust least square data fitting technique with the least absolute residuals method that minimizes the absolute difference of the residuals. The end of the process gives the result as a model coefficient (with 95% confidence), known as a regression coefficient, denoted by 'R-squared'

or R^2. The curve-fitting regression model gives the relation between the force and vibration variables. In the curve fitting model, R-squared statistically evaluates how close the data are to the fitted regression line and the goodness-of-fit that measured the linear regression model. In the curve fitting model, R-squared represented the strength of the relationship between the model concerning the data on a convenient 0 to 100% scale.

The least squares method was adapted to fit the data using a curve-fitting regression model. The model coefficient estimated the output of the curve fitting method, i.e., regression coefficient, represented by R-square. The present study determines the regression coefficient between force and vibration using Eq. 4.3 [167].

If the arbitrary function $V = P(F)$ is used to characterize the data,

The characterization error is given by

$$E_i = P(F_i) - V_i, \text{ for } i = 1, 2, \ldots \ldots n.$$

where, $V_i,$ = Data value

V = Obtained from the function $P(F_i)$

The least-square conditions used to fit the function $P(F)$ is given by Eq. 4.3,

$$R^2(\%) = \left(1 - \frac{A}{B}\right) \times 100 \tag{4.3}$$

where, $A = \sum_{i=1}^{n} [P(F_i) - V_i]^2$, A is the sum of the square of the residuals,

$B = \sum_{i=1}^{n} [P(V_i) - \bar{V}]^2$, B is the sum of the square of the V value from their mean.

4.7 Results

4.7.1 Curve fitting of raw signals

The output of linearly fitted data points of raw signals with maximum values of force and vibration is shown in Fig. 4.11 (a) and 4.12 (a) for WOG and TS files, respectively. Similarly, Fig. 4.11 (b) and 4.12 (b) show the results for minimum force values concerning the minimum value of vibration. The variation in RMS values of force with respect to

vibration for a linearly fitted model is shown in Fig. 4.11 (c) and Fig 4.12 (c). Further, variation in the kurtosis value of force concerning vibration for a linearly fitted model is shown in Fig. 4.11 (d) and 4.12 (d). From these obtained R-squared values, it can be inferred that the linearly fitted RMS model has a good strength of the relationship between force and vibration. The highest correlation value of RMS may be the reason for material dislodging during RCT and the transfer of vibration from the handpiece [74,161,168]. During RCT, a higher amount of force may cause the failure of the endodontic file. In each reciprocating motion, the endodontic file dislodges and erosion the root canal material. After some time, the file blunts due to continuous drilling inside the root canal. After specific usage, the endodontic file erodes the root canal material and causes vibration. The same is confirmed as the calculated R-squared value for this case is 0.90, which is the highest among them.
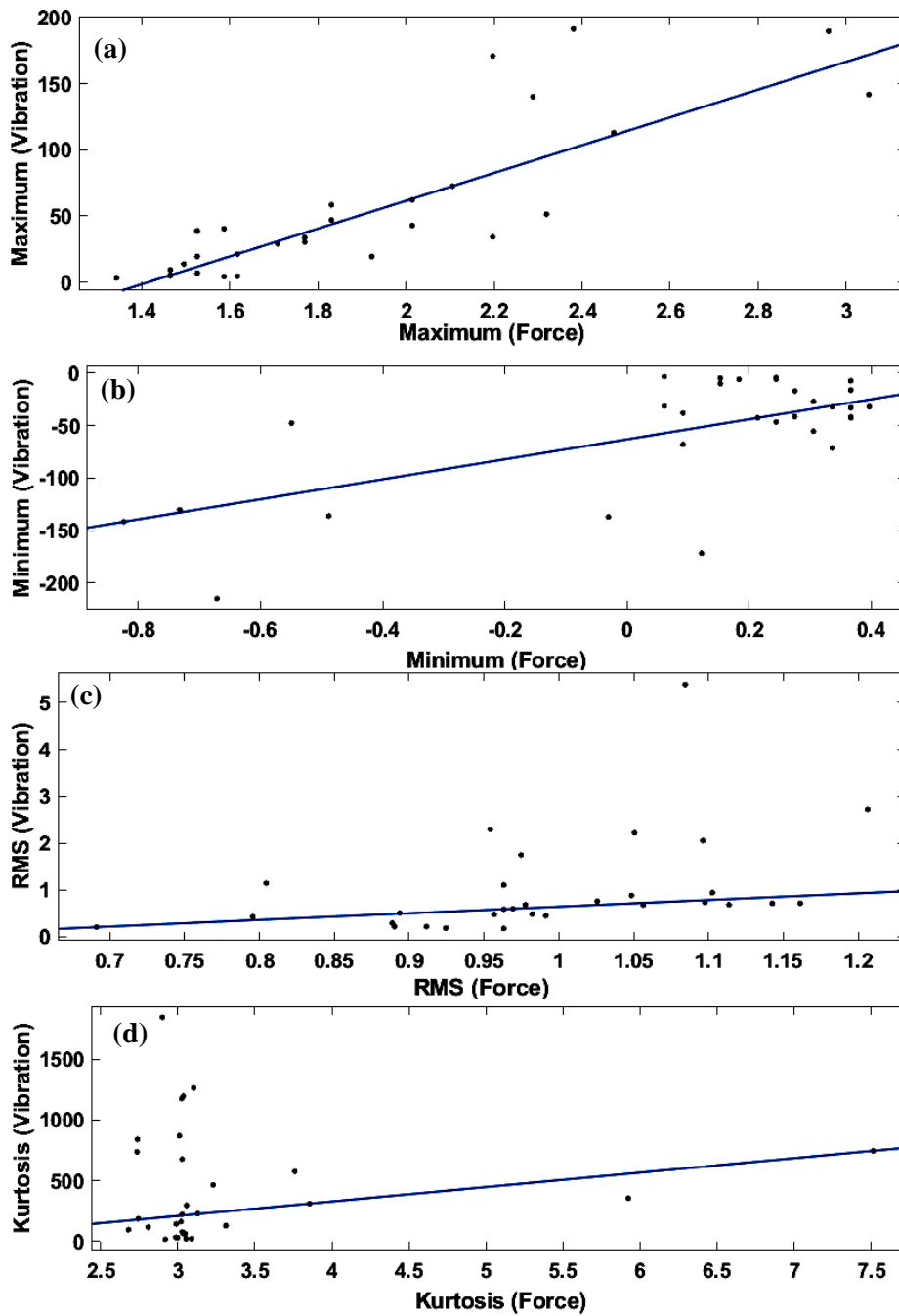
Figure 4.11 Linear relationship between force and vibration for WOG raw data signal of curve fitting model (a) maximum, (b) minimum, (c) root mean square, (d) kurtosis
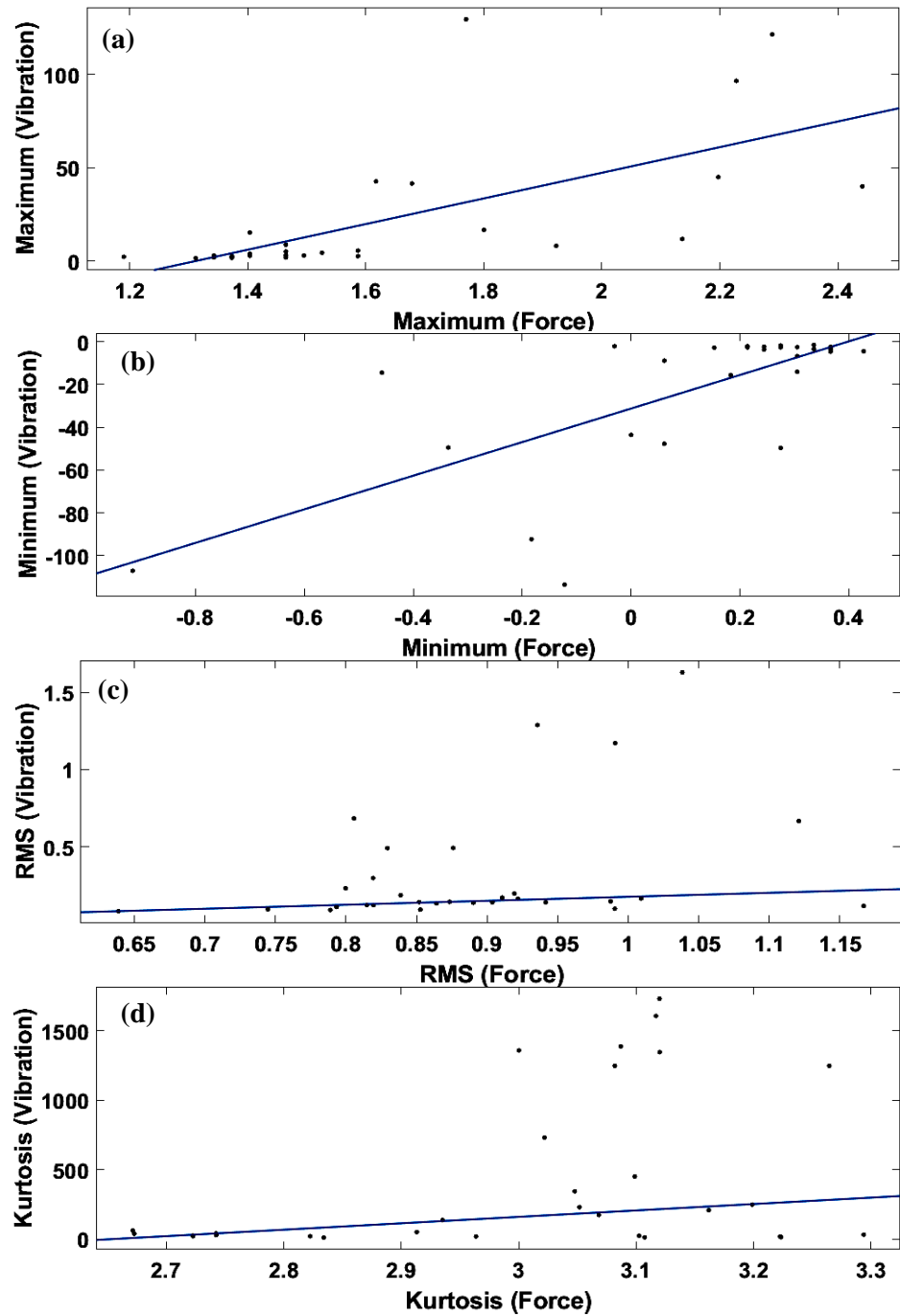
Figure 4.12 Linear relationship between force and vibration for TS raw data signal of curve fitting model (a) maximum, (b) minimum, (c) root mean square, (d) kurtosis

4.7.2 Curve fitting of denoised signal

Fig. 4.13 (a) and 4.14 (a) represent the output of linearly fitted data points of denoised signals with maximum values of force and vibration for WOG and TS files, respectively. Similarly, the outputs for minimum values of force with respect to the minimum value of vibration are shown in Fig. 4.13 (b) and 4.14 (b). The variation in RMS values of force and vibration for a linearly fitted model is shown in Fig. 4.13 (c) and 4.14 (c) for WOG and TS files, respectively. In contrast, variation in kurtosis of force with respect to kurtosis of vibration for a linearly fitted model is shown in Fig. 4.13 (d) and 4.14 (d). By visually inspecting all the obtained plots, it was observed that most of the data points are either lying on the linearly fitted line or in close vicinity, i.e., fewer data points amounted to be called outliers. The mathematical observation adheres to this. Therefore, the R-squared value is highest in Fig. 4.13 (a) and 4.14 (b). Model statistical measures the R^2 value in the raw and denoised signal of vibration and force explain collectively, as shown in Table 4.1 for both WOG and TS endodontic files. The methodology adopted for this study is shown in Fig. 4.15. Sample values of extracted features for force and vibration signals of both WOG and TS endodontic files are mentioned in Tables 4.2 and 4.3.
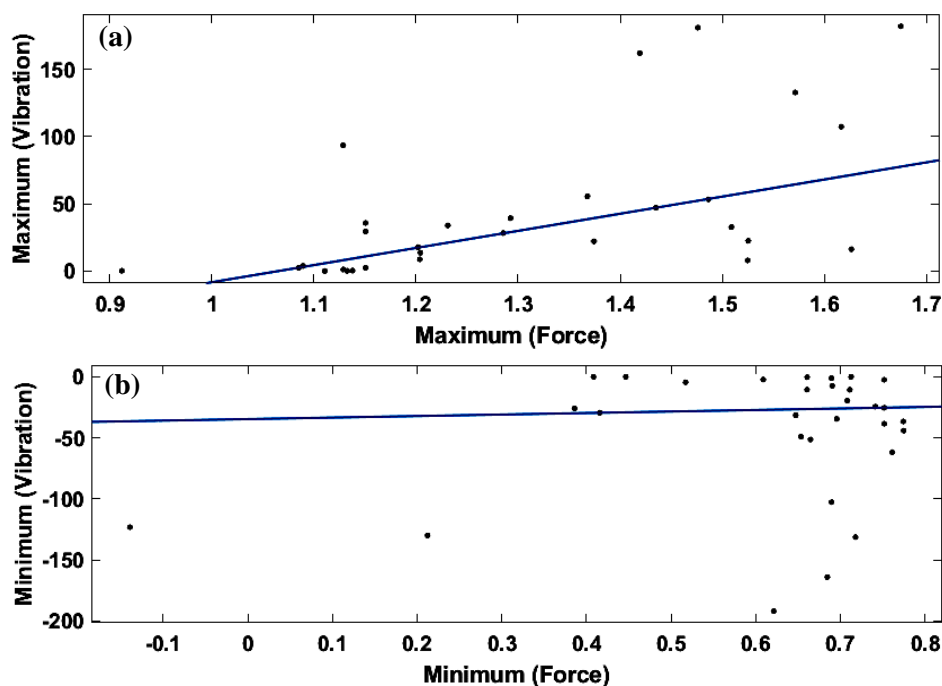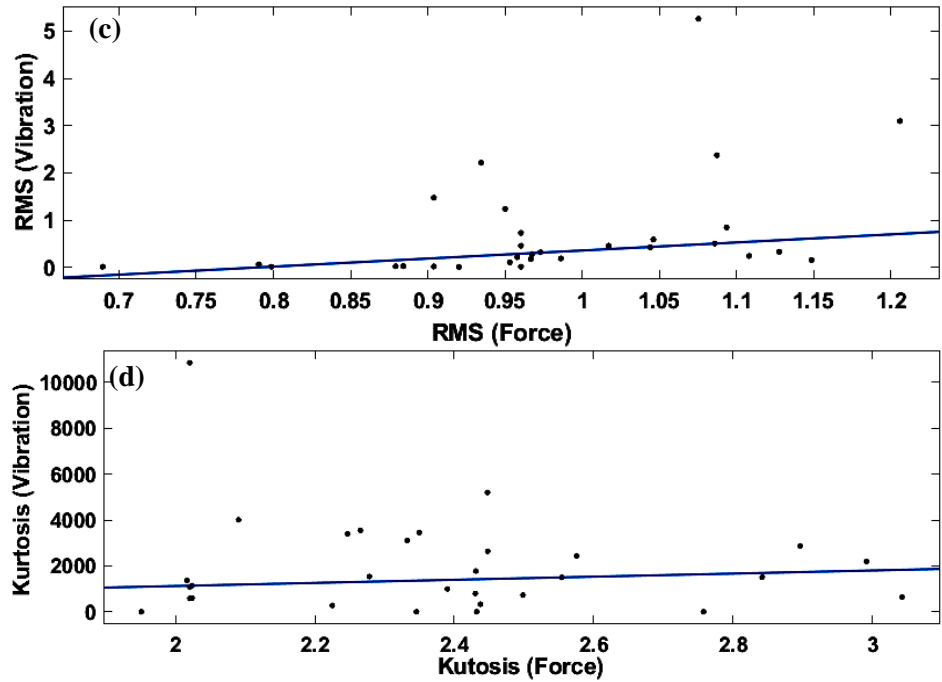
Figure 4.13 Linear relationship between force and vibration for WOG denoised data signal of curve fitting model (a) maximum, (b) minimum, (c) root mean square, (d) kurtosis
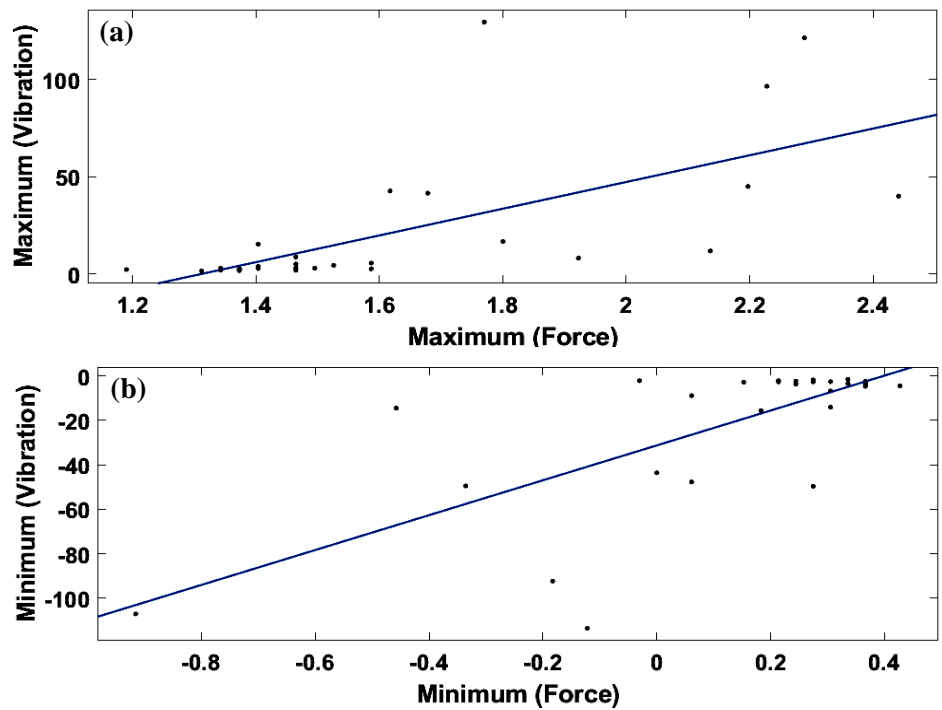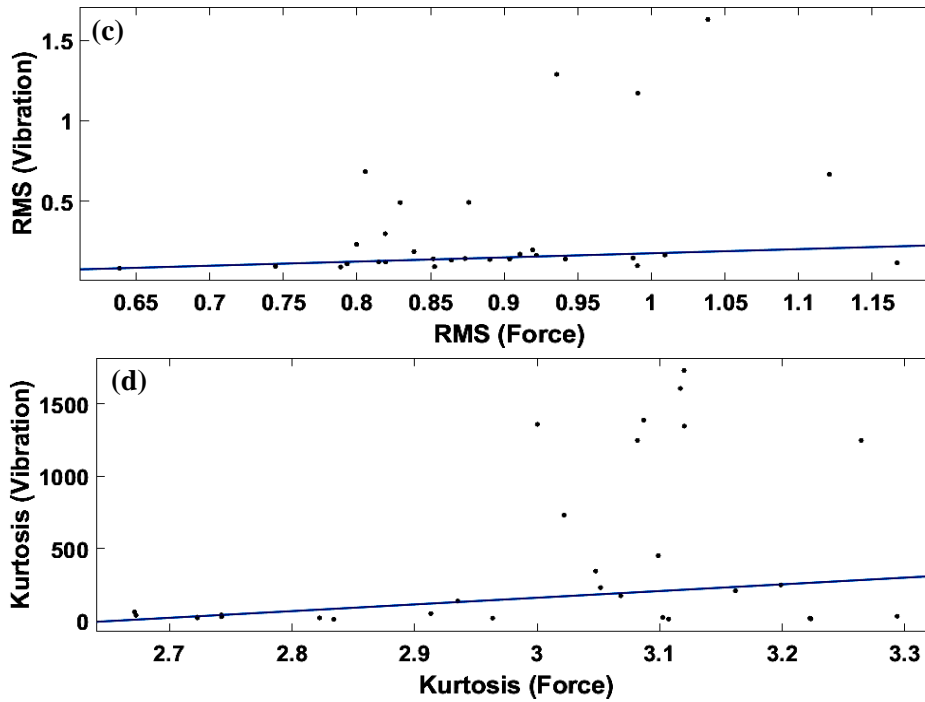
Figure 4.14 Linear relationship between force and vibration for TS denoised data signal of curve fitting model (a) maximum, (b) minimum, (c) root mean square, (d) kurtosis

Table 4.1 Comparison of the R^2 value of WOG and TS endodontic file from the different features in curve fitting regression model

Sr. No	Feature	R^2 value (%) (WOG file)		R^2 value (%) (TS file)	
		Raw signal	Denoised signal	Raw signal	Denoised signal
1	Maximum	69.63	92.25	42.21	89.85
2	Minimum	47.05	88.93	50.54	89.25
3	Root mean square	90.10	90.10	89.10	89.47
4	Kurtosis	88.31	88.45	86.89	88.66
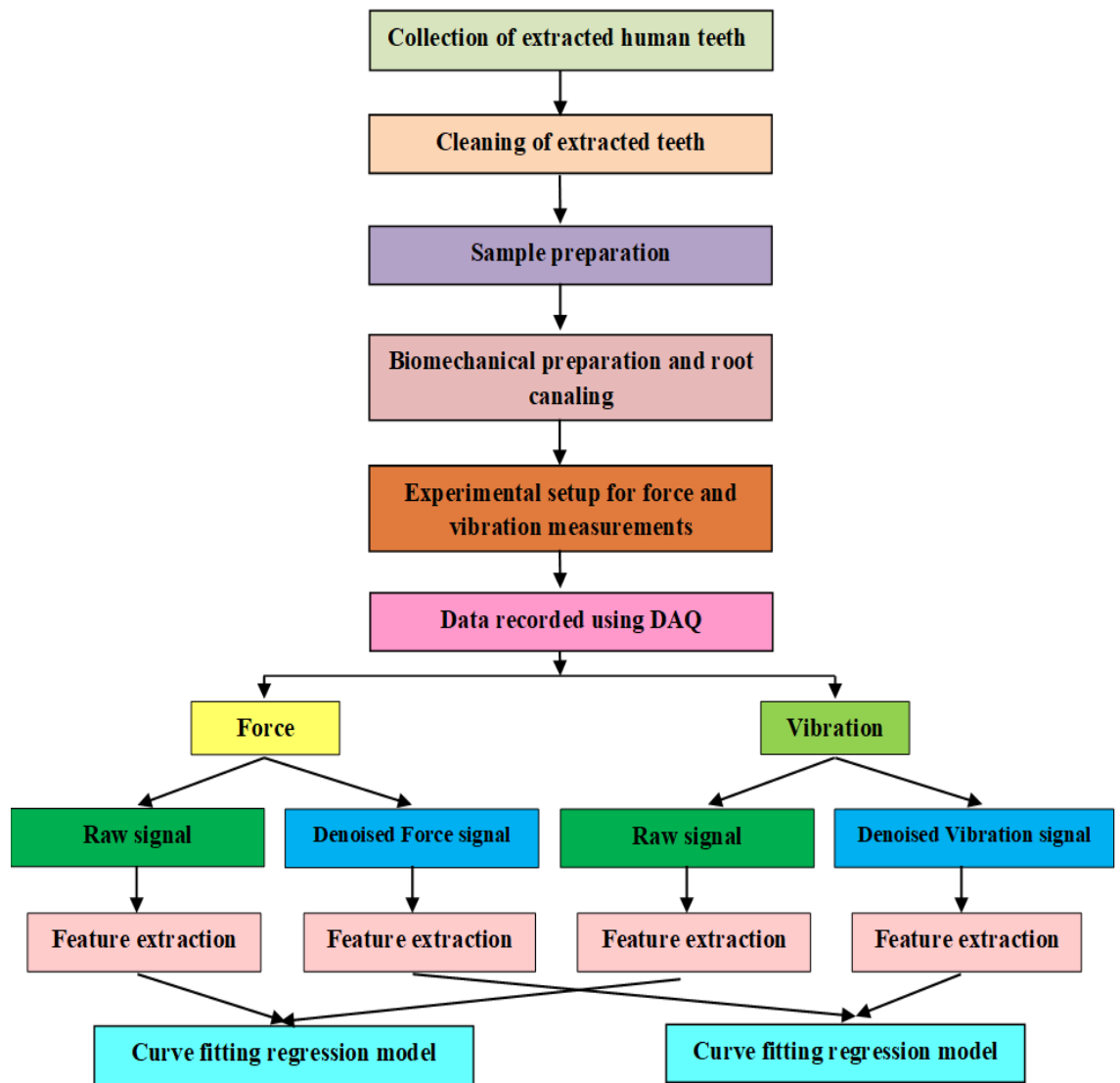
Figure 4.15 Methodology adopted for force and vibration analysis in reciprocating endodontic files system during root canal cleaning and shaping

Table 4.2 Samples values of extracted features for force and vibration signals of the WOG file

Sr. No.	Force (N)								Vibration (mm/s²)							
	Raw data				Denoised data				Raw data				Denoised data			
	Max	Min	RMS	Kurtosis	Max	Min	RMS	Kurtosis	Max	Min	RMS	Kurtosis	Max	Min	RMS	Kurtosis
1	2.11	0.34	1.05	2.74	1.43	0.66	1.04	2.09	72.59	-71.44	0.88	840.40	47.05	-51.34	0.43	4010.14
2	1.83	0.31	1.10	2.73	1.49	0.65	1.09	2.35	58.44	-55.50	0.73	738.24	53.29	-49.13	0.50	3460.19
3	2.96	-0.67	1.08	5.92	1.48	0.62	1.08	2.44	189.52	-214.78	5.39	354.86	181.07	-191.94	5.26	330.05
4	2.38	0.12	1.21	3.01	1.67	0.68	1.21	2.50	191.25	-171.79	2.72	870.15	182.08	-164.10	3.10	731.11
5	2.01	0.37	1.14	2.74	1.51	0.65	1.13	2.28	42.89	-41.94	0.71	185.34	32.74	-31.49	0.33	1540.83
6	2.29	-0.49	0.97	3.76	1.57	0.21	0.95	2.90	140.06	-136.16	1.75	576.67	132.81	-130.01	1.24	2868.60
7	2.47	-0.73	0.95	3.23	1.62	-0.14	0.93	3.04	112.88	-130.32	2.30	464.23	107.33	-123.17	2.21	647.67
8	1.92	0.27	1.11	2.68	1.52	0.69	1.11	2.22	19.53	-16.97	0.68	94.90	7.85	-7.34	0.24	278.37
9	1.71	0.06	0.97	2.81	1.37	0.39	0.96	2.58	28.86	-31.53	0.60	115.68	22.07	-25.82	0.21	2440.04
10	2.20	-0.03	1.10	2.90	1.42	0.72	1.09	2.02	170.72	-137.12	2.05	1847.66	162.20	-131.38	2.37	1368.98
11	1.50	0.37	0.96	3.04	1.20	0.71	0.95	2.33	13.90	-16.08	0.47	62.54	8.62	-10.67	0.11	3112.35
12	1.53	0.37	0.96	3.03	1.15	0.75	0.96	2.02	38.31	-32.87	0.59	677.37	29.36	-25.32	0.46	1084.35
13	1.62	0.40	0.99	3.06	1.20	0.74	0.99	2.25	21.36	-32.00	0.45	296.22	17.67	-24.38	0.19	3404.56
14	1.59	0.27	0.98	3.03	1.23	0.70	0.97	2.45	40.51	-41.48	0.48	1196.83	33.83	-34.47	0.32	5202.74
15	1.62	0.24	0.92	2.99	1.11	0.71	0.92	1.95	4.68	-4.28	0.18	32.83	0.04	-0.05	0.01	3.45

Sr. No.	Force (N)								Vibration (mm/s²)							
	Raw data				Denoised data				Raw data				Denoised data			
	Max	Min	RMS	Kurtosis	Max	Min	RMS	Kurtosis	Max	Min	RMS	Kurtosis	Max	Min	RMS	Kurtosis
16	1.83	0.24	1.06	3.02	1.29	0.77	1.05	2.43	46.98	-46.60	0.68	1176.47	39.30	-44.11	0.59	1777.52
17	1.77	0.21	1.03	3.13	1.29	0.77	1.02	2.39	33.70	-42.74	0.76	227.42	28.18	-36.62	0.46	996.86
18	2.20	0.34	1.16	3.31	1.63	0.66	1.15	2.84	34.14	-32.27	0.72	128.15	16.19	-10.55	0.16	1510.82
19	2.32	-0.55	0.80	3.86	1.13	0.41	0.80	2.76	51.43	-47.72	1.14	310.55	0.10	-0.08	0.01	4.92
20	1.34	0.06	0.69	3.09	0.91	0.45	0.69	2.43	3.31	-3.41	0.20	21.03	0.10	-0.08	0.01	4.92
21	2.01	0.09	1.10	3.10	1.37	0.76	1.09	2.55	62.31	-68.03	0.94	1265.87	55.55	-61.75	0.85	1501.59
22	1.77	0.09	0.98	3.02	1.53	0.42	0.97	2.99	30.43	-38.12	0.68	160.89	22.49	-29.49	0.28	2201.88
23	1.53	0.37	0.96	3.03	1.15	0.75	0.96	2.02	39.03	-42.80	1.10	222.74	35.72	-38.50	0.73	589.56
24	1.53	0.37	0.96	3.03	1.15	0.75	0.96	2.02	6.88	-7.35	0.17	75.12	2.31	-2.45	0.01	10858.62
25	1.46	0.18	0.89	3.00	1.09	0.61	0.88	2.27	5.30	-5.97	0.21	28.70	2.24	-2.31	0.02	3550.86
26	1.53	0.31	0.89	2.99	1.20	0.71	0.97	2.45	19.52	-27.10	0.51	142.06	13.46	-19.61	0.17	2639.34
27	1.59	0.24	0.89	3.05	1.14	0.66	0.88	2.35	4.44	-5.76	0.29	20.48	0.25	-0.28	0.02	4.80
28	1.46	0.15	0.91	2.92	1.13	0.69	0.90	2.02	4.84	-4.80	0.21	15.67	1.05	-1.13	0.02	599.72
29	3.05	-0.82	1.05	7.51	1.13	0.69	0.90	2.02	141.77	-141.63	2.22	746.50	93.49	-102.68	1.47	1142.29
30	1.46	0.15	0.80	3.05	1.09	0.52	0.79	2.43	9.35	-10.05	0.42	60.61	3.74	-4.51	0.06	797.33

Table 4.3 Samples values of extracted features for force and vibration signals of TS file

Sr. No.	Force (N)								Vibration (mm/s²)							
	Raw data				Denoised data				Raw data				Denoised data			
	Max	Min	RMS	Kurtosis	Max	Min	RMS	Kurtosis	Max	Min	RMS	Kurtosis	Max	Min	RMS	Kurtosis
1	2.29	-0.18	0.94	2.74	1.46	0.47	0.93	2.29	121.34	-92.33	1.29	28.33	114.39	-85.19	1.06	3.92
2	1.77	-0.12	1.04	2.83	1.53	0.38	1.03	2.64	129.38	-113.49	1.63	10.73	119.29	-107.63	1.42	4.21
3	2.44	0.27	1.12	2.72	1.67	0.57	1.12	2.49	40.04	-49.67	0.67	25.12	34.90	-42.64	0.49	5.54
4	2.20	0.00	0.99	2.82	1.57	0.38	0.99	2.60	44.99	-43.63	1.17	20.16	41.04	-38.95	0.87	28.40
5	2.23	-0.92	0.81	2.96	1.24	-0.06	0.80	2.47	96.44	-107.04	0.68	18.57	92.02	-103.83	0.60	18.04
6	2.14	-0.46	1.01	2.91	1.41	0.50	1.00	2.26	11.92	-14.57	0.17	49.63	5.66	-7.59	0.04	3.27
7	1.92	0.43	1.17	2.67	1.58	0.70	1.16	2.32	8.25	-4.54	0.12	38.24	1.68	-1.15	0.02	42.28
8	1.80	0.18	0.99	2.67	1.38	0.50	0.98	2.33	16.79	-15.66	0.15	61.79	11.41	-9.73	0.06	905.77
9	1.62	0.06	0.88	2.72	1.36	0.32	0.87	2.42	42.74	-47.74	0.49	20.54	35.37	-37.61	0.34	9.77
10	1.68	-0.34	0.83	2.74	1.28	0.25	0.82	2.31	41.59	-49.53	0.49	40.42	32.16	-39.91	0.35	5.45
11	1.40	0.31	0.82	3.11	1.04	0.57	0.81	2.61	15.39	-14.15	0.30	12.21	11.76	-9.95	0.13	4.33
12	1.59	0.31	0.92	3.22	1.17	0.73	0.92	3.85	5.71	-6.84	0.17	18.18	1.94	-1.83	0.06	4.72
13	1.46	0.06	0.80	3.29	0.94	0.66	0.79	2.74	8.80	-8.96	0.23	31.72	3.39	-4.77	0.08	4.44
14	1.31	0.34	0.81	3.16	1.01	0.64	0.81	3.40	1.65	-1.66	0.13	207.91	0.14	-0.11	0.02	22.68
15	1.50	0.31	0.89	2.94	1.17	0.64	0.88	2.34	3.05	-2.64	0.14	136.25	0.65	-0.73	0.03	748.32

Sr. No.	Force (N)								Vibration (mm/s²)							
	Raw data				Denoised data								Raw data			
	Max	Min	RMS	Kurtosis	Max	Min	RMS	Kurtosis	Max	Min	RMS	Kurtosis	Max	Min	RMS	Kurtosis
16	1.40	0.37	0.86	3.10	1.04	0.70	0.86	2.80	3.97	-3.79	0.14	24.11	2.29	-2.27	0.04	18.68
17	1.46	0.24	0.79	3.22	1.00	0.60	0.78	3.15	5.21	-3.72	0.09	13.56	0.32	-0.34	0.01	3.54
18	1.34	0.24	0.85	3.05	1.04	0.64	0.85	2.64	2.04	-2.43	0.10	229.98	0.15	-0.20	0.02	479.28
19	1.37	0.27	0.87	3.07	1.06	0.69	0.87	2.44	2.44	-1.86	0.15	173.01	0.16	-0.14	0.02	106.51
20	1.46	0.27	0.91	3.10	1.11	0.72	0.90	2.78	2.02	-2.00	0.17	450.51	0.16	-0.17	0.03	2098.92
21	1.37	0.21	0.74	3.26	1.01	0.58	0.74	3.32	2.13	-2.78	0.10	1247.45	0.20	-0.19	0.03	3652.71
22	1.34	0.27	0.85	3.12	1.09	0.65	0.85	3.19	3.06	-2.74	0.14	1607.46	0.34	-0.40	0.02	4932.09
23	1.53	0.37	0.94	3.08	1.19	0.68	0.94	2.88	4.52	-4.76	0.14	1247.45	2.32	-2.04	0.03	10009.28
24	1.37	0.15	0.79	3.20	0.97	0.53	0.79	3.22	2.63	-2.88	0.11	248.05	0.95	-0.86	0.05	1216.02
25	1.19	-0.03	0.64	3.02	0.86	0.35	0.63	2.44	2.38	-2.20	0.09	731.34	0.11	-0.10	0.02	8500.31
26	1.40	0.21	0.82	3.12	1.09	0.53	0.81	3.03	2.91	-2.54	0.12	1346.88	0.73	-0.66	0.03	9504.95
27	1.46	0.34	0.92	3.05	1.21	0.68	0.91	2.94	3.24	-3.59	0.20	344.27	0.75	-0.84	0.04	589.87
28	1.50	0.37	0.90	3.00	1.18	0.68	0.90	2.62	3.07	-3.12	0.14	1359.19	0.28	-0.36	0.04	2449.15
29	1.37	0.21	0.84	3.09	1.03	0.66	0.83	2.79	1.86	-2.21	0.19	1388.34	0.16	-0.16	0.02	1774.22
30	1.59	0.37	0.99	3.12	1.20	0.75	0.99	3.19	2.73	-2.54	0.10	1731.70	0.19	-0.18	0.02	2372.72

4.8 Discussion

The in-vitro experimental setup gives the real explorer of the root canal shaping during the RCT. Most of the authors used the J-shaped, L-shaped and S-shaped simulated root canal to evaluate and analyze the RCT signals [67,74,149,150,161,169]. The simulated root canal does not provide the actual behaviour of the root canal because they have used either a curve or a straight root canal, but the root canal in humans varies from patient to patient. However, human extracted tooth provides the actual behaviour of the root canal because of the distinct morphology of the canal.

The biomechanical preparation of the root canal system is recognized as the most crucial stage of root canal treatment. This process consists of three steps: access opening, cleaning and shaping, and obturation. These steps are equally crucial for the ultimate success of the procedure. However, this in-vitro experimentation study uses only access opening, cleaning, and shaping. Many practitioners consider pulp removal as the only objective of RCT and consider dentine removal unnecessary [170]. Due to this misconception, there is a significant failure rate for RCT [170]. Bacteria are present in dentinal tubules, which produce bacterial toxins. These toxins were causing the problem of peri-apical disease. These bacteria mostly affect the non-vital teeth. Even after the clean shaving cannot ensure that the infected dentine was removed completely [37,170]. Hence, removing inflamed and infected dentin is essential. Thus, RCT is necessary for disinfecting the root canal system.

During the acquisition of the signal, some noise in the signal was also recorded. A stationary wavelet transform algorithm was employed for smoothing these signals using the specified lowpass and highpass wavelet decomposition filters. The signals proceeded to each level's appropriate lowpass and highpass filters to produce the two sequences to the next level [171,172]. Each wavelet transform step applied the scaling function to the raw signal. The wavelet transform step applied the scaling function to calculate the denoised signal. The smoother signal was stored in the lower half of the raw signal [171,173]. While

denoising, the R2 value of WOG and TS endodontic signals are obtained using curve fitting with different features and compared with the R2 value of the raw signal. It is observed that essential signal information remained unchanged, whereas the regression value gets enhanced. Several studies have compared the efficiency of SWT with various denoising techniques for vibration signals, including Fourier transform (FT), empirical mode decomposition (EMD), wavelet packet transform (WPT), etc. Zhang et al. [174] and Wang et al. [175] evaluated the efficacy of SWT, EMD, DWT, and WPT in denoising a rolling bearing vibration signal. Based on evaluations of the feature, the study discovered that SWT was the most efficient technique for reducing noise while maintaining the signal's properties [174–176]. Likewise, Vafaeian et al. [177] investigated the SWT, Fourier transform, and EMD methods for denoising vibration signals deriving from gear faults. Based on SNR, RMSE, and kurtosis measurements, the study discovered that SWT was the most efficient technique for reducing noise while maintaining the signal's characteristics.

In this work, Fig. 4.11 (c) and 4.12 (c) show that the RMS of the force and vibration in the curve fitting is closely fitted to the regression line. The maximum RMS of WOG and TS endodontic file observed in Fig. 4.11 (c), and 4.12 (c), because of the transfer of vibration from the handpiece [168] and may be the cause of material dislodging [74]. Fig. 4.13 (a) and 4.14 (a) observed the maximum regression value compared to the three remaining features. In contrast to the kinematics, the WOG has a higher incremental taper and tip diameter than the TS1 or TS2, allowing for a greater cut depth at the same feed rate. The deeper cut increases cutting force and causes more vibration excitations in WOG. The vibration isolation of the root canal instruments is challenging [74]. For the perfection of the endodontic instrument or root canal instruments, researchers are still working, nevertheless need to address the problem of vibration and force initiation.

From the clinical significance point of view, in most cases, the fracture occurred due to procedural error and inappropriate instrumentation during the RCT [178]. Failure of the endodontic instruments is the cause

of root canal therapy, which increases undesirable negative consequences like ledge formation, blockages, and perforation [179]. The ledge formation is the iatrogenically created irregularity that obstructs the access of the instrument to the apex, resulting in insufficient or incorrect instrumentation of the root canal [27]. The packing of the tissue debris caused the blockage of the canal due to improper procedure, and it can be prevented by appropriate parameters of the root canal preparation [27]. The perforation may occur during access cavities preparation and internal resorption into peri-radicular tissue [28] and can be prevented using the optimum parameters during RCT. These complications have been recognized as the improper concepts of the shaping and cleaning of the root canal [179]. To avoid unfortunate occurrences, procedural accidents, and endodontic mishaps, Jafarzadeh et al. suggested using the optimum instruments driving parameter during cleaning and shaping [179]. The practitioner used the most important parameter, such as force, to use the access amount of force during the instrumentation. Due to these, chances of increasing the amplitude of vibration which cause the instrument to fail.

The root canal experimentation process proceeded with high experience and well-trained dentists. Each root canal was cleaned using the new endodontic file for data recording. This would help to avoid errors during the acquisition of the signal. Considering it is the analysis of force and vibration during the biomechanical preparation of the canal. Hence, distinct morphological human extracted teeth were used to study the actual behaviour of the signal and drilling condition for the NiTi alloy endodontic instrument.

4.9 Conclusions

In this experimental study, root canal preparation was carried out using the reciprocating and rotary endodontic file system. The effect of the force and vibration on healthy and unhealthy endodontic files has been studied. A linear relationship was established between acquired force and vibration signals during root canal preparation using a curve-fitting

regression model for raw and denoised signals. The following key conclusion can be drawn from this study:

- In biomechanical preparation during root canal treatment, it was observed that as the force increases, consequently, the amplitude of vibration also increases by a significant amount. A higher magnitude of vibration and force amounted to the root canal preparation using failed endodontic files because of overloading in uneven morphology of the root canal.

- The FESEM of the endodontic files shows that as the file's health condition deviates, the edges wear out, and chips are formed at the surfaces. These debris and chips can remain embedded in the tooth when root canalling is done with these files. Also, the blunt files lose their sharpened tip and thus need higher force for the canaling operation, which can adversely affect the human tooth.

- The importance of denoising was observed in the regression analysis; the denoised signals established a good association between force and vibration. Thus, noise removal from raw data was recommended. The best R^2 values for WOG and TS endodontic files found for root mean square values with raw signals were 90.1%, and 89.1%, respectively. In comparison, 92.25% and 89.85% for WOG and TS endodontic file correlation were established for the maximum values of the denoised signals.

This chapter presents the curve fitting method for analyzing force and vibration signals in endodontic files during root canal treatment. The statistical features of the vibration and force signals followed by the curve-fitting to establish the relationship between them. It helps identify the endodontic file's health with the fitted R^2 value. The results conveyed that the denoised signal established a decent association between vibration and force signal. The raw signal obtained the best regression with RMS value, whereas for the denoised signal best correlation was established for the maximum value.

In the subsequent chapter, fault diagnosis of the endodontic instruments during biomechanical preparation of the root canal has been carried out. Additionally, the effect of oversampling on the performance of force signals during RCT is investigated.

Chapter 5

The implication of oversampling and fault diagnosis of endodontic instruments during RCT

This chapter provides an innovative approach for fault diagnosis of an endodontic instrument during root canal therapy (RCT). An endodontic instrument may sometimes fail for reasons beyond the dentist's control. A thorough evaluation and decision-support system for an endodontist may prevent failures. This work suggests a machine learning and artificial intelligence-based method for evaluating the health of an endodontic instrument. With the help of a dynamometer, force signals are acquired during the RCT, and statistical features are retrieved from the obtained signals. Oversampling of datasets is necessary to prevent bias and overfitting because there are fewer instances of the minority class (i.e., failure/moderate class). In order to improve the minority class, the synthetic minority oversampling technique (SMOTE) is used. Additionally, the performance of machine learning techniques, such as Gaussian Naïve Bayes (GNB), quadratic support vector machine (QSVM), fine k-nearest neighbor (FKNN), and ensemble bagged tree (EBT) is assessed. Comparatively, the EBT model performs significantly superior to the GNB, QSVM, and FKNN. Machine learning algorithms can accurately diagnose the endodontic instrument's faults by monitoring the force signals. The EBT and FKNN classifiers are trained exceptionally well, with an area under the receiver operating characteristic curve of 1.0 and 0.99, respectively. Machine learning (ML) can improve treatment and improve RCT results. This work uses ML methodologies for fault diagnosis of endodontic instruments, providing practitioners with an adequate decision support system.

5.1 Introduction

One of the critical procedures in endodontics is the biomechanical preparation of root canal structure [37]. This process includes the access opening, cleaning, and shaping of canals. Endodontic treatment aims to remove unwanted smears and debris from the surface of a root canal's inner portion using an endodontic file [7,8]. The endodontic file or instruments are essential for removing decay and contaminated tissues from the root canal. These instruments are made of Nitinol (NiTi) alloys, commonly known as shape memory alloys, which are super-elastic and flexible [32,105,116]. The endodontic instrument may fracture during the RCT, often without visible signs of deterioration. The damaged instrument retains the remnant in the canal, which necessitates a further effort to extract it [141]. The implications of such instrument remnants impact the endodontic treatment's completion accuracy [139]. The initial assessment of this deterioration during the primary stages of failure is required. Thus, a thorough evaluation, severity prediction, and treatment approach are essential components of a successful endodontic procedure [78,180].

In past studies, technology has been employed in numerous parts of biomedical and dental research to find ways to analyze clinical health data. These studies can aid throughout the assessment of a medical condition, decision- making and the initiation of adequate care. Morch et al. [76] presented a systematic review of implementing artificial intelligence (AI) in dentistry. The authors included the traditional, neural, and combination of learning techniques. Later, the study suggested the involvement of AI in dentistry. Qu et al. [82] used the machine learning (ML) approach for endodontic micro-surgery prognosis prediction. Random forest (RF) and gradient boosting machine (GBM) algorithms were used. Additionally, they evaluated the predictive sensitivity, accuracy, and specificity. The receiver operating characteristic curve (ROC) curve and area under the curve (AUC) were

used to assess the performance of RF and GBM techniques. The authors observed that the GBM model was better than the RF model.

Hung et al. [79] used ML techniques to diagnose and forecast root caries. ML and AI were used to provide the most significant aspects and examine the model's performance to categorize the absence and presence of dental decay. A model capable of classifying classes was built utilizing various supervised ML techniques. The authors state that clinicians have been urged to adopt the study's algorithms for primary prevention in treatment. The diagnosis of the endodontic instrument is required to examine the health condition of the instrument during root canal treatment. The current study used the force signal for analyzing the endodontic characteristic through biomechanical preparation. The machine learning algorithms have been employed to assess the model's performance, namely Gaussian Naïve Bayes (GNB), quadratic support vector machine (QSVM), fine k-nearest neighbor (FKNN), and ensemble bagged tree (EBT).

5.2 Methodology

5.2.1 Biomechanical preparation and data acquisition

The College of Dental Science and Hospital Indore, India, provides the extracted teeth samples. Since these extracted teeth contain harmful bacteria, disinfection through hydrogen peroxide is required after collecting from the hospital. The previous chapter explained the sample preparation process in detail. This chapter also follows the same preparatory procedure. The biomechanical preparation setup involves the dental trolley and the air compressor. The dental trolley consists of three components: the first one is a micro-motor for creating a glide path, second is an air rotor which is used to give an initial ditch to the crown of the teeth. The last one is two ways syringe, which provides water and air during the sample preparation, as depicted in the biomechanical preparation portion of Fig. 5.1.

The RCT utilizes this study's wave one gold (WOG) endodontic file. Dentsply Maillerfer, Switzerland, manufactures these endodontic files,

which are used in accordance with the manufacturer's guidelines. The RCT experimental rig consists of two sub-systems. The first one is for biomechanical preparation, where the extracted teeth are cleaned, and samples are prepared, as shown in Fig. 5.1. In the second, an endodontic file is used to clean and shape the teeth., as shown in Fig. 5.1. A dynamometer with a sampling frequency of 7100 Hz is used to record the data. Force measurement sensor made by the Kistler group in Winterthur, Switzerland. The sensor has a sensitivity of nearly -7.5 pC/N (*x, y*-direction) and -23.5 pC/N (*z*-direction) and can measure forces up to 10 kN. For data transfer, DAQ is paired to a dedicated laptop. MATLAB (MathWorks, USA) software is used to analyze the signals. The methodology used in this study is shown in Fig. 5.2.

5.2.2 Unbalanced and balanced datasets

This work considers three classes: *success*, *moderate*, and *failure.* A file is categorized as a class *success* if it is in healthy condition after the RCT procedure. The file that has faults during the procedure is considered in class *failure*. In contrast, the file with a moderate level of damage is assessed in class *moderate*. Minority classes have fewer occurrences, and a class with a superior number of instances is titled a majority class. The minority class includes *failure* and *moderate*, whereas the majority class includes success instances. The unbalanced dataset problem happens in many domains. In an unbalanced dataset problem, one of the predefined classes has fewer instances than the others [181], as illustrated in Fig. 5.3. There are fewer minority class occurrences, and ML models may overlook or fail to recognize a minority class, thus providing unfair outcomes [181].

Biomechanical preparation setup

Root canal treatment experimental setup

Recorded force signal of healthy, moderate, and faulty
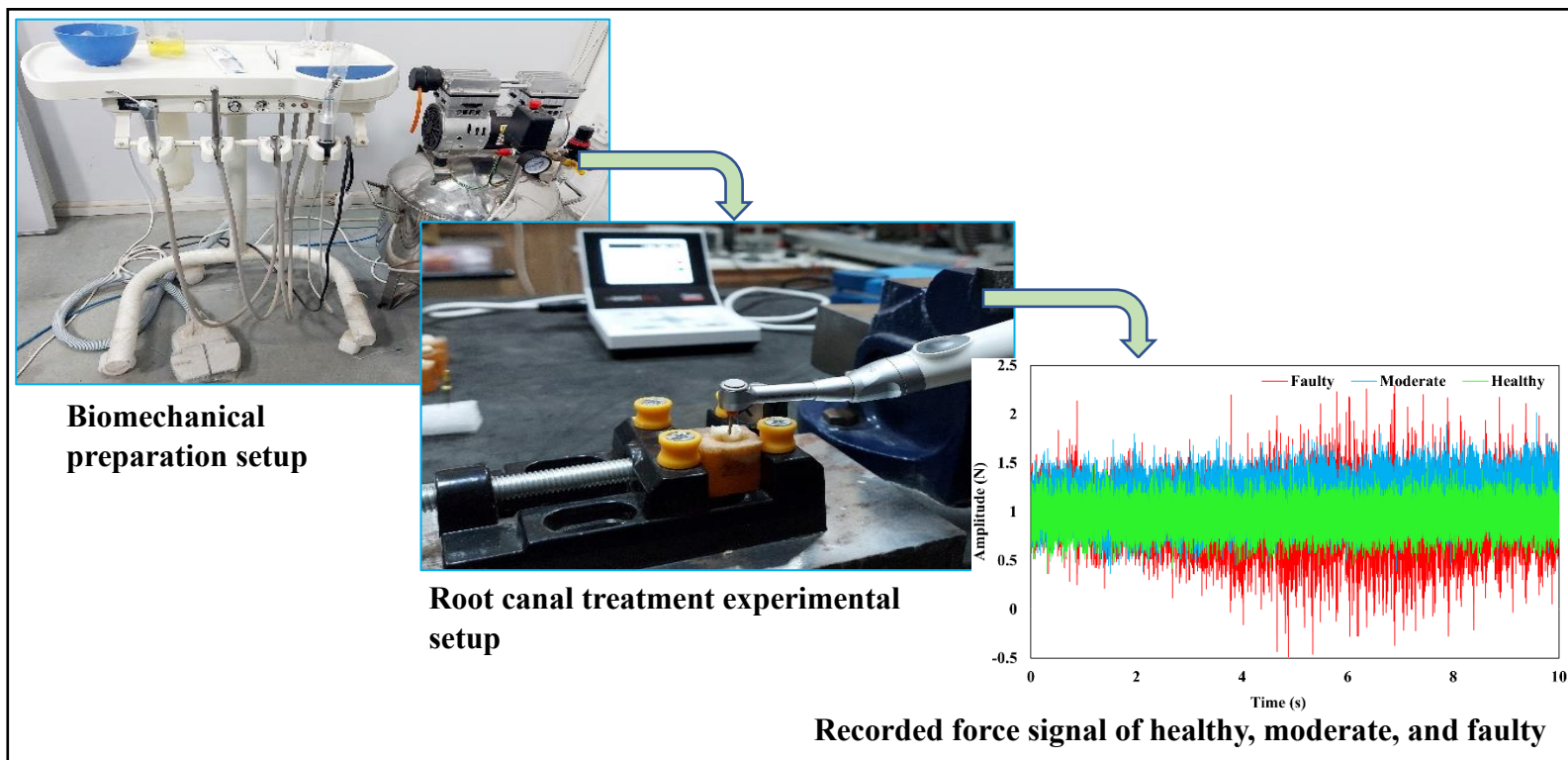
Figure 5.1 Experimental setup for the biomechanical preparation of root canal, with the recorded signal for healthy, moderate, and faulty endodontic fil
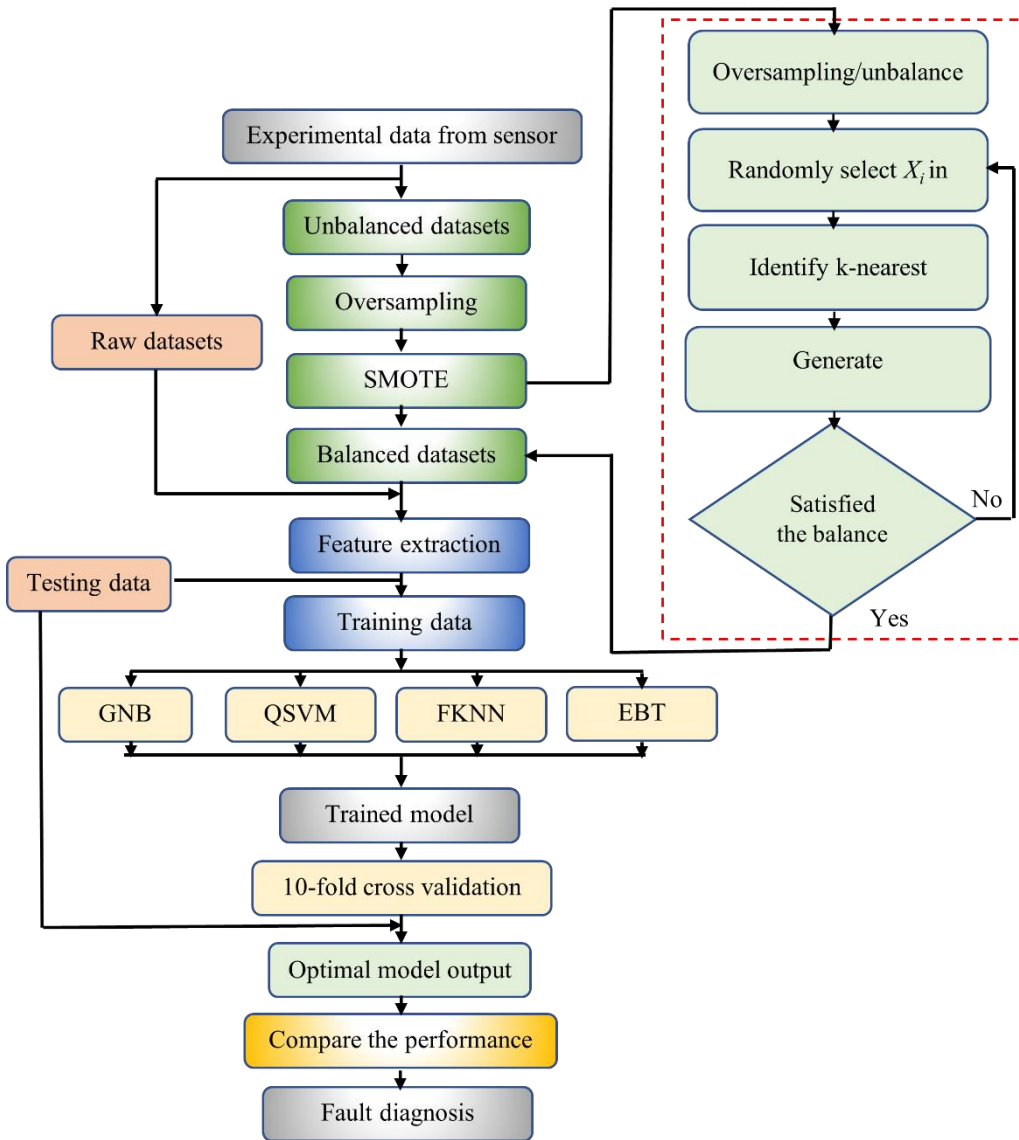
Figure 5.2 Flow chart of the methodology adopted for fault diagnosis of the endodontic instrument

5.3 Synthetic Minority Oversampling Technique (SMOTE)

The unbalanced distribution of the datasets means the minority class (*faulty* and *moderate* class) is much less than the majority class (*healthy /success* class). If the problem of unbalanced data is addressed in advance, the classifier model's effectiveness will improve. Most predictions are for the *success* class, while the *faulty* and *moderate* class features might be discarded because of the borderline points and treated

as data noise [182]. As a result, the model will have a significant bias. The technique of synthetic minority oversampling, i.e., SMOTE, is employed to balance the dataset.
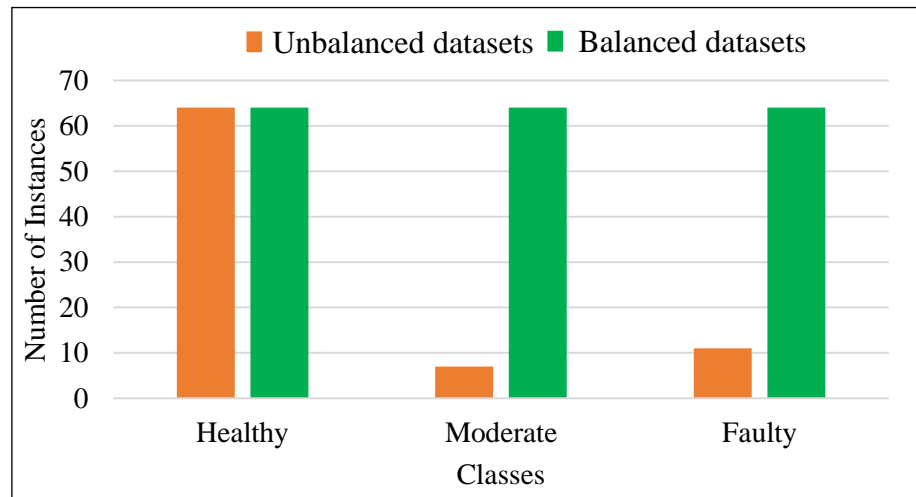
Figure 5.3 The unbalanced and the balanced classes of the datasets

The SMOTE is one of the essential techniques in generating artificial instances for the minority class. This technique is easier to address the challenges of overfitting produced by random oversampling. The SMOTE emphasizes the feature space to make a new number of instances by interpolating between minority instances close together, as shown in Fig. 5.4.

A few techniques are discussed in the literature, such as SMOTE (Synthetic Minority Oversampling Technique) [183,184], safe level-SMOTE [185], Borderline-SMOTE [186], SMOM (Synthetic Minority Oversampling Technique for Multiclass) [187], and ADASYN (Adaptive Synthetic Sampling Approach) [188]. The SMOTE models function admirably and provide the majority of accurate predictions [187]. Additionally, rather than eliminating several duplicates, SMOTE methods generate new unique data [187,189]. Since SMOTE reduces the probability of overfitting [183], this study uses SMOTE to balance the datasets.

5.3.1 SMOTE algorithm

The function in Eq. 5.1, generates new observations using a k-nearest neighbor technique and existing (input) data. Only neighbors within the same class are evaluated if multiple classes are provided as input [183,184,190].
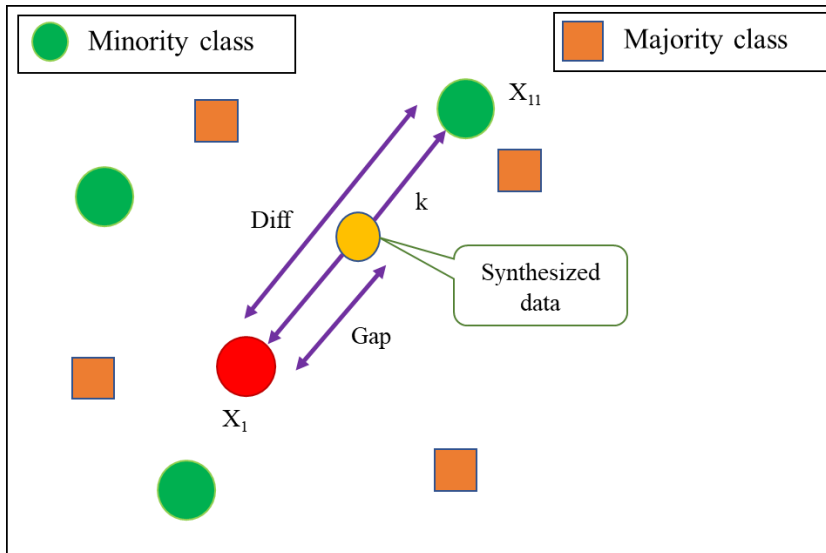
Figure 5.4 Synthetic Minority Oversampling Technique (SMOTE) algorithm

$$function\ [X, C, Xn, Cn]\ =\ smote\ (X, [N, k]) \qquad (5.1)$$

where, in input; X: Original datasets

N: Oversampling amount (i.e., $1 = 100\%$), N can be a vector with the same number of objects as the number of classes if the variable 'Class' is set.

k: Consider the number of closest neighbors, k can be a vector with the same number of objects as the number of classes if the variable 'Class' is set.

Output; X: the entire dataset (before and after SMOTE)

C: Complete dataset classes

Xn: Observations after SMOTE

Cn: Classes of synthesized observation

The following steps are followed for the SMOTE algorithm [183]:

Step 1: Initialisation of datasets and minority class sets in oversampled border regions

Step 2: Calculate the sample datasets for the majority and minority classes

Step 3: Calculate the boundary area and the lower approximation decision.

Step 4: Create synthetic data from minority class datasets.

Step 5: Return: end function

The above algorithm synthesizes the fresh minority class observations so that the total observation for every class equals the total observations for the majority class.

5.3.2 Feature extraction

Statistics are used to calculate a wide range of features from the sensor's signals [163,191,192]. These statistical features are commonly used for health and condition monitoring of the systems or components [191]. These extracted features are discussed below.

1. *Root mean square (RMS)*: The RMS is the square root of the signals' arithmetic mean.

$$RMS = \sqrt{\frac{1}{2} \sum_i x_i^2} \tag{5.2}$$

2. *Standard deviation (STD)*: The standard deviation (SD) is a measure of how much datasets deviate from the mean.

$$\sigma^2 = \frac{1}{n-1} \sum_{i=0}^{n-1} (x_i - \mu)^2 \tag{5.3}$$

3. *Kurtosis*: The flatness and sharpness of the peak of the signal corresponding to the normal distribution are evaluated by kurtosis.

$$Kurtosis = \left[\frac{n(n+1)}{(n-1)(n-2)(n-3)} \sum \left(\frac{x_i - \mu}{\sigma} \right)^4 \right] - 3 \frac{(n-1)^2}{(n-2)(n-3)} \qquad (5.4)$$

4. *Skewness*: The asymmetry in a statistical distribution is referred to as skewness, symmetry evaluation.

$$Skewness = \frac{n}{(n-1)(n-2)} \sum \left(\frac{x_i - \mu}{\sigma} \right)^3 \qquad (5.5)$$

5. *Crest factor*: The crest factor is the ratio of the data's absolute greatest value to its root mean square value.

$$crest\ factor = \frac{|x_{max}|}{RMS} \qquad (5.6)$$

6. *Clearance indicator*: The ratio of a data's maximum absolute value to the data's square root amplitude value is known as the clearing indication.

$$clearance\ Indicator = \frac{max|x_i|}{\left(\frac{1}{n} \sum_{i=1}^{n} \sqrt{|x_i|} \right)^2} \qquad (5.7)$$

7. *Shape factor*: The root mean square value to the data mean ratio is used as a shape factor.

$$Shape\ factor = \frac{max(|x_i|)}{\frac{1}{n} \sum_{i=1}^{n} |x_i|} \qquad (5.8)$$

5.4 Machine learning models

The supervised ML-based classifier approach has been applied for model training and evaluation. The fundamental aim is to figure out a class for the observed data. The following ML models are used in this study:

5.4.1 Gaussian Naïve Bayes

The Gaussian Naïve Bayes (GNB) classifier is a supervised machine learning and probabilistic distribution model where the Bayes hypothesis is utilized as a framework [193,194]. This hypothesis is used to classify observations into one of the predefined classes utilizing a dataset. GNB classifiers evaluate the conditional probabilities that data

corresponds to a particular class through the response variable. The Gaussian distribution assumes that variables of response classes are conditional independent in the Naïve Bayes model. The probability of the observed instances and class is calculated as per the following [195]:

$$P(c|x) \propto P(c) \prod_{i=1}^{n} P(x_i|c) \tag{5.9}$$

where the conditional probability terms $P(x_i|c)$ of x_i occurred in the variable of class c. $P(x_i|c)$ measures how much evidence x_i provides that c is the correct class. The probability of observing instances falling into class c is $P(c)$.

The following equation can be employed to evaluate the conditional probability [195,196]:

$$P(x|c) = \frac{1}{\sqrt{2\pi\sigma}} e^{\frac{-(x-\mu)^2}{2\sigma^2}} \tag{5.10}$$

where x is an observation, c is class, $\mu,$ and σ are mean and standard deviation, respectively.

5.4.2 Quadratic support vector machine

The SVM is a supervised learning method that aids multi-dimensional function estimation [197]. A structural minimization of risk and statistical learning theory are the foundations of the SVM approach. By converting input values into a multi-dimensional space, the SVM seeks to learn the boundary between the two classes [198,199]. A quadratic support vector machine (QSVM) was introduced to make optimization problems free from dual form and kernel [200].

A quadratic function is defined as [198,200]:

$$f(X) = \frac{1}{2} X^T W X + b^T X + c \tag{5.11}$$

$$\text{where } W = W^T = \begin{bmatrix} w_{11} & w_{12} & \cdots & w_{1m} \\ w_{12} & w_{22} & \cdots & w_{2m} \\ \vdots & \vdots & \vdots & \vdots \\ w_{1m} & w_{2m} & \cdots & w_{mm} \end{bmatrix}; b = \begin{bmatrix} b_1 \\ b_2 \\ \vdots \\ b_m \end{bmatrix} \tag{5.12}$$

Eq. 5.11 has two terms; the first is non-linear, and the remaining two represent linear terms. This makes Eq. 5.11 efficient enough to separate (non-linearly) the data into two classes. The QSVM optimization problem for *m* training data becomes:

$$Minimize \ \sum_{i=1}^{m} \|\Delta f(X_i)\|^2 \tag{5.13}$$

subject to $\gamma(i) \geq 1$ for $i = 1, m$ (5.14)

5.4.3 Fine k-nearest neighbor

The k-nearest neighbor (KNN) is a modest classifier among the all-machine learning algorithm [201]. The nearest k training dataset in the feature space makes up the datasets, where k denotes the integer. The datasets are categorized by determining the most common class from the k-nearest neighbors. These neighbours are evaluated based on their distance from the test sample. The KNN classifier uses a variety of distance metrics to apply the categorization model. The distance matrices are Euclidean distance, Minkowski distance, cosine similarity and weighted distance [202]. In this work, data is classified using a Fine KNN (FKNN) classifier, a type of KNN that identifies k-nearest neighbors using a small number of training samples. FKNN algorithm uses Euclidean distance to estimate the closest neighbors [203].

5.4.4 Ensemble bagged tree

An ensemble technique is an approach that combines predictions from various decision algorithms to provide more accurate predictions than those from any single algorithm [204]. Bagging is the term for bootstrap aggregation, an ensemble learning that generates data using sequential and parallel approaches [205]. In most cases, bagging uses a similar weak classifier and trains them simultaneously [205]. Several decision tree learners are used in this ensemble; each is trained on a different portion of the training set. Furthermore, the majority vote of the estimations is used to make the final prediction of an ensemble bagged tree classifier (EBT), for instance, through the individual decision trees. The EBT model has one of the most significant features: despite training the model frequently with various feature subsets, the significance of features can be assessed throughout the training phase.

5.5 Results

5.5.1 Model parameters for performance analysis

In this work, seventy percent of the dataset is chosen at random for the training, and thirty percent is utilized as a test set to assess the effectiveness of the machine learning models. The same ratio for training and testing is used for balanced and unbalanced datasets to carry out the experimentations. The ML models are trained using a stratified 10-fold cross-validation technique. Moreover, to overcome the unbalanced class problem and avoid overfitting, the approach of synthetic minority oversampling is used.

True positive (TP) and false positive (FP) signify that a positive class is detected correctly as positive and a negative class is incorrectly detected as positive, respectively. The true negative (TN) and false negative (FN) denote that the negative class is adequately detected as negative and the positive class is incorrectly detected as negative, respectively. For the unbalanced and balanced model, sensitivity, specificity, precision, NPV, and F1-score of the datasets are employed to evaluate the efficiency of predictions [190,206–208]. The following are their definitions:

1. *Sensitivity or recall*: It is referred to as a true positive rate, a quantity of positive class that the classifier has classified.

$$\frac{TP}{TP+FN} \tag{5.15}$$

2. *Specificity*: It is referred to as the true negative rate. It is a quantity of negative classes that have been classified as negative by the classifier.

$$\frac{TN}{TN+FP} \tag{5.16}$$

3. *Precision:* It is the proportion of the number of classes exactly classified as positive to the total number of positive classes detected. It also demonstrates the accuracy of positive prediction.

$$\frac{TP}{TP+FP} \qquad (5.17)$$

4. *Accuracy* is the percentage of accurate predictions from the total number of predictions.

$$\frac{TP+TN}{TP+TN+FP+FN} \qquad (5.18)$$

5. *F1-Score*: It's a weighted average of precision (recall) and sensitivity.

$$\frac{2\times precision\times sensitivity}{precision+sensitivity} \qquad (5.19)$$

5.5.2 Implementation of machine learning model

5.5.2.1 Effect of datasets prior to oversampling

The confusion matrix of the classifier model is obtained utilizing raw unbalanced data (before the oversampling). Gaussian Naïve Bayes, quadratic support vector machines, fine *k*-nearest neighbor, and ensemble bagged tree classifier are used to acquire the confusion matrix as shown in Fig. 5.5. For the unbalanced datasets, GNB, QSVM, FKNN, and EBT models achieved accuracies of 91.46 %, 95.12%, 97.56%, and 97.56%, respectively. The Fine KNN and EBT measured the decent value of the specificity through the model. However, as we compare it with the GNB and QSVM, it is a much higher value than Gaussian and quadratic classifiers, as mentioned in Table 5.1. The sensitivity value of the quadratic classifier is predicted as minimum compared with the other classifiers because it precisely detected the class.
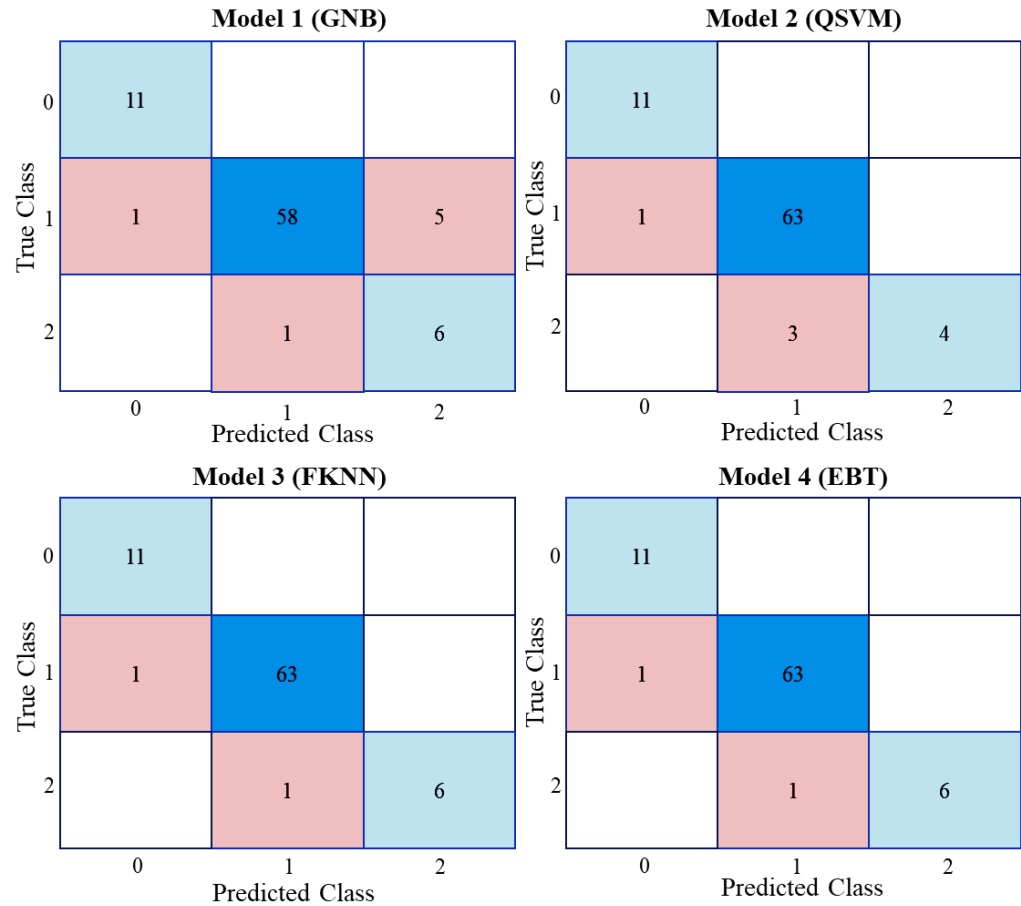
Figure 5.5 Confusion metrics of ML model before oversampling (unbalanced)

5.5.2.2 Effect of datasets after the oversampling

The SMOTE approach is implemented to balance the dataset. Both classification model's performance has improved after resampling, as shown in the confusion matrix of Fig. 5.6. The true positive rate of the GNB, QSVM, FKNN, and EBT classifier is increased. The accuracy of the balanced class is observed to be higher after utilizing the oversampling technique with the acquired confusion matrices. The FKNN and EBT classifiers have higher accuracy than the Gaussian and quadratic classifiers in the balanced class, and the noted higher accuracies are 98.95% and 98.95%, respectively. The precision value for all the classifiers is observed to be higher after utilizing the SMOTE approach, as shown in the performance metrics for the classifier model in Table 5.1.
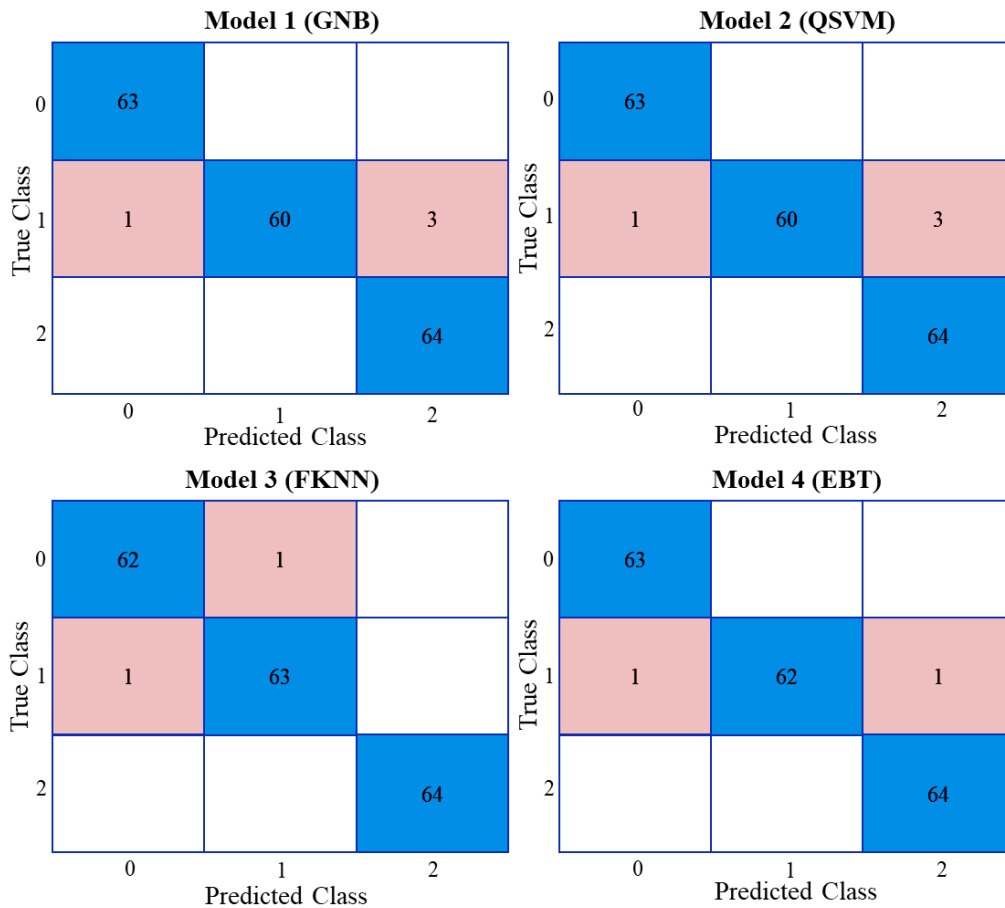
Figure 5.6 Confusion metrics of ML model after oversampling (balanced)

5.6 Discussion

In endodontics, machine learning techniques may predict periapical diseases, vertical root fracture, apical foramen, root morphologies, retreatment, and endodontic surgeries [76,77,79,82,160,209–211]. The current study includes the diagnosis of endodontic instrument failure. The typical endodontic RCT mechanics makes it laborious and prone to error in fault diagnosis estimation. Therefore, accurate techniques and enhancing RCT approaches for diagnostics are implemented to aid in successful decision-making. It suggests that the multiple class associations can be analyzed quickly using machine learning algorithms. The oversampling effect is investigated on the acquired force signal during the RCT. Furthermore, it established that the ML classifier model could effectively diagnose the endodontic file.

Table 5.1 Performance metrics for GNB, QSVM, FKNN, and EBT classifications

Performance	Gaussian Naïve Bayes		Quadratic SVM		Fine KNN		Ensemble Bagged Tree	
	Imbalanced	Balanced	Imbalanced	Balanced	Imbalanced	Balanced	Imbalanced	Balanced
Precision (%)	81.51	97.61	95.71	97.99	96.70	98.95	96.70	98.95
Sensitivity (%)	92.11	97.92	85.19	97.92	94.72	98.95	94.72	98.95
Specificity (%)	95.46	98.74	93.97	98.95	97.68	99.48	97.68	99.48
Accuracy (%)	91.46	97.56	95.12	97.91	97.56	98.95	97.56	98.95
F1 Score (%)	85.54	97.70	88.43	97.90	95.47	98.95	95.47	98.95

In this work, results of the cleaning and shaping procedures are analyzed using Gaussian Naïve Bayes (GNB), quadratic support vector machines (QSVM), fine k-nearest neighbor (FKNN), and ensemble bagged tree (EBT) classifiers. The investigation is constrained by the minority class dataset that can be related to the comparatively satisfactory outcomes of endodontic instruments during RCT. The unbalanced classes may affect model performance; therefore, SMOTE algorithm is employed to resolve the problem [190,212]. The GNB, QSVM, FKNN, and EBT classifications algorithms are implemented and found to create the most accurate prediction when performing the RCT. Fig. 5.7 and 5.8 show the scatter plot of the classifier model for unbalanced and balanced class datasets, respectively. The features of the models have a significant relationship, which is also observed in unbalanced and balanced scatter plots. The graph shows that the classifier usually predicts positive and negative classes accurately, as shown in Fig. 5.7 and 5.8. There are only a few instances where the model predicts incorrectly. The clustered bar chart of the classifier model represents the performance of unbalanced and balanced classes, as shown in Fig. 5.9. This figure analyzes the comparison of all four-classifier model performances based on the precision, sensitivity, specificity, accuracy, and F1 score, respectively.
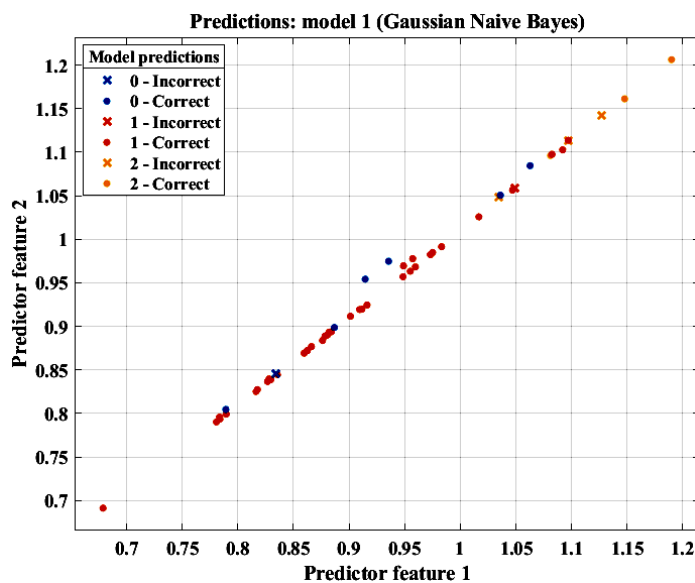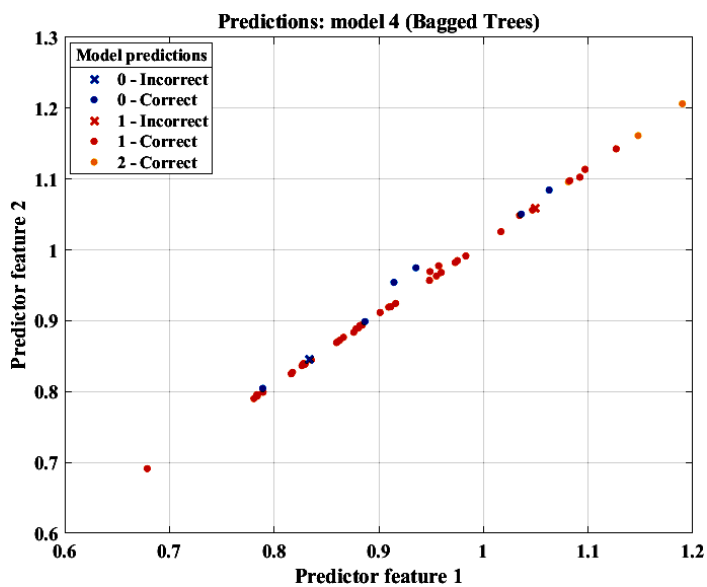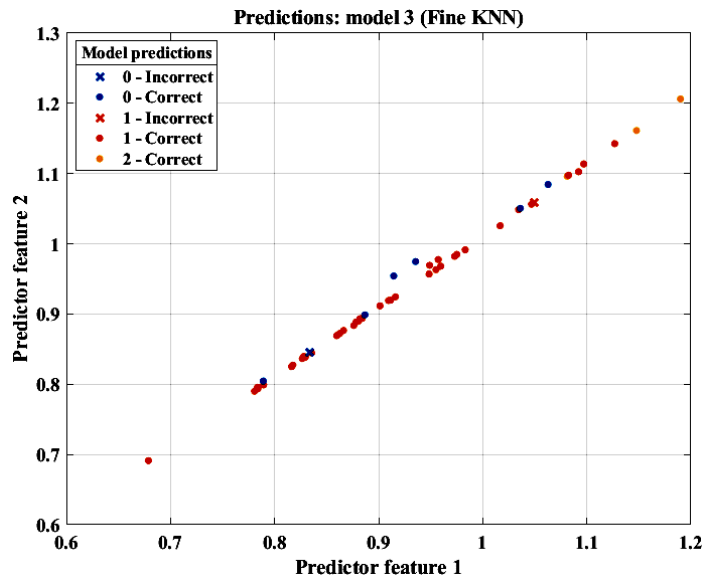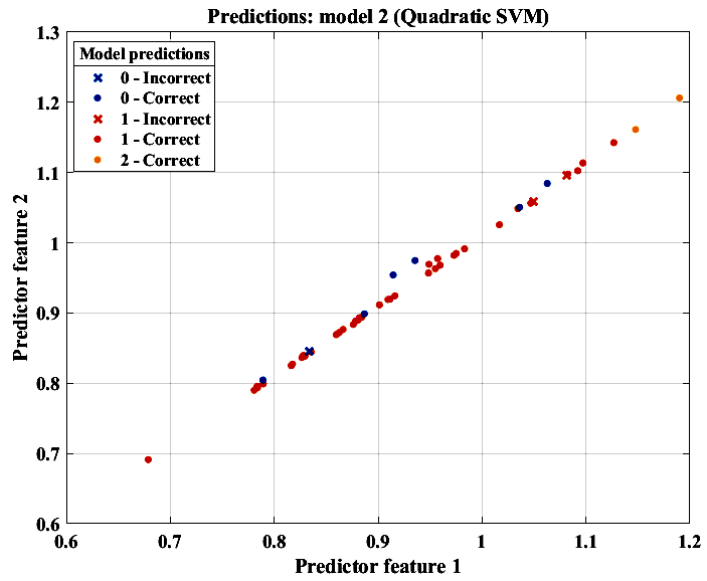
Figure 5.7 Scatter plot for unbalanced datasets of GNB, QSVM, FKNN, and EBT classifiers between the predictors

Fig. 5.10 depicts the receiver operating characteristic (ROC) curve and area under the curve (AUC) of the unbalanced dataset. These curves are utilized to evaluate the accuracy of predictions. For unbalanced datasets, the area under the curve of the GNB, QSVM, FKNN, and EBT classifier is observed at 0.95, 0.98, 0.96, and 0.99, respectively, as shown in the positive class. For the balanced dataset, the AUC of the GNB, QSVM, FKNN, and EBT classifiers is noted as 1.0, 0.99, 1.0, and 1.0, the positive class, respectively, as shown in Fig. 5.11. The FKNN and EBT classifiers reported accuracy improvements. This is possible because of the SMOTE approach, which has increased the minority class, resulting in a performance improvement.
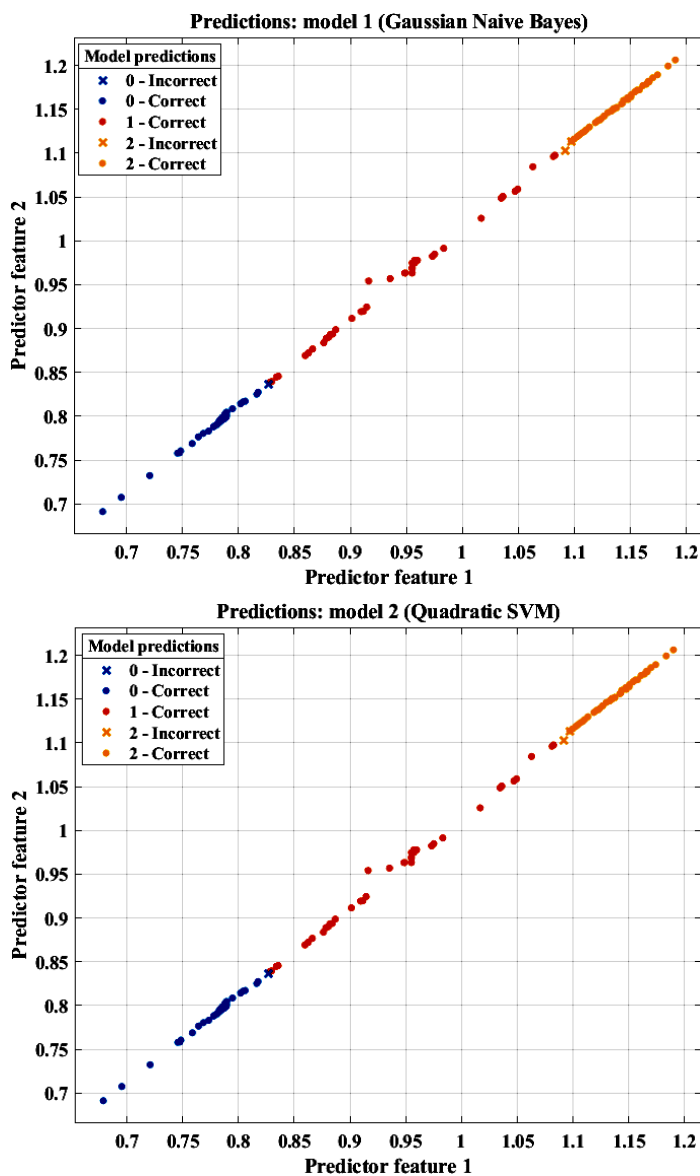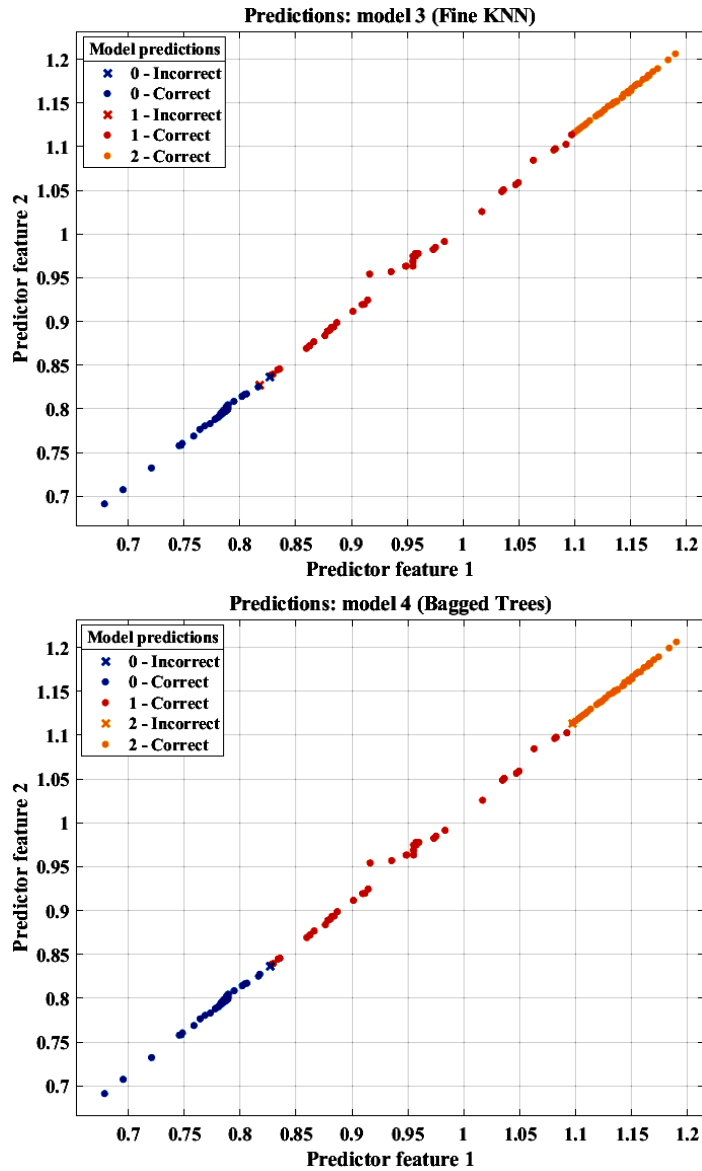
Figure 5.8 Scatter plot for balanced datasets of GNB, QSVM, FKNN, and EBT classifier between the predictors

Fine KNN and EBT models performed well in this study compared to all four classifiers, with an accuracy of 97.67%, 97.67% for unbalanced, 98.95%, and 98.95% for balanced, respectively. High precision, specificity, accuracy, and F1 score are very relevant when evaluating their performance, as shown in Table 5.1. It is essential to prevent classes that are completely treated as untreated. It may have an actual impact on teeth which can lead to teeth extraction due to catastrophe instrumentation.
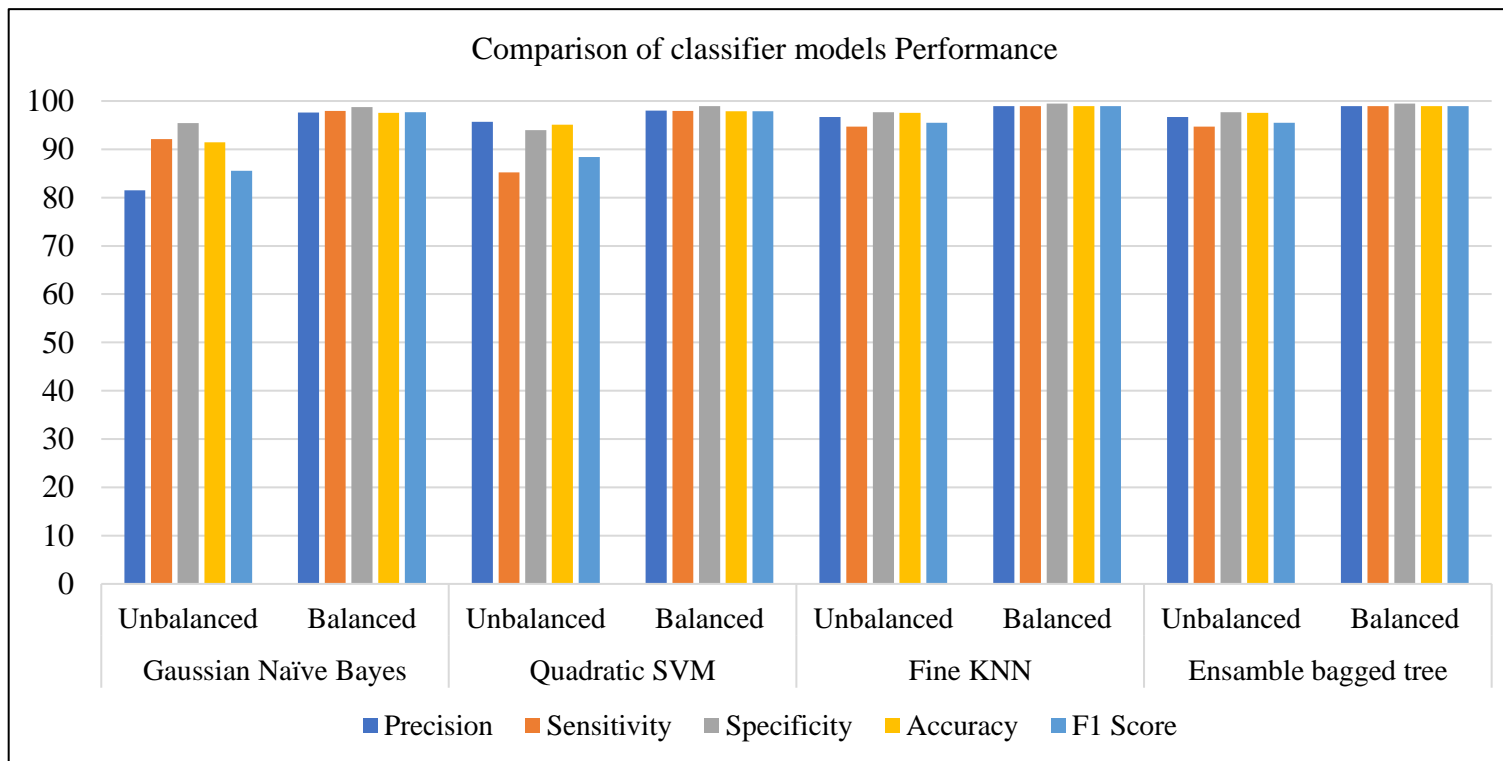
Figure 5.9 Comparison of a clustered bar chart for the classifications model performance

In this regard, the balanced EBT is even more accurate, specific, and sensitive. However, the accuracy and F1 score of the balanced FKNN classifier are similar to the EBT classifier. In contrast to the FKNN and EBT, the GNB and QSVM have a chance of misclassifying classes with adverse predictions with favourable fault diagnoses. Altogether, the QSVM and EBT models performed better after resampling, with an AUC of 1.0. The FKNN model also performed well in estimating endodontic instrument fault diagnosis, with an AUC of 0.99.
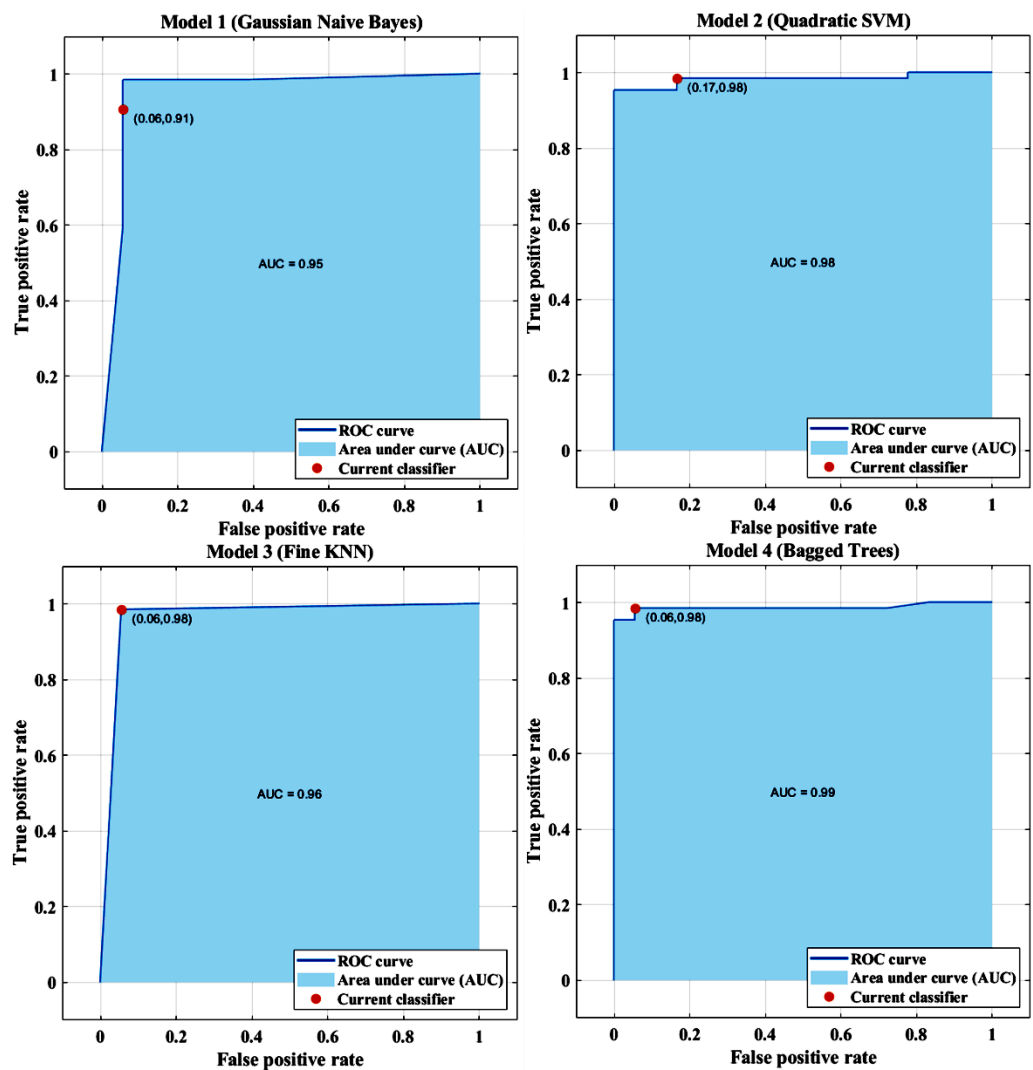
Figure 5.10 ROC performance curve and AUC for unbalanced data
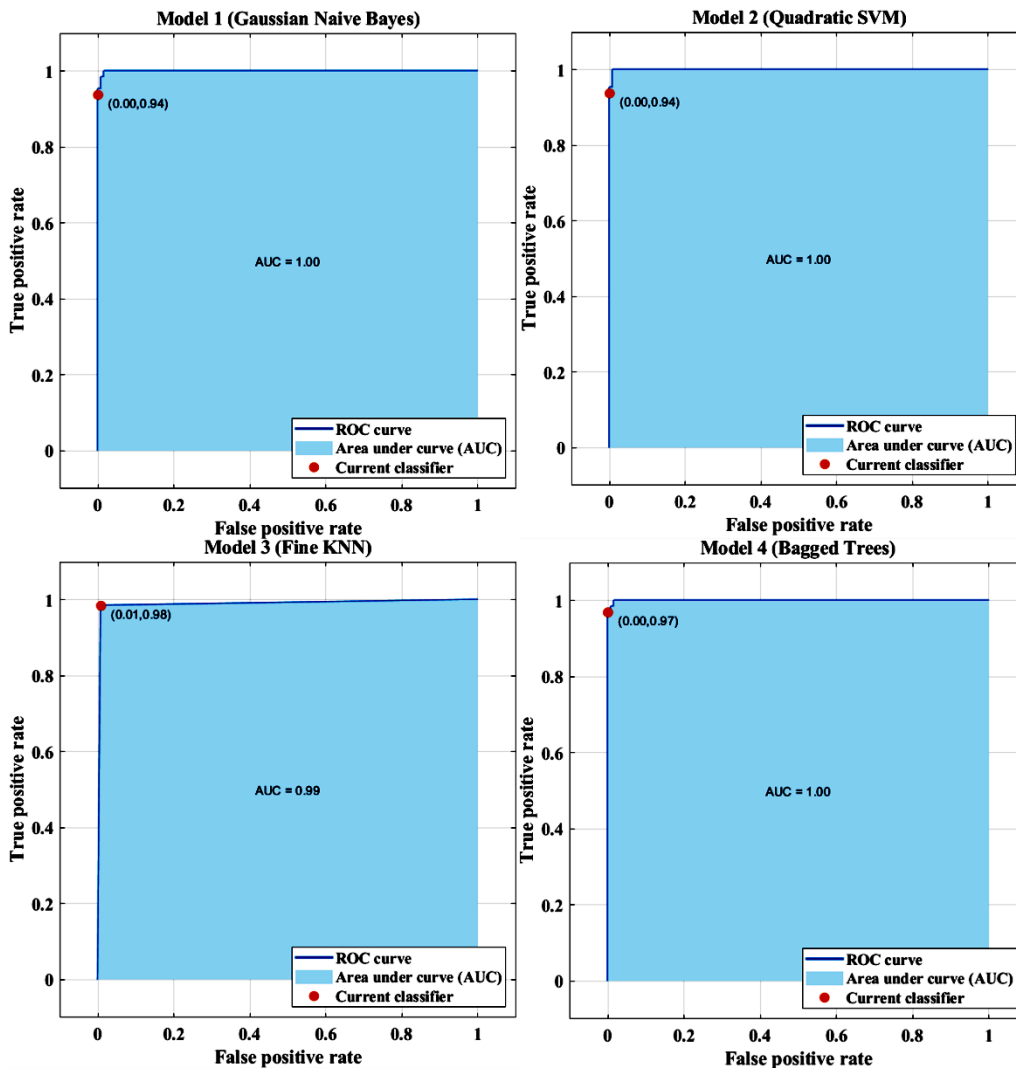
Figure 5.11 ROC performance curve and AUC for balanced data

Recently, ML algorithms have been used to classify endodontic treatments based on the Case Difficulty Assessment Form (CDAF) of the American Association of Endodontists (AAE) [180]. The ML approach is employed for estimating endodontic RCT complexity regarding the endodontic instrument [213]. This will substantially benefit the clinician in making referred judgments and enhancing patient satisfaction [180,213].

From the perspective of clinical relevance, according to the National Library of Medicine (NLM) and the National Institutes of Health (NIH) in the US, dentistry is one of the specialties where MLs are implemented

[76,87]. The research has yielded tangible outputs based on the scientific literature, including endodontics and orthodontics [76,87].

5.7 Conclusions

This study presents the implications of reciprocating endodontic instruments to shape and clean root canals by acquiring the force signals for different healthy and faulty conditions. These force signals are acquired while performing RCT and are subsequently used to train three supervised machine learning models. The following conclusions are drawn from the current research:

- The health diagnosis of endodontic files while carrying out RCT can be performed effectively by analyzing the force signals using QSVM, GNB, and FKNN with higher precision, sensitivity, and other performance metrics parameters.
- The SMOTE algorithm improves classification accuracy significantly.
- The current study reveals that the ensemble bagged tree (EBT) and fine k-nearest neighbor (FKNN) improves the performance evaluation of training and testing datasets compared to other methods. EBT and FKNN are equally accurate, with 98.95% and 97.56% for balanced and imbalanced data, respectively.
- The present study provides practitioners with appropriate clinical decision support systems by using machine learning approaches to diagnose the health condition of endodontic instruments.

This chapter presents the influence of oversampling on the effectiveness of force signals in predicting faults in the endodontic instrument. In the subsequent chapter, the endodontic file's health prediction and fault prognosis has been analyzed. The machine learning algorithm and degradation model have been utilized to analyze the force signals during the root canal treatmen

Chapter 6

Health prediction of the endodontic instrument based on machine learning and exponential degradation models

This chapter proposes an intelligent health prediction and fault prognosis of the endodontic file during root canal treatment. The force signals are acquired using a dynamometer during the RCT. Subsequently, statistical features are retrieved from the force signals. Through the window-wise feature extraction method, the extracted features are selected. Time-domain features of the signals are analyzed as characteristic features for endodontic file prognostics. Extracted features do not have relevant information due to noise in the signals. Hence the smoothing of the feature is required at this stage to observe a trend in the signals. The health of the endodontic instrument is predicted using machine learning techniques and an exponential degradation model. This model is intended to forecast the degradation of the endodontic instrument so that measures can be implemented before actual failures occur. The proposed approach can investigate endodontic instrument malfunctions and the initiation of failure. Endodontics practitioners can use machine learning models and an exponential model to estimate the endodontic instrument's health condition. This research may assist practitioners in improving the effectiveness of endodontic instrument performance and the efficacy of root canal treatment.

6.1 Introduction

Root canal treatment is necessary to prevent deterioration, pain, and toothache. The endodontic file is an essential instrument for the RCT

[37]. The RCT is an intricate procedure usually handled by dental practitioners. Endodontic instruments shape and clean the root canal [7,37]. Sometime, the instrument gets stuck between the root canal due to its intricated shape, resulting in the formation of a ledge [27]. The micro-crack can be initiated during the process, and there may be chances of endodontic instrument failure [110].

A health prognosis of the endodontic instrument is required to avoid failure of the instrument. The machine learning model predicts the endodontic instrument's degradation while preparing the root canal. Several approaches have been used for prognosis and health monitoring of endodontic instruments, including micro-CT technology, optical micrograph, fractographic analysis, SEM, AFM, statistical features, etc. Barbosa et al. [209] showed the internal and external defects of the endodontic instruments through micro-computed tomography. Additionally, they visualized the endodontic instrument's exterior surface and progressive deterioration. Rosa et al. [210] compared the strength and flexibility of the NiTi endodontic instruments with stainless steel instruments. Burklein et al. [144] discussed the axial force and dynamic torque during the RCT using three different endodontic motors. The rotary instrument is given a higher torque than the manual preparation [144]. Kataya et al. [214] compared the endodontic instrument's debris retention and cutting efficiency through the computer image analysis program. Afterward, it concluded that electro-polishing could enhance and improve the instrument's wear resistance. Gerek et al. [142] showed the adequate force involved in removing the fractured instrument during the RCT. Two different techniques, namely Masserann and ultrasonic, were compared. This study concluded that there was no significant difference between these techniques, but the reduced force was observed when the fractured instrument was removed vertically. Tokita et al. [64] analyzed the vertical force and dynamics torque during the RCT preparation through the NiTi rotary instrument with distinct reciprocal rotational modes. Further, they concluded that the maximum torque reduces considerably due to the decrement of stress

initiation affected by screw-in force. In this study, machine learning techniques are used with an exponential degradation model to forecast the degradation of the endodontic instrument.

6.2 Material and methods

6.2.1 Samples and root canal preparation

The College of Dental Science and Hospital Indore India has supported us in providing human extracted teeth. The methodology of this study is presented in Fig. 6.1. After collecting human extracted teeth, cleaning is mandatory through hydrogen peroxide (H_2O_2) because these extracted samples have germs and bacteria. The sample preparation for holding the extracted teeth has been made through the cold mountings process. In chapter 4, I have briefly described the stepwise sample selection and preparation process. The same sample selection and preparation procedure is also adopted for this chapter.

6.2.2 Experimentation and data acquisition

In this study, WaveOne Gold (WOG) endodontic reciprocating file system performs the RCT. The WOG (Dentsply Maillefer, Switzerland) endodontic file is utilized based on the directions given by the makers. The endodontic handpiece holds the endodontic file connected to the endomotor (X-smart Plus, Dentsply Sirona, United States). The experimental setup helps to shape and clean the root canal. A tooth sample is mounted over a vice fixed over the dynamometer. The vice is used for providing rigid support in the mounted specimen. During RCT, force signals were acquired using the dynamometer (Kistler Group, Winterthur, Switzerland), as shown in Fig. 6.2.

The dynamometer measures force up to 10 kN, and the sensitivity of the sensor is approximately $\approx$ -7.5 pC/N (Fx, Fy) and $\approx$ -23.5 pC/N (Fz). The force signal from the sensor is sampled at 7.1 kHz [66]. The dynamometer is directly connected through the data acquisition (DAQ) system, and DAQ is connected to the dedicated computer for transferring the data. The DAQ converts the current and voltage signals

into their corresponding value of the force signal. After that, the recorded data is analyzed and post-processed in MATLAB software.
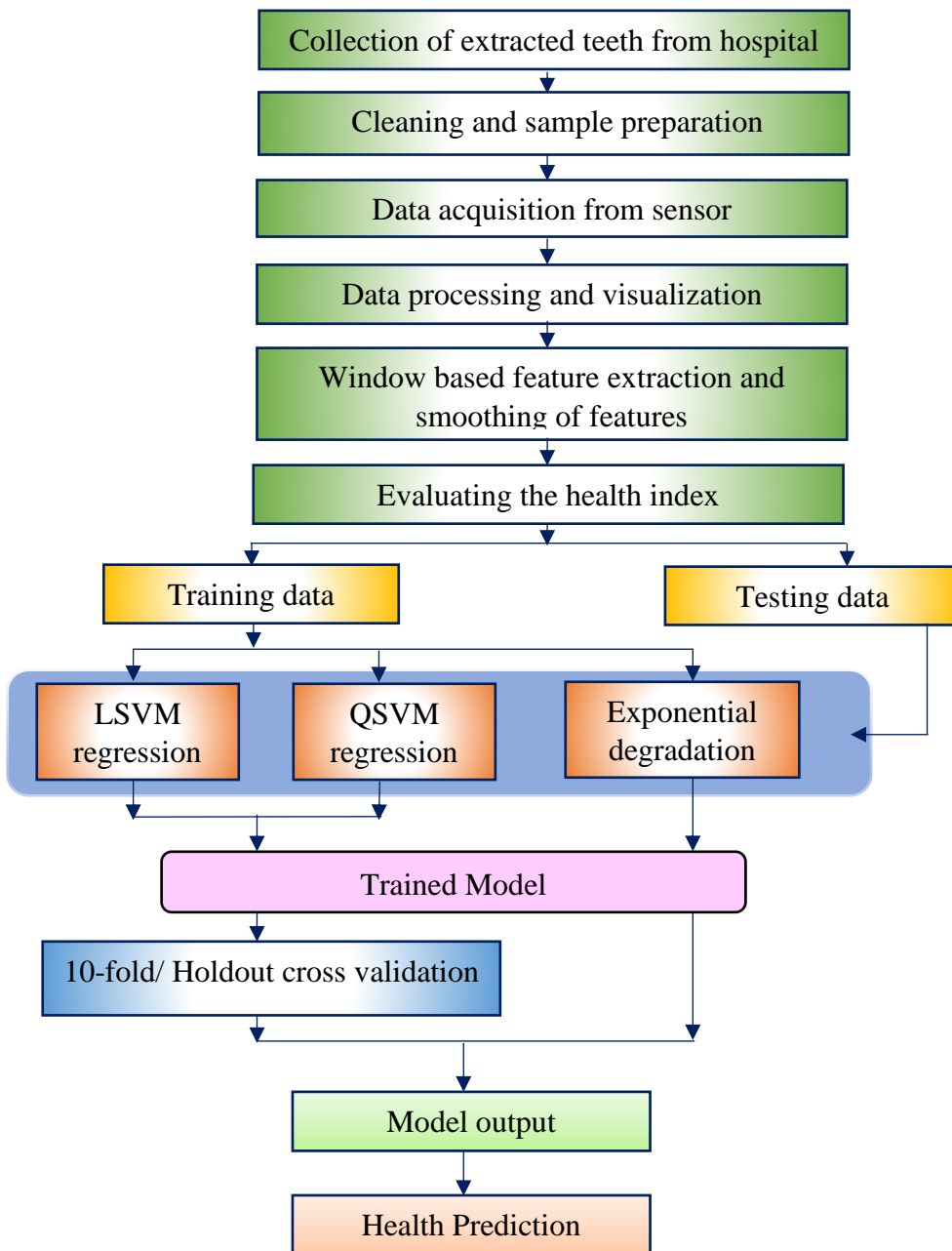
Figure 6.1 Methodology adopted for health prediction of endodontic files system during RCT
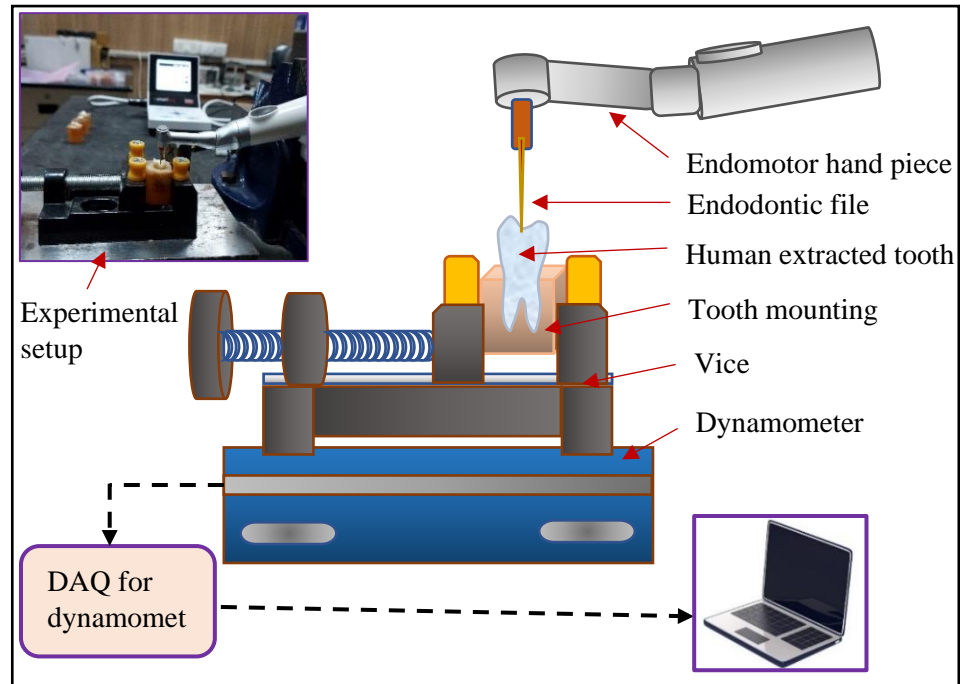
Figure 6.2 Schematic diagram of the experimental setup for RCT

6.2.3 Data processing and exploring

The data have been processed and visualized in MATLAB software. The force signals are represented as time responses, as shown in Fig. 6.3 (a-c). The force amplitude increases as the endodontic file approach the canal's curved and apical portion. The force signals are categorized into three categories based on the degradation status of a file: healthy, moderate, and faulty. The retraction and insertion signals of the endodontic instruments from the root canal wall are observed during the RCT, as shown in Fig. 6.3. The retraction and insertion signatures of the endodontic instruments are clearly visualized in the graph. Furthermore, these healthy, moderate, and faulty signals are used for feature extraction.

6.2.4 Microscopic analysis

The severity level of failure of the endodontic instrument has been examined under an optical stereo-microscope system (Leica DMS300; Leica Microsystems Inc. USA). Fig. 6.4 (a) shows the Longitudinal and cross-sectional view of the healthy condition of the endodontic file,

which has a sharp and clean edge. After some time, the irregularities and file tip wear have been observed during the cleaning and shaping, as shown in Fig. 6.4 (b). The smear layer and debris substances [155] have also remained at the cutting edge during the process, as shown in Fig. 6.4 (b) [155,215]. After that, failure origination and tip break along the grove [157] have been observed on the file surface while RCT, as shown in Fig. 6.4 (c).

6.2.5 Feature extraction

For the different fault severity mentioned in section 2.3, well-known statistical features such as standard deviation, kurtosis, means, skewness, shape indicator, clearance indicator, impulse indicator, root mean square, etc., have been calculated [162,192]. Four features based on the trendability and monotonicity of the features, i.e., standard deviation (σ), kurtosis, skewness, and root mean square [164,192], are considered for further analysis.

1. Root means square (RMS): RMS calculates the average value over a period of time.

$$RMS = \sqrt{\frac{1}{2}\sum_i x_i^2} \tag{6.1}$$

2. Kurtosis: Kurtosis measure the flatness and sharpness of the peak of the signal corresponding to the normal distribution.

$$Kurtosis = \left[\frac{n(n+1)}{(n-1)(n-2)(n-3)}\sum\left(\frac{x_i-\mu}{\sigma}\right)^4\right] - 3\frac{(n-1)^2}{(n-2)(n-3)} \tag{6.2}$$

3. Skewness: Skewness refers to a measure of asymmetry, the lack of symmetry.

$$Skewness = \frac{n}{(n-1)(n-2)}\sum\left(\frac{x_i-\mu}{\sigma}\right)^3 \tag{6.3}$$

4. Standard deviation (STD): The STD measures fluctuations of force signal from the mean.

$$\sigma = \sqrt{\frac{1}{n-1}\sum_{i=0}^{n-1}(x_i-\mu)^2} \tag{6.4}$$

where μ is the mean, and n is the number of samples.
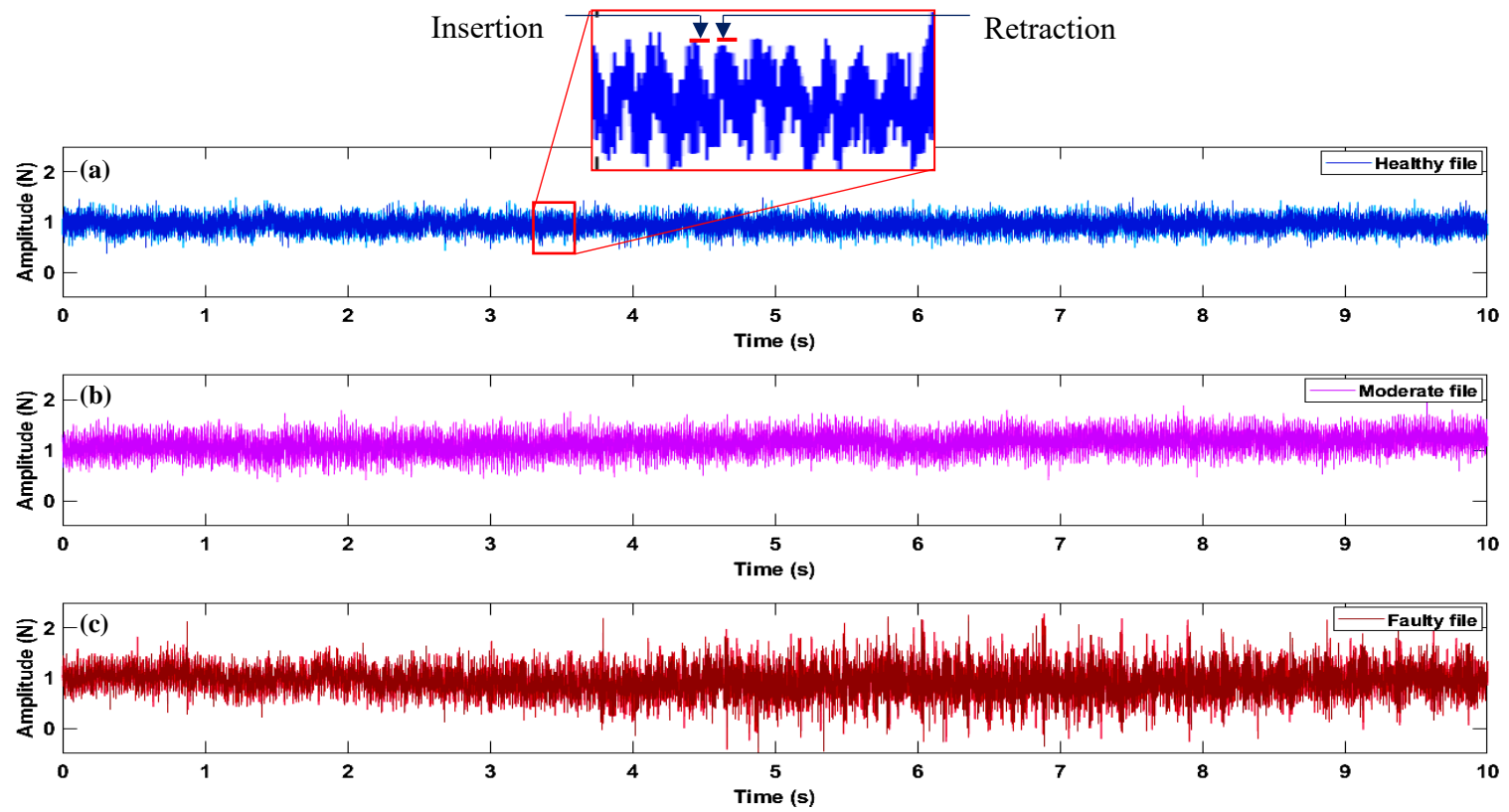
Figure 6.3 Force signal during the RCT (a) healthy file, (b) moderate file, and (c) faulty file
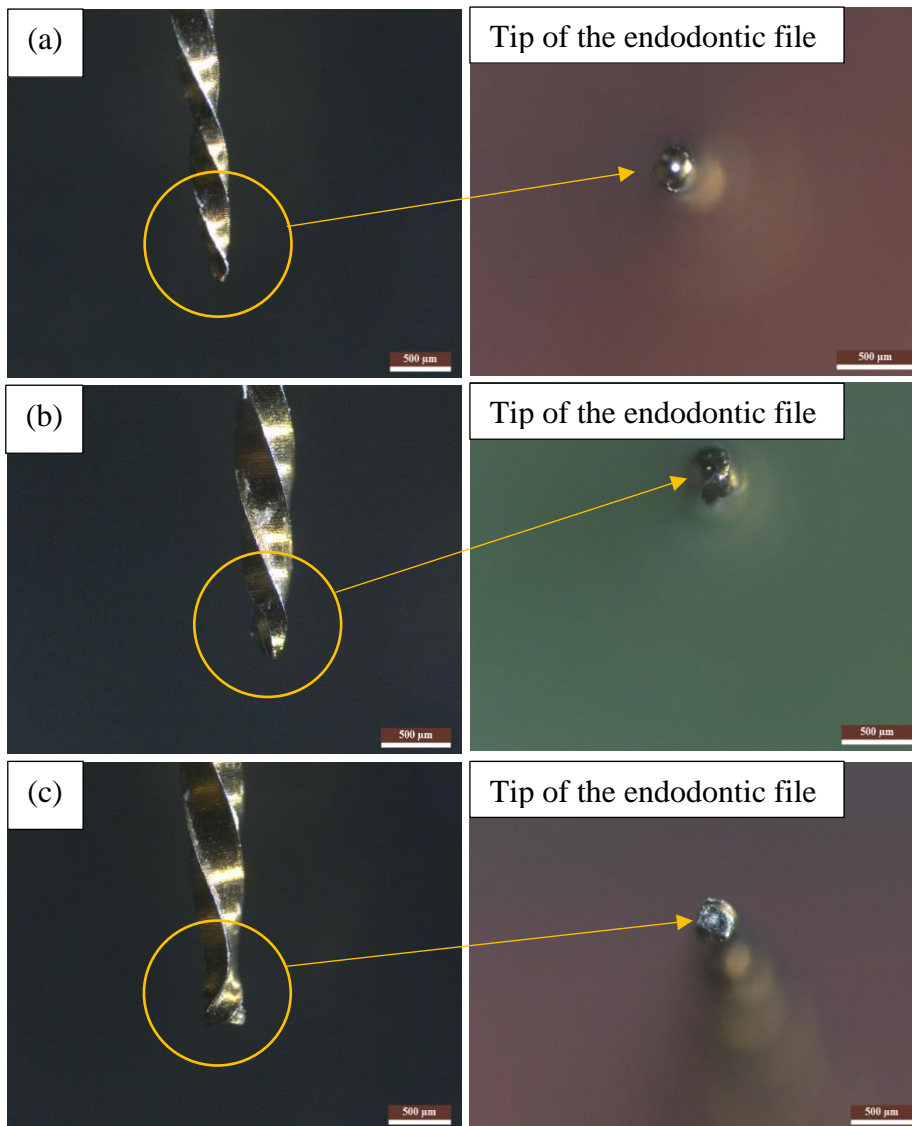
Figure 6.4 Longitudinal and cross-sectional aspects of representation of the endodontic reciprocating instruments (a) healthy, (b) moderate, and (c) faulty file

6.2.6 Window-wise feature extraction

Window-wise feature extraction is needed to obtain the appropriate feature trend [216,217]. After choosing three selected endodontic files, healthy, moderate, and faulty files, a window is employed in each time-domain signal, as shown in Fig. 6.5. Features are extracted according to the window-wise feature extraction process. Afterward, the trends of these features are analyzed for different file conditions.
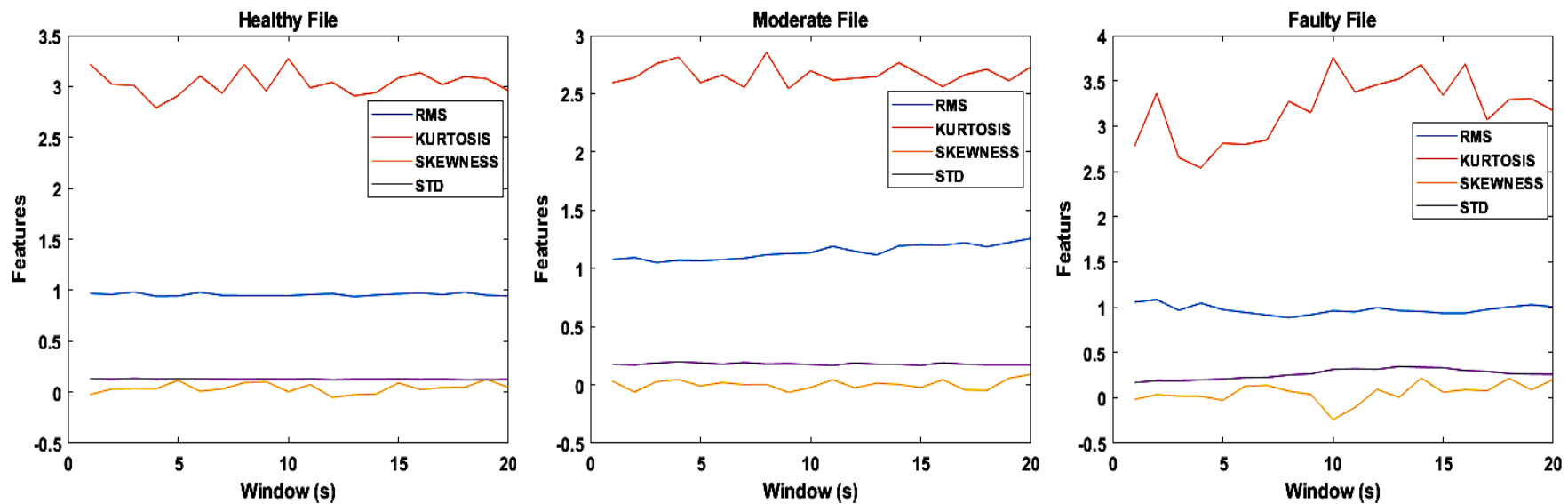
Figure 6.5 Extracted features in the time domain, i.e., RMS, kurtosis, skewness, and standard deviation of the endodontic file, namely: healthy file, moderate file, and faulty file, respectively
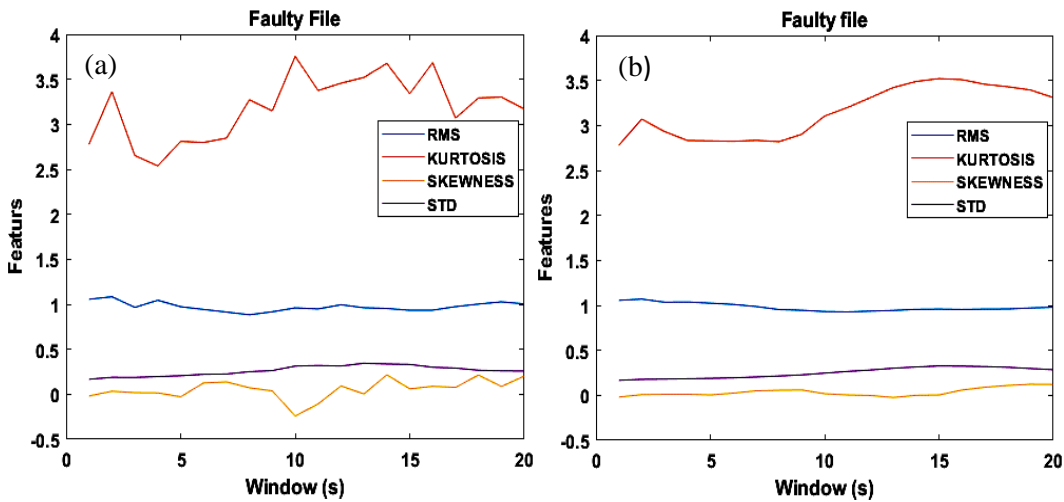
Figure 6.6 Smoothing the extracted feature of the faulty file (a) without smooth features, (b) with smooth features

6.2.7 Smoothing the feature data

To avoid unnecessary noise from extracted features, smoothing of the feature is required. The noisy feature can sometimes be inaccurate in measuring the health prediction. Therefore, the lag window of five steps with a moving means filter is employed to extract the features of the signal. Fig. 6.6 (b) shows the effect of feature smoothing.

6.2.8 Health Index

The health index (HI) is employed to predict the health status of the endodontic instruments. Various techniques can define the health index. A few of them include principal component analysis (PCA) [199,218], kernel PCA [199], diffusion mapping (DM) [199], window wise feature extraction [216], maximum variance unfolding (MVU) [199], self-organizing mapping (SOM) network [200] and isometric feature mapping reduction technique (ISOMAP) [197]. This work determines the health index using PCA and the window-wise method. In this method, the windowing of 20-second data is used. Each window measures the one-second data, as shown in Fig. 6.7. The best health index is obtained from the window-wise feature extraction method, as

124

shown in Fig. 6.7 (b). The curves are plotted between the window (second) and features (standard deviation i.e., STD). The standard deviation feature is optimized using the RefliefF feature selection technique that is defined as a health index. After selecting the healthy, moderate, and faulty file features (i.e., RMS, kurtosis, skewness, and STD), then applied the window method for each selected file according to the health condition of the endodontic file. Since this work aims to the health prediction of the endodontic instrument thus, a faulty file is chosen for analyzing the health index.
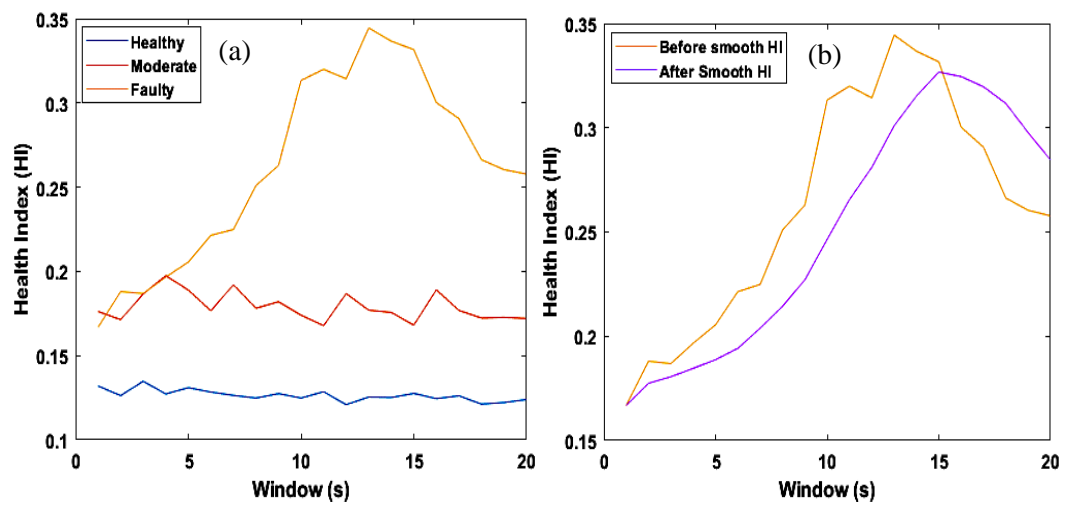
Figure 6.7 (a) Health index of healthy, moderate, and faulty file, and (b) health index of the faulty file

6.3 Machine learning models

6.3.1 Linear support vector regression

Vapnik et al. [218] proposed the Linear Support Vector Regression (LSVR), which is used as a highly popular application of SVMs [82,199,218]. The LSVR depends on the kernel function. Therefore, it is considered a nonparametric technique. The LSVR mainly focused on estimating a functional relationship of the random variable between input and output under the assumptions. The assumption is that the input and output variable of joint distribution is entirely unknown. The outcomes of the linear support regression model have shown in Fig. 6.8.

125

The general approach behind the LSVR is to analyze the best fit line. The best fit line means there is a hyperplane on which the maximum number of points lies. The regression algorithm helps to reduce the deviation between the actual value and the predicted value.

The LSVR evaluation can be formalized as a function of y [219]:

$$y = f(x) \tag{6.5}$$

depend on the training dataset $= [(x_i, d_i), i = 1, 2, \dots \dots n]$,

where, $x_i \in R^n$: i$^{\text{th}}$ input vector for the training dataset,

$x_i \in R$: Target value for the i$^{\text{th}}$ training dataset,

n : number of the training set.

The training LSVR model corresponds to obtaining a regression function:

$$f(x) = \sum_{i=1}^{n}(\varphi_i - \varphi_i^*)k(x_i, x) + b \tag{6.6}$$

where, $G(x_i, x)$: positive definite kernel function,

$\varphi: (\varphi_1, \varphi_2, \dots \dots \varphi_n)^T$
$\varphi: (\varphi_1^*, \varphi_2^*, \dots \dots \varphi_n^*)^T$
b: model parameter
ε: epsilon margin

To obtain the expression, construct a Lagrangian function by establishing a non-negative multiplier φ_n and φ_n^* for each observation x_n. This leads to expression, which requires minimizing the objective function.

$$L(\varphi) = \frac{1}{2}\sum_{i=1}^{n}\sum_{j=1}^{n}(\varphi_i - \varphi_i^*)(\varphi_j - \varphi_j^*)x_i' x_j + \varepsilon \sum_{i=1}^{n}(\varphi_i +$$
$$\varphi_i^*) + \sum_{i=1}^{n} y_i(\varphi_i^* - \varphi_i) \tag{6.7}$$

Subject to,
$$\sum_{i=1}^{n}(\varphi_i - \varphi_i^*) = 0 \text{ and } \varphi_I, \varphi_I^* \in [0, C] \tag{6.8}$$

where, ε and C is hyperparameters.

According to the above concept of support vector (SV), the simplified function of the SVR is as follows:

$$f(x) = \sum_{i=1}^{n} (\varphi_i - \varphi_i^*) G(x_i, x) + b \tag{6.9}$$

where, $G(x_i, x)$ is kernel function, so for LSVR, $G(x_i, x) = x_i', x_j$.
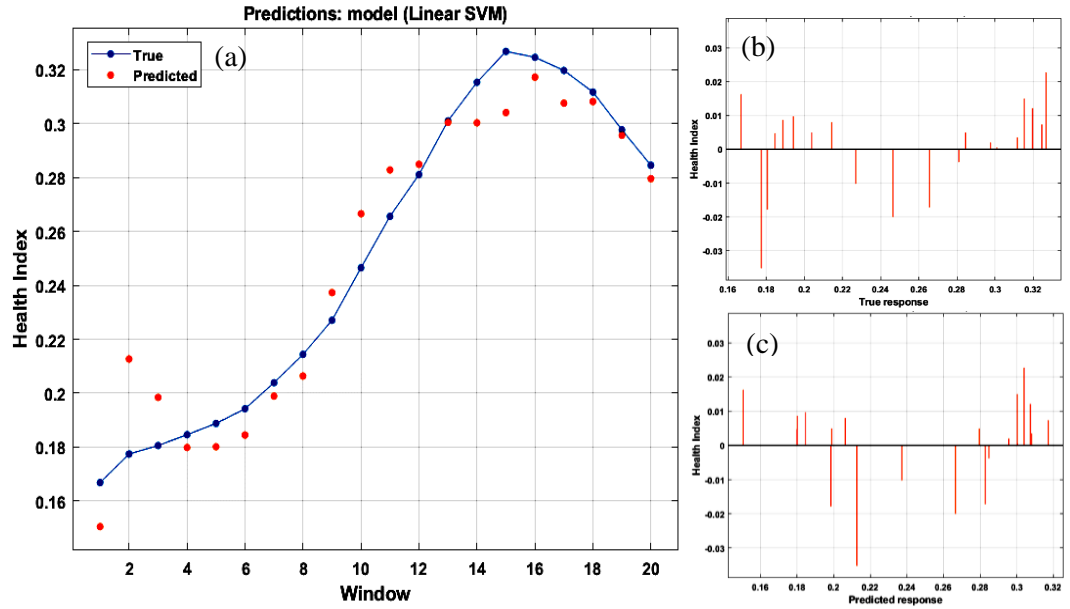
Figure 6.8 (a) Linear support vector regression prediction model, (b) residual of true response, and (c) predictive response

6.3.2 Quadratic support vector regression

The quadratic support vector regression (QSVR) is also called a quadratic kernel-free non-linear support vector regression machine [200]. The quadratic regression function can separate both linear and non-linear data [200]. The optimization problem for quadratic support vector regression is similar to the linearly separable data (dual form). The QSVR optimization contains two forms: the first is associated with the linear segment of the quadratic function, and the next is associated with the non-linear quadratic function. For the quadratic optimization problem, Eq. 6.7 and Eq. 6.8 can be used to solve for the two parameters [197]. Fig. 6.9 shows the outcomes of the quadratic support vector regression.
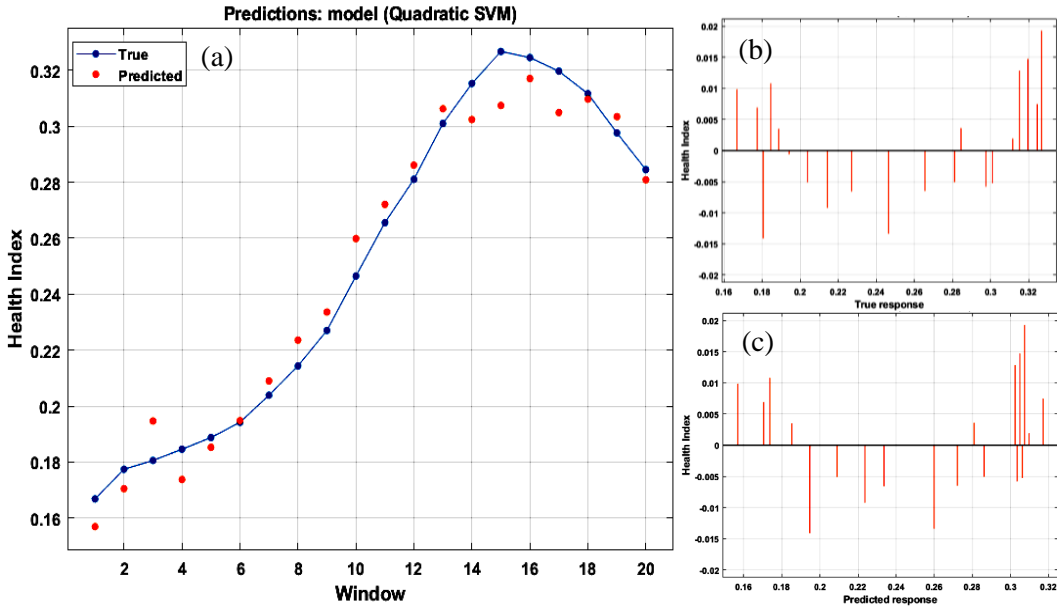
Figure 6.9 (a) Quadratic support vector regression prediction model, (b) residual of true response, and (c) predictive response

6.3.3 Exponential degradation model

In the exponential degradation model (EDM), a dynamometer-based signals feature measures the occurrence of the degradation behavior of an endodontic instrument [220]. The residual life of a partially degraded instrument can be estimated statistically through the health indicator. The degradation frameworks operating in the field inform the residual life up to the degradation threshold of the endodontic instruments. For characterizing the assessment of the degradation signal, exponential degradation modeling is used [221–224]. The EDM is employed to model an exponential degradation process for estimating the health of the endodontic instruments, as shown in Fig. 6.10.

The health degradation of the instrument can mathematically be expressed as [220,221]:

$$H(t) = \alpha' + \theta' \exp\left(\beta't + \epsilon' - \frac{\sigma^2}{2}\right) \qquad (6.10)$$

where $H(t)$ is a health indicator,

α' is the intercept term considered as a constant,

θ' and β' are random parameters. θ' and β' are lognormal-distributed and Gaussian-distributed, respectively.

On every step t, the distribution of θ and β is updated to the subsequent based on the latest observation of $H(t)$.

ϵ' is a gaussian noise yielding to $N(0, \sigma^2)$.

The exponential degradation model can be expressed as [220]:

$$E[H(t)_{\theta,\beta}] = \alpha' + \beta' \exp(\beta't) \tag{6.11}$$

Here is a health index $[H(t)_{\theta,\beta}]$ that is extracted from the feature extraction model is fitted to the exponential degradation model.

For the EDM, the model primarily has confidence in the observed data. Therefore, the slope parameters are chosen arbitrarily with significant variance [220]:

$$E(\theta) = 1, Var(\theta) = 10^6, E(\beta') = 1, Var(\beta') = 10^6 \tag{6.12}$$

The α' is set to be '-1' because the model depends on the observed data; therefore, here, we set the value of α so that the model will start from zero [220,221],

$$E[H(0)] = \alpha' + E(\theta) \tag{6.13}$$

Degradation models evaluate health conditions by predicting when a health index will cross a threshold as an expression given in Eq. 6.14 and Eq. 6.15 [225]. Thus, the association between the variation of noise and the variation of health index can be obtained as:

$$\Delta H(t) \approx [H(t) - \alpha'\nabla \in (t)] \tag{6.14}$$

The standard deviation of the noise is supposed to affect 10% of the adaptation of the health index. Thus, the standard deviation of the signal can be expressed as:

$$\frac{10\%.threshold}{(threshold - \alpha)} \tag{6.15}$$
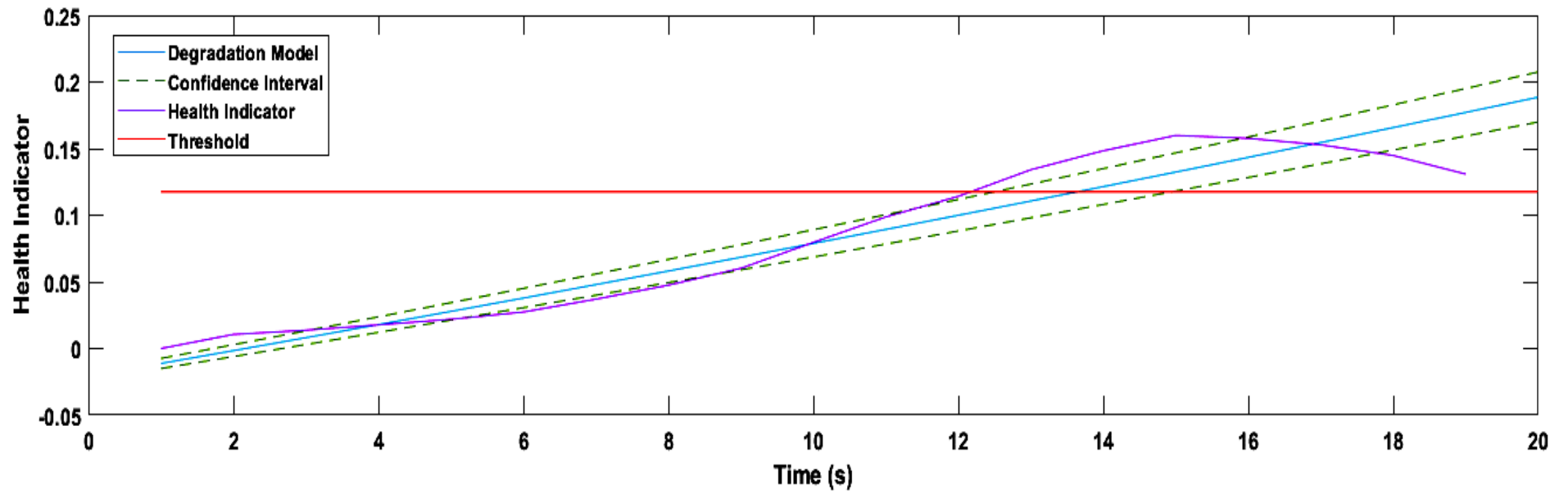
Figure 6.10 Exponential degradation model trajectory of the endodontic instrument

The EDM model additionally presents a functionality to estimate the importance of the slope. When a significant slope of the health index is identified, the EDM model will not recall the earlier interpretation and resume the assessment on the original observations. The slope can only be acknowledged if the p-value is smaller than the confidence interval. So, here 0.05 is set to be a confidence interval.

6.4 Discussion

Few authors worked for the endodontic instruments in RCT mechanics, endodontics, and dentistry [66,76,160,161,226–228]. This study implements a novel approach that helps the practitioner to understand the health condition and fault prognosis of the endodontic instrument based on machine learning models. It can assist in preventing endodontic instrument failure while performing the RCT.

The biomechanical procedure of the root canal system is a crucial step of RCT. The opening of access, preparation of the canal (shaping and cleaning), and obturation are the three major steps in the RCT process [37]. These steps are significant for the accomplishment of root canal procedures. Due to the limitation of in-vitro experimentation, we have used only two steps, the opening of access and the canal preparation in this study. The endodontic file removes inflamed and infected dentin tissue during shaping and cleaning. While disinfecting the infected and inflamed dentin, endodontic files may sometimes stick between the root canal, resulting in file failure, as exhibited in Fig. 6.4 (c). The machine learning model has been employed to monitor the health of the endodontic instrument.

The SVR algorithm is used in this study. The LSVR and QSVR are evaluated to optimize the best algorithm and proportional outcomes mentioned in Table 6.1. This table compared the outcomes in terms of the following parameter, i.e., R-squared (R^2), mean absolute error (MAE), and root mean squared error (RMSE). Through these models, the optimum results are obtained from the quadratic regression. The maximum R^2 value of 0.98 was obtained from the QSVR, and the

observed points are strongly suited to the regression line, as shown in Fig. 6.11. The regression algorithm provides the relationship between the true and predicted responses. The regression model showed the goodness of fit and data fitting through the regression line. Root mean squared error (RMSE) [229] and mean absolute error (MAE) are used to analyze the accuracy, performance, and effectiveness of the prediction outcomes [222]. The RMSE [229] and MAE [222] are employed as assessment indexes for the estimation outcome of the two models. Based on these two indexes, RMSE and MAE can be calculated from the following expression [222,230]:

$$RMSE = \sqrt{\frac{1}{n'}\sum_{i=1}^{n'}(x_i - x_i^*)^2} \qquad (6.16)$$

$$MAE = \frac{1}{n'}\sum_{i=1}^{n}\frac{|x_i - x_i^*|}{n'} \times 100\% \qquad (6.17)$$

where x_i and x_i^* are the observed value and predicted, n' is the number of samples.

Table 6.1 Comparison between the models

Machine learning model	R^2	RMSE	MAE
LSVR	0.95	0.014	0.011
QSVR	0.98	0.005	0.008

Fig 6.8 shows the regression curve of the signals using the LSVR model. A linear kernel function is used to execute the algorithm. Additionally, Fig. 6.8 illustrates the residual of the true response and the predictive response graph. The QSVR obtained the maximum regression value compared to the LSVR, and quadratic regression data are closely fitted to the regression line, as shown in Fig. 6.9. The quadratic kernel function is employed for quadratic regression. In terms of the root means squared error (RMSE) in LSVR and QSVR, quadratic regression gives better precision than linear regression, as discussed in Table 6.1. Therefore,

the QSVR model is implemented to investigate the health degradation of endodontic instruments.
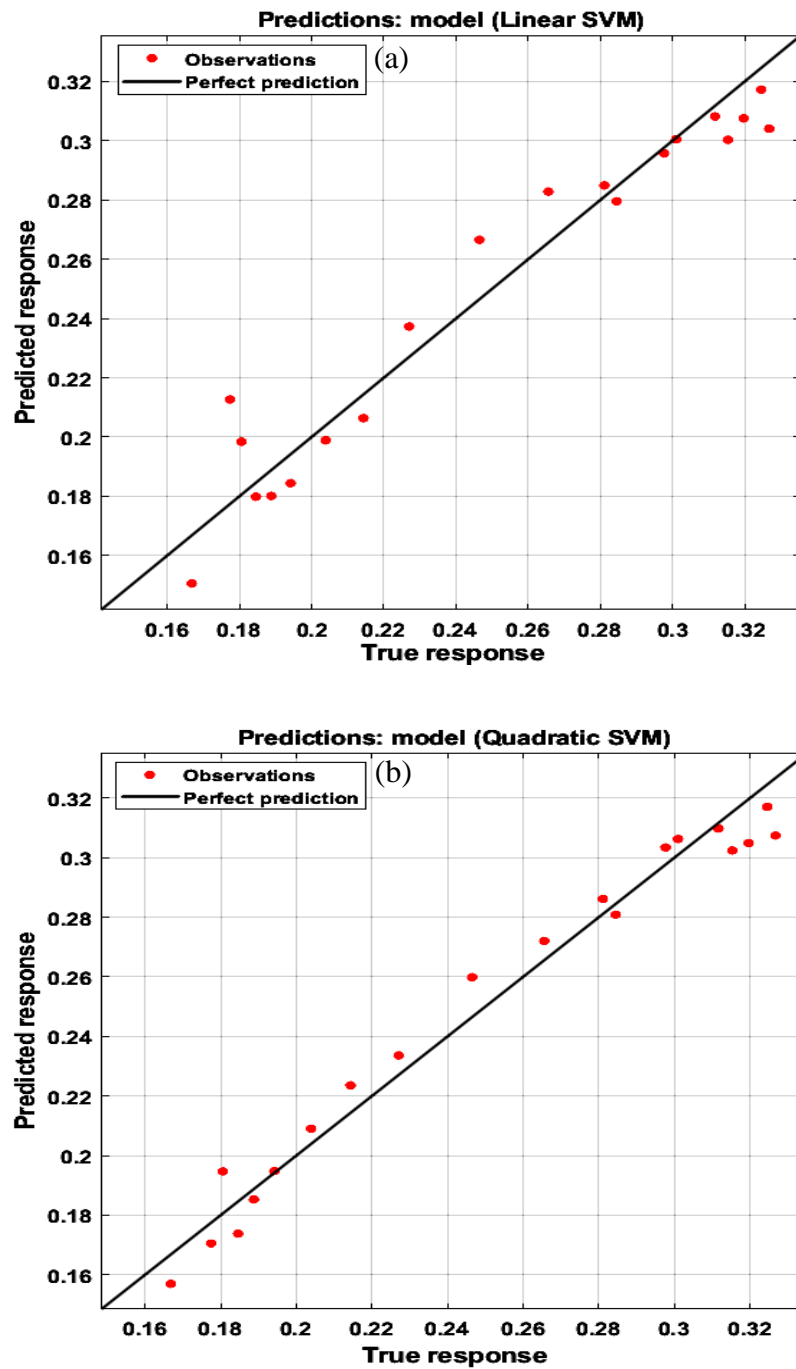
Figure 6.11 Support vector regression model (a) LSVR and (b) QSVR

The exponential degradation model curve reveals the degradation of endodontic instruments concerning the health index, as shown in Fig. 6.10. The threshold value obtained is approximately 12 to 12.5 seconds. After that, the health index increases due to the deterioration of the

endodontic instrument. The obtained model is perfectly fitted within the confidence interval, as shown in Fig. 6.10. Generally, the dental practitioner took a few seconds to complete the root canal preparation. According to the American Association of Endodontists [231], utilizing the continuous rotation motion instrument takes 46.42 ± 18.12 seconds, whereas the reciprocating motion instrument takes 21.15 ± 6.70 seconds to complete the RCT [231]. Endodontic instrument does not wear enough during the canal preparation because of the simulated periodontal ligament of the oral cavity in an in-vitro study. Due to that, the deformation occurs in wider mid-file lands and narrow lands of the tip region. Simultaneously, heat initiation is started. Heat dissipation occurs in the endodontic instruments while performing the RCT [39,40], resulting in micro-fracture and instrument failure [138,141,143,232].

6.5 Conclusions

The root canal is shaped and cleaned in this study through the WOG reciprocating endodontic instrument. The influence of the force signal on healthy, moderate, and faulty files has been investigated. The successive inferences are taken from the current study:

- The reciprocating WOG endodontic faulty instrument significantly generated a higher force amplitude with respect to time than the healthy and moderate endodontic file.
- The force signal shows the excellent performance capabilities of the QSVR algorithm statistically compared to the LSVR with the help of kernels, i.e., quadratic and linear, respectively.
- The exponential degradation model accomplished the reliability and degradation characteristics of the endodontic instrument with sensory signals. The computed stochastic parameter acquired the information and comprehensively characterized the state of degradation of endodontic instruments. This state further evolves in the future health condition of the endodontic file.
- In most cases, fracture or failure of the instrument happens due to repeated use. The flexural fracture occurred due to repeated

tension and compression in the curved root canal, and torsional failure occurred due to the twisting of the file through its longitudinal axis while the file was stuck in the canal at one end in the curved root canal.

Chapter 7

Prediction of apical extent using ensemble machine learning techniques

This chapter aims to evaluate the dimensions of the apical extent following preflaring with primary treatment and retreatment on human extracted teeth under endodontic therapy using ensemble machine learning techniques. The nickel-titanium (NiTi) endodontic instruments are used for the root canal's biomechanical preparation. Inadequate biomechanical RCT procedure frequently leads to post-operative apical periodontitis. This results in severe gum inflammation that harms the soft tissues, if left untreated, may harm the bones of the root canals supporting teeth. Therefore, the dimension of the apical extent has been analyzed to obtain the proper RCT instrumentation and endodontic treatment. For this chapter, digital intraoral radiographic images have been recorded with the help of the Kodak Carestream Dental RVG sensor (RVG 5200). The RVG sensor is directly coupled with the CS imaging software (Carestream Dental LLC, NY) to acquire radiographs. Furthermore, the recorded images have been used to measure the dimensions of apical length. The ensemble classifiers are used in this chapter to classify the apical condition, such as apical extent, beyond the apical, and up to apical or perfect RCT, respectively. The ensemble bagged, boosted, and RUSboosted trees classifiers are used in this analysis. The maximum accuracy obtained through the ensemble bagged trees model is 94.2 %, the highest among the models. The machine learning approaches can improve the treatment practice, improve RCT results, and provide a suitable decision support system.

7.1 Introduction

The RCT is recommended when a bacterial infection has harmed the pulp [136]. It has been deemed essential to estimate the apical dimension using an endodontic instrument to provide an adequate root canal during RCT [74,137,141]. Therefore, the measurement of the apical extension has been investigated in this work to achieve the appropriate RCT procedure.

The technology has been employed in earlier studies in several areas of endodontics and dentistry research to assess dimensions of the epical extent. Few works dealt with the apical size, and some studies discussed the dimensions of a root canal. Ibelli et al. [45] measured the maxillary lateral incisors' apical size as an effect of cervical preflaring. Anatomically significant differences were observed in the apical dimension. Additionally, they showed that the correlation between anatomical data and file dimensions was accurate. Gesi et al. [233] investigated the apical extent dimension following the preflaring. The dimensions of the apical were established electronically using the largest instrument. The Mann-Whitney U test was employed to observe the distinction between the treatment group. The root canal's apical region seemed to have a larger diameter when there was periapical radiolucency. It includes checking each attribute to ensure that such tools are of appropriate sizes for successful canal operation. Kumar et al. [234] examined the influence of the apical dimension on vertical root failure. The authors used the lateral compaction technique to prepare the root canal using the rotary nickel-titanium (NiTi) or nitinol alloy instrument. The radiographic apex was used to acquire the apical root filling. Hung et al. [79] worked on root caries for diagnostic prediction using machine learning. The authors developed the support vector machine model to observe the best performance. Artificial intelligence applications were developed for the diagnosis of treatment, decision-making, and prediction [77,191].

The approach of dimension analysis of apical extension has been established in this chapter. This work used the digital radiographic sensor for image scanning, whereas CS imaging software is used for image acquisition and dimensional measurement. The ensemble machine learning technique has been employed to classify the apical condition of the root canal. This work helps to analyze the apical extent measurement after preflaring the root canal through endodontic treatment. The methodology and materials are briefly explained, which includes the sample preparation, biomechanical preparation, and root canal treatment. The principle and procedure of the digital radiograph through the RVG sensor are explained. This chapter also discussed the perfect filled, underfilled, and overfilled classes of the RCT-treated teeth, which have been examined for the current research. The measured apical dimension of the canal has been used as input for the machine-learning technique. The ensemble learning classifiers, such as bagged, boosted, and RUSboosted trees, are employed to predict the apical extension following the RCT. This chapter concludes that the maximum accuracy and performance are obtained in the ensemble bagged trees classifier compared to the boosted and RUSboosted classifier.

7.2 Material and methodology

7.2.1 Sample preparation

Three hundred human-extracted teeth were obtained from the College of Dental Science and Hospital Rau, Indore, India. Out of these, one hundred seventy-one human extracted teeth have been chosen for the biomechanical preparation. The hospital provided the extracted teeth contaminated with bacteria and germs. In this stage, extracted teeth require a cleaning process. Thus, before sample preparation, kept these teeth in hydrogen peroxide for a week to properly eliminate the bacteria from the surface. As mentioned in chapter four, the manual sample preparation method is also used in this chapter, as shown in the updated procedure in Fig. 7.1. After being kept for a week, clean each tooth again. After that, use the cold setting powder and liquid material to make

the cold mounting. Once dried, remove the mould and get the final produced tooth sample.
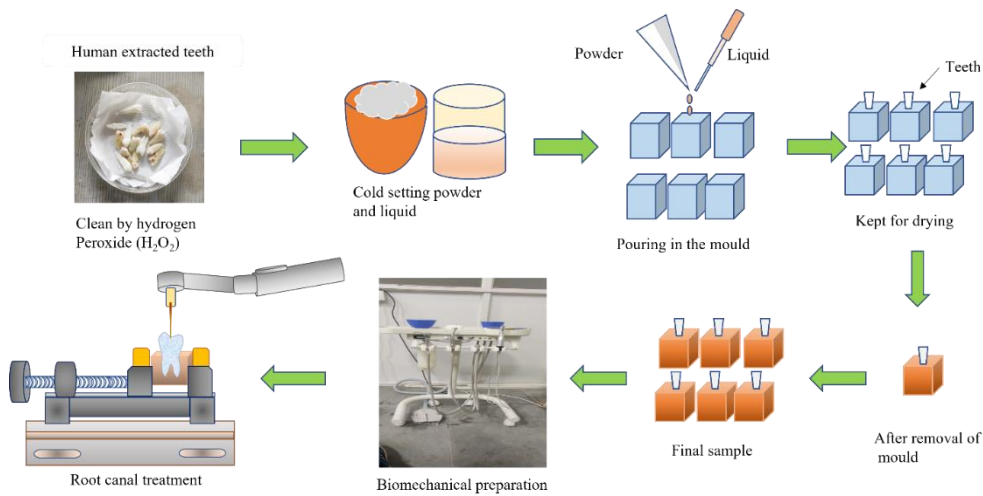
Figure 7.1 Methodology for the sample selection and preparation

For collecting the human-extracted teeth, the individual from whom the teeth samples had been collected were free from other diseases or systemic conditions. In the current research work, the following inclusion criteria was used:

- No previous treatment: any prior endodontic procedures, such as root canal therapy or apicoectomy, have not been performed on the extracted tooth because they can alter its morphology and functional characteristics.
- Posterior teeth were preferred: the back teeth, including the premolars and molars, are referred to as posterior teeth.
- No restoration: after extraction, restorations like fillings or crowns should not change the anatomy and characteristics of the tooth.
- Initial carries teeth were carefully chosen with good root morphology.
- Extracted teeth with more than one root canal or multiple root canal teeth were preferred.

- While teeth from various age groups may have various features and characteristics, the age of the tooth donors may also be an important consideration. Thus, the donor age considered in this study was in between 21 to 50 years.

7.2.2 Biomechanical preparation (BMP)

Following the teeth samples' preparation, the biomechanical preparation process begins to locate the root canals. An airotor is used to commence the canal preparation. The airotor provides the initial ditch to the tooth's enamel rotating at a very high speed. Since the enamel is the hardest part of the body, it requires the optimum ditching speed using pneumatic pressure. Preliminary, the round diamond burr and the straight diamond burr (Prime Dental Product Pvt. Ltd.) are used to open the access. Simultaneously, water injection and irrigation are provided continuously throughout the root canal preparation with the help of a three-way syringe [5,151,235]. The biomechanical preparation process includes irrigation, which aids in eliminating necrotic tissue when finding and cleaning the root canal [5,111,151]. The hand-driven endodontic file system and micromotor were employed to observe the root canal in the teeth sample. To make the canals lengthen, more uniformly shaped and enlarge them using a series of hand-driven endodontic files. Once the root canal is identified, endodontic treatment can then begin. The proposed approach predicts the apical extent during endodontic treatment using a machine learning technique, as shown in Fig. 7.2.
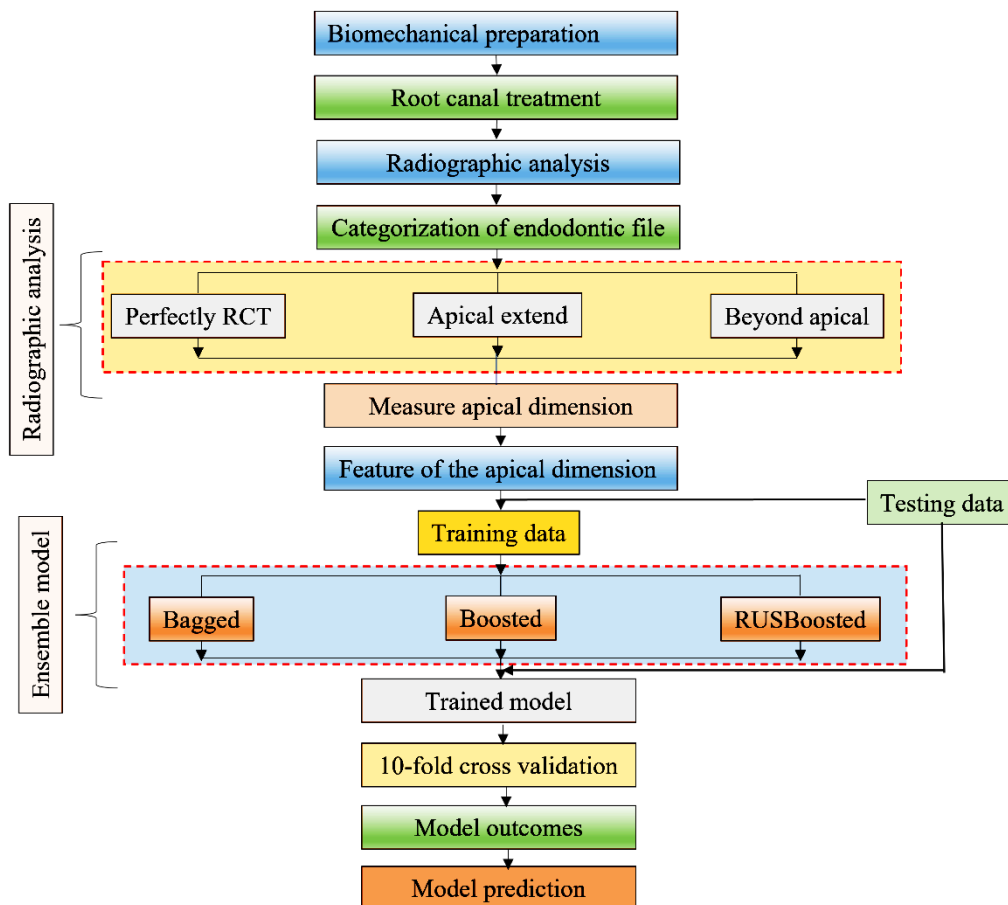
Figure 7.2 Proposed methodology of analysis of apical extent dimension

7.2.3 Root canal treatment (RCT)

Once the root canal has been found from the mounted sample, the RCT process can begin after biomechanical preparation is done. Through RCT, the infected and inflamed pulp is removed with the help of an endodontic instrument. The flat top of the tooth, known as the crown, is opened using an endodontic file to gain access to the soft tissue inside (i.e., pulp) and eliminate any leftover infected debris [7]. The X-smart plus endo-motor (Dentsply, Maillefer, Switzerland) and the motor-driven endodontic file are used for shaping and cleaning during the RCT. Following the pulp removal, the root canal is cleaned and lengthened, so filling it might be achievable [48,236]. The duration of the procedure increases with the number of roots a tooth possesses. Root canal therapy is an effective treatment for preserving the tooth and curing the infection.

7.3 Digital radiographic analysis

The digital radiograph has been taken from the Kodak Carestream Dental RVG 5200 Sensor, which is very sophisticated, sensitive, and reliable. This sensor is used for medical imaging and dentistry for digital radiographs [237], as shown in Fig. 7.3. In 1987, the French dentist Dr. Francis Mayen invented digital radiography for medical imaging. Various adjustments are made, and current concepts are being established for its application due to this digital technology's effectiveness. RadioVisioGraphy is another name for digital radiography, and this procedure employs an RVG sensor [238,239]. In dentistry, this technology is utilized in place of x-ray radiography [238]. The sensor provides higher photos attributable to the cooperation of a high-sensitivity scintillator, fiber optics, and high-resolution rugged CMOS (complementary metal-oxide semiconductor) sensor. The Kodak Carestream Dental provides two sides of the RVG sensor, one side provides the sensor, and another gives the cable connector. The X-ray radiation is used to expose the endodontic treated sample for examination, and then the sensor records the light that has been refracted. The recorded photograph is immediately processed and transformed into digital data through analog-to-digital converters using CS imaging software (Carestream Dental). The dedicated laptop receives the digital data and enables reviewing of the images immediately.

7.3.1 Perfect RCT

Analyze the obtained digital radiograph in this step. In a perfect RCT or perfect filled category, the apical region of the endodontic file is filled to the apical portion. The endodontic procedure is completed without any inaccuracies.
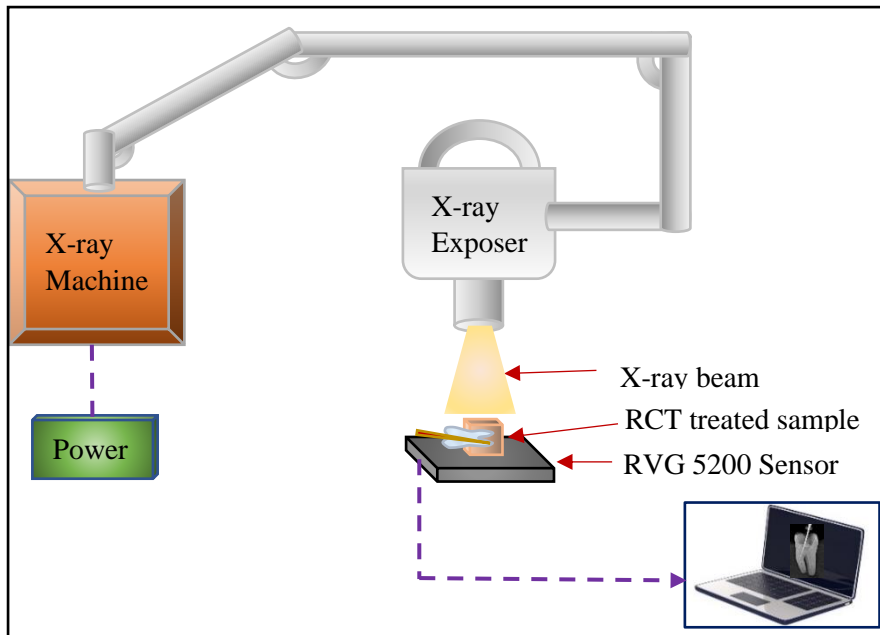
Figure 7.3 Schematic diagram of digital radiographic analysis

7.3.2 Apical extent

The effects of the post-RCT process appear to be most significant at the apical level. In this condition, the endodontic file suffered too short of the radiographic apex, and the file did not reach out to the root canal apical section. The underfilling happens due to the canal blockages inside the root canal, which is visible as an outcome.

7.3.3 Beyond apical

The endodontic instrument reaches beyond the apical portion of the apical root canal; this situation is overfilled or beyond the apical. Sometimes, the endodontic file proceeds beyond the root canal due to excessive force during the endodontic treatment. The treatment becomes overfilled.

7.4 Results

7.4.1 Apical dimension measurement

The dimensional analysis of apical extent has been carried out following the endodontic treatment and retreatment. Through the RVG sensor,

images have proceeded with the help of CS Imaging software (Carestream Dental LLC, NY). During the radiograph acquisition, there is a time limit for the x-ray exposing the treated sample. Depending on the objects and scanning equipment, the optimum exposure times for digital scanning ranged from 0.02 to 0.13 seconds [240,241]. This analysis utilized the 0.09 seconds as an x-ray expose time for exposing and scanning the tooth. This is the optimal exposure time for object observations and sensing equipment. The high-resolution radiograph with proper sharpness is achieved through the optimal parameters, as shown in Figs. 7.4 and 7.5. The digital images must be adjusted by altering the contrast and brightness through the CS Imaging software to maximize the visibility of measurement areas.

7.4.1.1 Radiographic images before the dimensional measurement

The digital images are categorized into three categories after visualization: perfect RCT images, apical extension images, and beyond the apical images, respectively, as shown in Fig. 4. From the total of one hundred sixty-four endodontic RCT-treated teeth sample images, each category is analyzed, such as perfect RCT images ($n = 50$), apical extension images ($n = 88$), and beyond the apical ($n = 26$), respectively. In perfect RCT images, most endodontic files are penetrated up to the apex, as shown in Fig. 7.4 (a). However, Fig. 7.4 (b) shows the apical extension, where the endodontic file could not reach the apex position. In another case, the endodontic file penetrated beyond the apical length during the endodontic treatment, as shown in Fig. 7.4 (c).

7.4.1.2 Radiographic images after the dimensional measurement

After measuring the dimension of apical extension from the endodontic-treated root canals, digital radiographs are analyzed for all three categories, as shown in Fig. 7.5. The blue colour box denoted the zoomed images of the root canal after the cleaning and shaping, as shown in Fig. 7.5 (a-c). The green colour line represents the measured dimension of the canal in Fig. 7.5 (b-c), whereas Fig. 7.5 (a) shows only

the apex position of the endodontic file. The perfect RCT has been observed in Fig. 7.5 (a) because the root canal is entirely clean and shaped. The perfect apical length is observed when performing RCT in a straight root canal. In Fig. 7.5 (b), the RCT-treated image demonstrated the apical extent. It happened because of the chance of canal blockage in the presence of debris, dead tissue, the complexity of the root canal and complex canal anatomy, etc. Beyond the apical or overfilled endodontic treated radiographic image is shown in Fig. 7.5 (c). The endodontic tool penetrated beyond the apical length due to the improperly executed RCT or the access load applied to the instrument during the RCT. Measurement of the apical dimension during RCT with the following condition: perfect RCT, apical extent, and beyond the apical has been evaluated through the measured data, as shown in Fig. 7.6.
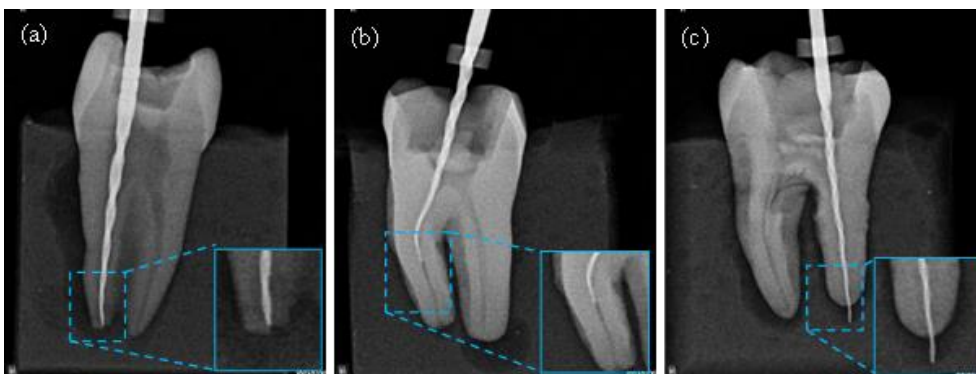
Figure 7.4 Radiographic images analysis before the dimensional measurement (a) perfect RCT, (b) apical extent, and (c) beyond apical
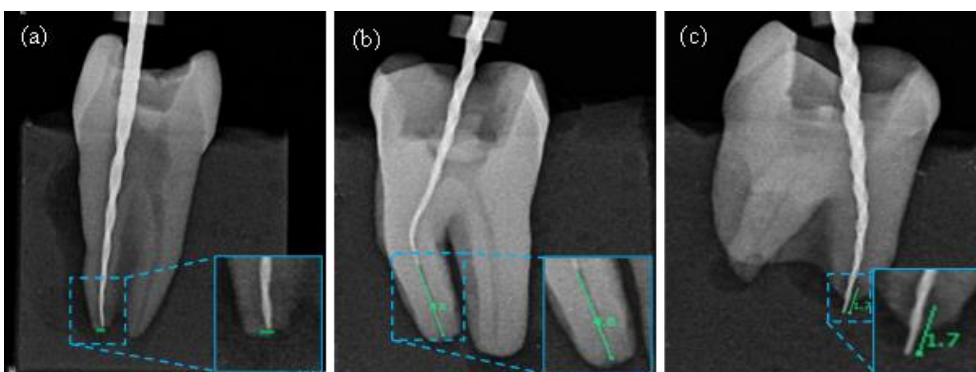
Figure 7.5 Radiographic images analysis after the dimensional measurement (a) perfect RCT, (b) apical extent, and (c) beyond apical
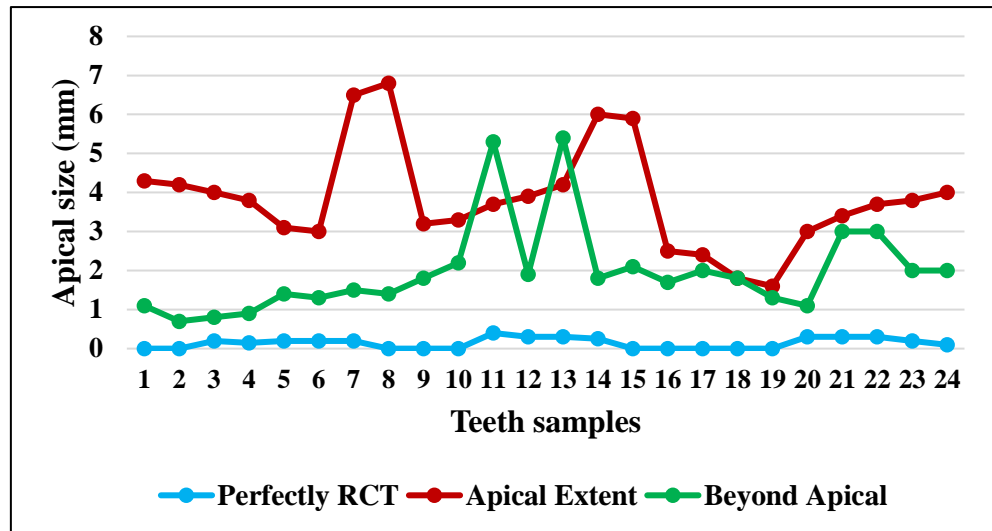
Figure 7.6 Apical dimensional measurement during RCT with the following condition: perfect RCT, apical extent, and beyond the apical

7.4.2 Performance of the ensemble models

The ensemble machine learning technique has been implemented in this study to classify the apical extension of the root canal during the RCT. The ensemble techniques combine multiple base models to create a single optimum predictive model. When using this learning technique, many different models are considered and averaged to create a final model. Analyze the optimum model accuracy with their performance through these ML approaches. This approach uses ensemble machine learning such as ensemble bagged trees, boosted trees, and RUSboosted trees.

7.4.2.1 Ensemble bagged trees

Bootstrap Aggregation, often recognized as Bagging, is also commonly referred to as ensemble learning because it establishes a model by combining Bootstrapping and Aggregation. Bagged trees are a well-known machine-learning approach that significantly boosts the prediction power of a single decision tree [242]. A key concept behind bagged trees is that they rely on various decision trees instead of one, which enables them to take advantage of the expertise of multiple models.

147

7.4.2.2 Ensemble boosted trees

Like the bagged trees, a collection of decision trees is combined with the boosting ensemble approach to produce boosted trees. Boosted trees correct mistakes made by earlier decision trees. The errors of trees from earlier rounds are considered while creating new trees. Consequently, new trees are produced following one another. Every tree depends on the one before it. Sequential learning is the name given to this sort of learning approach.

7.4.2.3 Ensemble RUSboosted trees

Random Under Sampling is referred to as RUS. The RUSBoosted is adept at recognizing unbalanced data and indicating that a training data class contains fewer entries than another. In contrast to individual trees, distributed training data are integrated into a robust classifier and repeatedly run-on base learners.

The confusion matrix shows that the training accuracy of the ensemble machine learning models is exceptionally good than the testing dataset, as shown in Fig. 7.7 and 7.8. The classifier successfully detects the model's positive class and true positive rate. The observed accuracy of the training model, such as ensemble bagged trees, boosted trees, and RUSboosted trees, are 94.2%, 91.7%, and 90.8%, respectively. Whereas the testing accuracies of the models are 88.2%, 90.2%, and 90.2%, respectively, as shown in Table 7.1. The performance of the models includes the precision, sensitivity, specificity, accuracy, and F1 score, respectively.
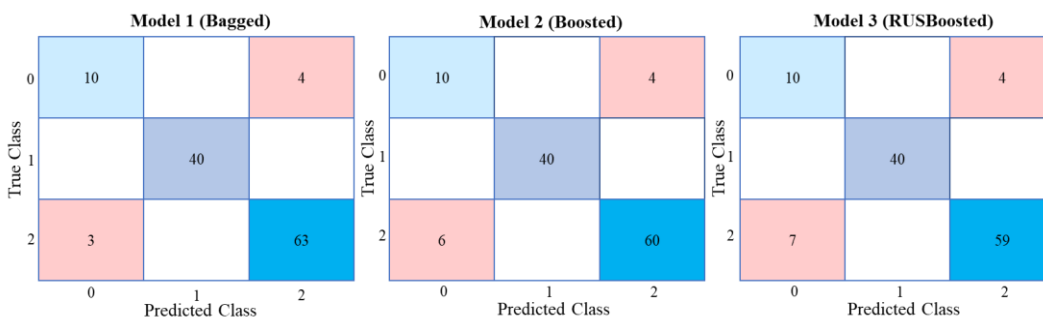
Figure 7.7 Confusion matrix of training data with their ensemble learning models
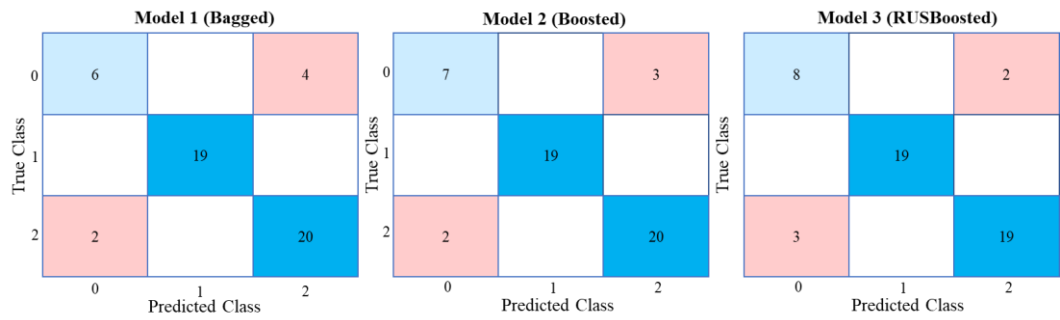
Figure 7.8 Confusion matrix of testing data with their ensemble learning models

Table 7.1 Performance evaluations of the ensemble machine learning models

Performance	Bagged tree		Boosted tree		RUS boosted	
	Train	Test	Train	Test	Train	Test
Precision (%)	90.32	86.11	85.41	88.24	84.15	87.73
Sensitivity (%)	88.96	83.63	87.44	86.97	86.94	88.78
Specificity (%)	96.85	93.77	95.64	94.92	95.33	95.26
Accuracy (%)	94.16	88.23	91.66	90.19	90.83	90.19
F1 score (%)	89.6	84.54	86.32	87.52	85.33	85.19

7.5 Discussion

In dentistry, machine learning (ML) may anticipate periapical illnesses, root canal failure, apical dimension, endodontic treatment, and retreatment procedures [66,76,77,79,82]. Several dental professionals believe that the primary intention of RCT is pulp removal and that dentine removal is superfluous [170]. It is a significant misperception that contributes to the high failure rate of RCTs [170]. Even after cleaning and shaping, it is impossible to be sure that all infectious dentine is removed. Consequently, removing the affected and inflammatory debris from the root canal is crucial. Otherwise, the endodontic file does not penetrate properly inside the root canal. Thereafter, the overfilled and underfilled endodontic treatments are

observed. The adequately filled, underfilled, and overfilled apical length dimensions are studied through the current work.

The Carestream Dental RVG 5200 sensor is used to acquire the radiographic images for the extent of apical dimensional analysis. The measurement data is post-processed through MATLAB software (MathWorks, U.S.). Fig. 7.9 and 7.10 represent the area under the curve (AUC) and receiver operating characteristic (ROC). This curve is used to estimate the accuracy of the model. The maximum and minimum AUC of the training datasets are 0.96 and 0.93, as shown in Fig. 7.9. The maximum and minimum AUC of the testing datasets are observed as 0.96 and 0.91, as shown in Fig. 7.10. Table 1 demonstrates the performance of the ensemble machine learning model, including the precision, sensitivity, specificity, and F1 score. The ensemble bagged trees model provides excellent results based on their outcomes. The bagged trees noticed the best accurate prediction model when analyzing the apical extension during the biomechanical preparation of the root canal.

Before figuring out the dimension of the apical extent, it's advised to preflare the mid and coronal parts of the canal. The margin of error in medical observations of the apical size cannot be eliminated, although it can be minimized [233]. In order to achieve appropriate apical section cleaning, a few of the works of literature have recommended that the root canal's apex section be extended three times higher than the initial files that clinically correlate to the working size [7,140,233,234,243]. Endodontic instruments are used more than the recommended size in straight root canals. It may be able to decrease the number of debris and germs still present in the section of the canal. Cleaner canals are produced in more significant apical lengths, which may help to enhance performance. Treatment failure may occur if canals are not cleaned, particularly near the apex [244]. The current work uses machine learning techniques to provide practitioners with appropriate clinical decision support systems for measuring the apical extent through biomechanical root canal preparation.
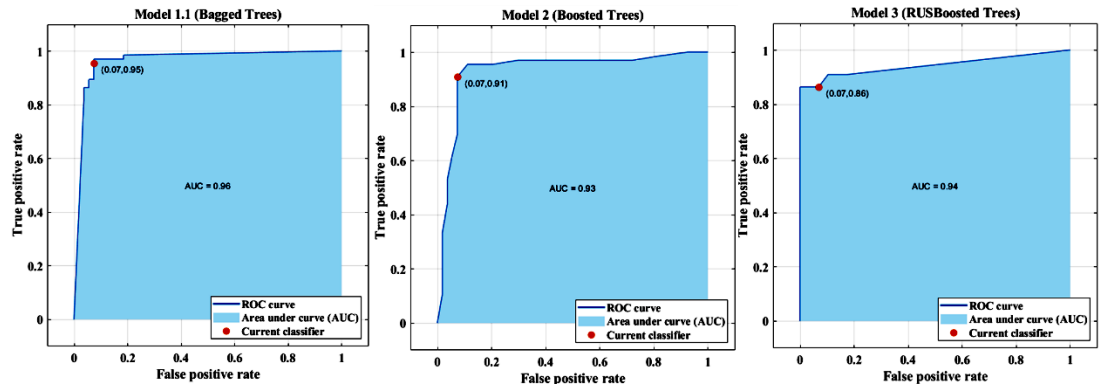
Figure 7.9 ROC and AUC performance curves of the training datasets
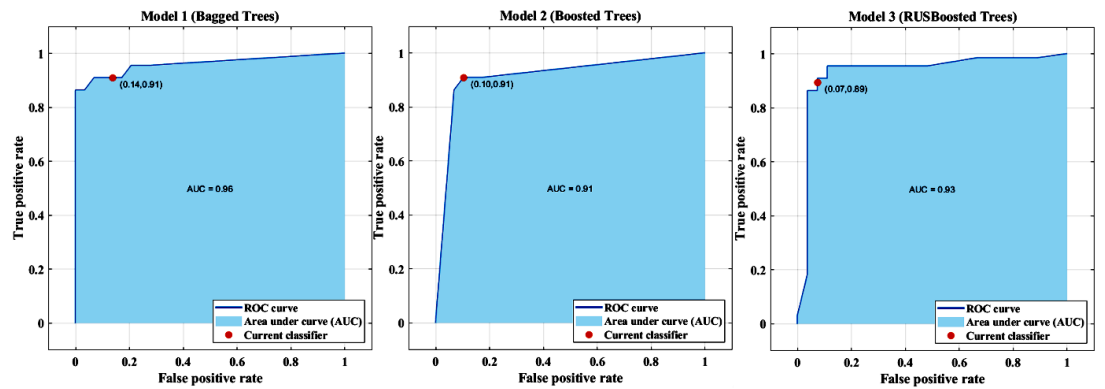
Figure 7.10 ROC and AUC performance curves of the testing datasets

7.6 Conclusions

In the current work, the dimensional analysis of apical extent on the root canal after primary treatment and retreatment on human extracted teeth during endodontic treatment has been studied using the machine learning technique. The apical extension measurement has been analyzed with the help of a radiographic examination. From this research, the following conclusions are drawn:

- The approach for analyzing digital radiography images worked incredibly well for determining the apical extent dimensions. Maintaining the post-preflaring using endodontic tools and examining the apical region of the root canals impact the degree of root canal curvature.

- Due to the root canal's anatomical foramen and anatomical variation, the dimension of the apical extension has been observed in the class of apical extent

151

- The maximum feature value is observed in the apical extent class. The minimum feature value is achieved in the perfect RCT or adequately filled endodontic-treated canal.

- According to the current investigation, ensemble bagged trees enhance the performance assessment of training and testing datasets compared to boosted trees and RUSboosted trees, with an accuracy of 94.2%.

The apical size of the root canal after the treatment is the measure concern while performing the RCT. This chapter offers an understanding of the radiographic analysis of the three different effects of post endodontic treatments. This research analyzes the root canal's apical extent following the endodontic treatment.

Chapter 8

Conclusions and scopes for future works

═══════════════════════════════════════

The research focuses on the endodontic instrument's force and vibration analysis during root canal treatment. Biomechanical preparation of human-extracted teeth, root canal cleaning, and shaping have been investigated in this research work. The significant contributions are highlighted, and the overall thesis research work is summarized in this chapter. Additionally, this chapter lists the research's potential continuation and future scope.

═══════════════════════════════════════

This thesis presents novel and innovative methodologies for force and vibration analysis of the endodontic file during the biomechanical preparation of RCT. Additionally, three-dimensional finite element analysis has been carried out to analyze the mechanical behaviour of endodontic instruments when penetrated inside the root canal. The tooth-file assembly has been modeled with the help of a micro-drilling approach to simulate the real-life condition of root canal preparation during RCT. Explicit dynamic simulations have been carried out in the computer-aided engineering package ANSYS for three different endodontic files: TwoShape (TS1 and TS2) and WaveOne Gold (WOG). The results obtained from the FEA modeling facilitate the accurate knowledge simulation and their respective contours. The outcomes revealed a significant difference in the deformation, equivalent elastic strain, equivalent stress of endodontic files, and tooth assembly.

The force and vibration analysis are carried out during RCT. Endodontic instruments for reciprocating and rotary motion have been used for root canal preparation. Force and vibration signals were recorded by dynamometer and accelerometer, respectively. In most cases, the failure occurred due to the improper use of the root canal instrumentation. The optimum force was used to avoid file failure and provide the proper

instrumentation. An endodontic instrument may sometimes fail for reasons beyond the dentist's control. A comprehensive assessment and decision support system for an endodontist may avoid several failures. This research proposes a machine learning and artificial intelligence-based approach that can help to diagnose instrument health.

An intelligent health prediction and fault prognosis of the endodontic file during RCT has been proposed using the recorded force signals. Characteristic features for endodontic file prognostics include time-domain features of the signals are evaluated. The health index is defined using denoised features to calculate the health condition of the endodontic instruments. A machine learning algorithm and exponential degradation model are used to predict the degradation of the endodontic file so that actions can be taken before actual failures happen. This approach can analyze the failure initiation of the endodontic instruments. To evaluate the dimensions of the apical extent after preflaring with the primary treatment and retreatment on human extracted teeth during endodontic treatment with the help of an ensemble of machine learning techniques. Utilizing the Dental RVG sensor, digital intraoral radiography images have been acquired. Additionally, the captured photos have been used to calculate apical dimensions. The measured apical dimension of the canal has been used for the machine learning technique to classify the apical condition, such as apical extent, beyond the apical, and up to apical or perfectly RCT.

8.1 Conclusions

The major conclusions from the present investigations are summarized as follows:

- The simulation outcomes show the value of maximum deformation in the TS1 endodontic file at the narrow lands of the tip region, wider mid-file lands, and shank region due to the flared root canal. The minimum von-Mises stress in WOG endodontic file is observed on the shank region and the point of

contact during RCT. The maximum von-Mises stress is observed in the TS1 endodontic file compared to the WOG and TS2 endodontic files. Thus, the root canal using TS2 and WOG endodontic files is more suitable in RCT than the TS1 endodontic file.

- The NiTi alloy-based endodontic instrument possesses superelastic behaviour. Because of the superelastic behaviour, the maximum equivalent elastic strain was obtained in the TS1 endodontic file at the narrow tip region and in the internal canal surface. It is observed when the endodontic file penetrates during the root canal preparation.

- In biomechanical preparation, it is observed that as the force increases, vibration amplitude increases significantly. The failure of endodontic files is caused by excessive vibration and force due to overloading in uneven morphology of the root canal.

- The importance of denoising is observed in the regression analysis as the denoised signals established a good association between force and vibration. The best R^2 values for WOG and TS endodontic files found for root mean square values with raw signals are 90.1% and 89.1%, respectively. In comparison, 92.25% and 89.85% for WOG and TS endodontic file association are established for the maximum values of the denoised signals.

- Endodontic file's health can be efficiently diagnosed by analyzing the force signals using QSVM, GNB, and FKNN with higher precision, sensitivity, and other performance parameters.

- The SMOTE algorithm, an oversampling approach with enhanced instances of minority classes, is found to balance the dataset so that the classification accuracy improves considerably. The study reveals that the ensemble bagged tree (EBT) and fine k-nearest neighbour (FKNN) enhances the performance of training and testing datasets compared to other methods. EBT and FKNN have shown 98.95% and 97.56%

accuracy, respectively.

- The current work uses machine learning techniques to diagnose the health condition of endodontic instruments, providing practitioners with adequate clinical decision support systems.

- The reciprocating WOG endodontic faulty instrument considerably produced a higher force amplitude with respect to time as compared to the healthy and moderate endodontic file. The force signal demonstrates the excellent performance capabilities of the QSVR algorithm compared to the LSVR with the help of kernels, i.e., quadratic and linear, respectively.

- The exponential degradation model accomplished the reliability and degradation characteristics of the endodontic instrument with sensory signals. The computed stochastic parameter acquired the information and comprehensively characterized the state of degradation of endodontic instruments. This model aids in predicting the future health condition of the endodontic file.

- The methodology for evaluating digital radiography images worked incredibly well for estimating the apical extent dimensions. Maintaining the post-preflaring using endodontic files and examining the apical region of the root canals impact the degree of root canal curvature. According to the current investigation, ensemble bagged trees enhance the performance assessment of training and testing datasets compared to boosted trees and RUSboosted trees, with an accuracy of 94.2%.

8.2 Scopes for the future works

The research and invention of a novel approach for force and vibrations signals-based endodontic treatment are described in this work. It can be expanded in certain aspects in facilitating decision-making for endodontic clinicians and dental health care. Establishing a system of clinical support will be beneficial. Additionally, this research can be beneficial for minimal invasive RCT treatment and improve the performance of the endodontic treatment.

156

- Development of the vibration characteristics model of endodontic instruments during RCT using the 3D- FEA analysis
- Develop the mechanical characteristic approach of endodontic instruments before and after the biomechanical preparation
- Similarity-based remaining useful life estimation can be utilized to analyze the health condition of the endodontic instruments during root canal preparation
- An artificial intelligence-based model can be developed to predict the endodontic instrument fracture and provide an indicator to avoid the facture of the instrument
- Development of the AI and ML-based model for faults diagnosis of the endodontic file during the RCT using current signals

References

[1]   J.R. Farley, Brief history of endodontics., Tex. Dent. J. 92 (1974) 9.

[2]   J.L. Gutmann, History of Endodontics, Ingle's Endod. 6th Ed. Philadelphia BC Decker Inc,. (2008) 36–85.

[3]   A. Castellucci, A Brief History of Endodontics, in: Italy Endod. Prato, 2004: pp. 2–5.

[4]   J.I. Ingle, Leif K. Bakland, Ingle's Endodontics 6, 2008.

[5]   A.G. Nisha Garg, Textbook of ENDODONTICS Third Edition, Third, Jaypee Brothers Medical Publishers (P) Ltd., Year: 2014, New Delhi, India, 2014.

[6]   L.I. Grossman, Endodontics 1776-1976: a bicentennial history against the background of general dentistry., J. Am. Dent. Assoc. 93   (1976)   78–87. https://doi.org/10.14219/jada.archive.1976.0606.

[7]   B.R.. Cohen S., Pathways of the Pulp, 6th edn., Mosby-Year Book, 1987. https://doi.org/10.1017/CBO9781107415324.004.

[8]   S. Kim, S. Kratchman, Modern Endodontic Surgery Concepts and Practice: A Review, J. Endod. 32 (2006) 601–623. https://doi.org/10.1016/j.joen.2005.12.010.

[9]   S.K. Singhrao, A. Harding, T. Simmons, S. Robinson, L. Kesavalu, S. Crean, Oral inflammation, tooth loss, risk factors, and association with progression of Alzheimer's disease, J. Alzheimer's   Dis.   42   (2014)   723–737. https://doi.org/10.3233/JAD-140387.

[10]   George T.-J. Huang, Dental pulp and dentin tissue engineering and regeneration: advancement and challenge, Front. Biosci. E3. (2011) 788–800.

[11]   S. Asgary, M. Fazlyab, S. Sabbagh, M.J. Eghbal, Outcomes of different vital pulp therapy techniques on symptomatic permanent teeth: A case series, Iran. Endod. J. 9 (2014) 295–300.

[12]   N. Akhlaghi, A. Khademi, Outcomes of vital pulp therapy in permanent teeth with different medicaments based on review of

the literature, Dent. Res. J. (Isfahan). 12 (2015) 406–417. https://doi.org/10.4103/1735-3327.166187.

[13] S. Gupta, S.P. Sodhi, G. Brar, R. Bansal, Endodontic treatment of immature tooth – a challenge, J. Pre-Clinical Clin. Res. 14 (2020) 73–79. https://doi.org/10.26444/jpccr/126280.

[14] A. Sujlana, P.K. Pannu, Direct pulp capping: A treatment option in primary teeth??, Pediatr. Dent. J. 27 (2017) 1–7. https://doi.org/10.1016/j.pdj.2016.10.001.

[15] S.C. Harlamb, Management of incompletely developed teeth requiring root canal treatment, Aust. Dent. J. 61 (2016) 95–106. https://doi.org/10.1111/adj.12401.

[16] J.I. Ingle, A standardized endodontic technique utilizing newly designed instruments and filling materials, Oral Surgery, Oral Med. Oral Pathol. 14 (1961) 83–91. https://doi.org/10.1016/0030-4220(61)90477-7.

[17] K. Gulabivala, Y.L. Ng, M. Gilbertson, I. Eames, The fluid mechanics of root canal irrigation, Physiol. Meas. 31 (2010). https://doi.org/10.1088/0967-3334/31/12/R01.

[18] C. Estrela, R. Holland, C.R. de Araújo Estrela, A.H.G. Alencar, M.D. Sousa-Neto, J.D. Pécora, Characterization of successful root canal treatment, Braz. Dent. J. 25 (2014) 3–11. https://doi.org/10.1590/0103-6440201302356.

[19] C.R. Glosson, R.H. Hailer, S.B. Dove, C.E. Rio, A Comparison of Root Canal Preparations Using Ni-Ti Hand, Ni-Ti Engine-Driven, and K-Flex Instruments, J. Endodonotics. 21 (1995) 146–151.

[20] D.M. Tucker, C.S. Wenckus, S.K. Bentkover, Canal wall planning by engine-driven nickel-titanium instruments, compared with stainless-steel hand instrumentation., J. Endod. 23 (1997) 170–173. https://doi.org/10.1016/S0099-2399(97)80269-5.

[21] Gary S P Cheung, C.S.Y. Liu, A Retrospective Study of Endodontic Treatment Outcome between Nickel-Titanium Rotary and Stainless Steel Hand Filing Techniques, J. Endod. 35

(2009) 938–943. https://doi.org/10.1016/j.joen.2009.04.016.

[22] P. Bansode, M.. Wavdhane, S. Pathak, S. Khedgikar, H. Rana, Evolution of Rotary NI-TI File Systems: A Literature Review Endodontic, Indian J. Appl. Res. 6 (2016) 91–94.

[23] S. Bhatia, V. Nagendrababu, O.A. Peters, A. Fawzy, U. Daood, Evaluation of usage-induced degradation of different endodontic file systems, Sci. Rep. 11 (2021) 1–10. https://doi.org/10.1038/s41598-021-88570-4.

[24] E. Schäfer, D. Lohmann, Efficiency of rotary nickel-titanium FlexMaster instruments compared with stainless steel hand K-Flexofile--Part 2. Cleaning effectiveness and instrumentation results in severely curved root canals of extracted teeth., Int. Endod. J. 35 (2002) 514–21. http://www.ncbi.nlm.nih.gov/pubmed/12190908.

[25] E. Schäfer, H. Florek, Efficiency of rotary nickel-titanium K3 instruments compared with stainless steel hand K-Flexofile. Part 1. Shaping ability in simulated curved canals, Int. Endod. J. 36 (2003) 199–207. https://doi.org/10.1046/j.1365-2591.2003.00643.x.

[26] M. Alrahabi, A. Alkady, Comparison of root canal apical transportation associated with Wave One , ProTaper Next , TF , and OneShape nickel – titanium instruments in curved canals of extracted teeth : A radiographic evaluation, Saudi J. Dent. Res. 8 (2017) 1–4. https://doi.org/10.1016/j.sjdr.2017.01.001.

[27] T. Lambrianidis, Ledging and blockage of root canals during canal preparation: causes, recognition, prevention, management, and outcomes, Endod. Top. 15 (2006) 56–74. https://doi.org/10.1111/j.1601-1546.2009.00235.x.

[28] A.K. Kakani, C. Veeramachaneni, C. Majeti, M. Tummala, L. Khiyani, A review on perforation repair materials, J. Clin. Diagnostic Res. 9 (2015) ZE09-ZE13. https://doi.org/10.7860/JCDR/2015/13854.6501.

[29] E.S. S. Bürklein, P. G. Jäger, Apical transportation and canal straightening with different continuously tapered rotary file

systems in severely curved root canals: F6 SkyTaper and OneShape vs Mtwo, Int. Endod. J. 50 (2017) 983–990. https://doi.org/10.1111/iej.12716.

[30] C. Zanesco, M.V.R. Só, S. Schmidt, V.R.C. Fontanella, R. Grazziotin-Soares, F.B. Barletta, Apical Transportation, Centering Ratio, and Volume Increase after Manual, Rotary, and Reciprocating Instrumentation in Curved Root Canals: Analysis by Micro-computed Tomographic and Digital Subtraction Radiography, J. Endod. 43 (2017) 486–490. https://doi.org/10.1016/j.joen.2016.11.006.

[31] M.J. Mahtabi, N. Shamsaei, M.R. Mitchell, Fatigue of Nitinol: The state-of-the-art and ongoing challenges, J. Mech. Behav. Biomed. Mater. 50 (2015) 228–254. https://doi.org/10.1016/j.jmbbm.2015.06.010.

[32] Dimitris C. Lagoudas, Shape Memory Alloys Modeling and Engineering Applications, Springer US, 2008. https://doi.org/10.1007/978-0-387-47685-8.

[33] S. Necchi, S. Taschieri, L. Petrini, F. Migliavacca, Mechanical behaviour of nickel-titanium rotary endodontic instruments in simulated clinical conditions: A computational study, Int. Endod. J. 41 (2008) 939–949. https://doi.org/10.1111/j.1365-2591.2008.01454.x.

[34] W.J. Buehler, J. V. Gilfrich, R.C. Wiley, Effect of Low-Temperature Phase Changes on the Mechanical Properties of Alloys near Composition TiNi, J. Appl. Phys. 34 (1963) 1475–1477. https://doi.org/10.1063/1.1729603.

[35] S. Tabassum, K. Zafar, F. Umer, Nickel-titanium rotary file systems: What's new?, Eur. Endod. J. 4 (2019) 111–117. https://doi.org/10.14744/eej.2019.80664.

[36] R. He, Modeling, analysis, and experimental investigation of root canal instrumentation process, PhD Theses, University of Michigan, 2007.

[37] M. Hulsmann, O.A. Peters, P.M.H. Dummer, Mechanical preparation of root canals: shaping goals, techniques and means,

Endod. Top. 10 (2005) 30–76. https://doi.org/10.1111/j.1601-1546.2005.00152.x.

[38] H. Schilder, Cleaning and shaping the root canal., Dent. Clin. North Am. 18 (1974) 269–296. https://doi.org/10.1016/s0011-8532(22)00677-2.

[39] A.J.E. Qualtrough J.D. Satterthwaite L.A. Morrow P.A. Brunton, Principles of Operative Dentistry, 2005. https://doi.org/10.1136/bmj.2.5263.1337.

[40] W.H. Clem, Endodontics: the adolescent patient., Dent. Clin. North Am. 13 (1969) 482–493. https://doi.org/10.1016/s0011-8532(22)02907-x.

[41] L.F. Morgan, S. Montgomery, An Evaluation of the Crown-down Pressureless Technique, J. Endod. 0 (1984) 491–498.

[42] N.M. Grande, G. Plotino, R. Sinibaldi, G. Gambarini, F. Somma, The impact of endodontic anatomy on clinical practice: A micro-CT study and tribute to Prof. Francesco Riitano, G. Ital. Endod. 29 (2015) 30–36. https://doi.org/10.1016/j.gien.2015.05.001.

[43] J.B. Roane, C.L. Sabala, M.G. Duncanson, The "balanced force" concept for instrumentation of curved canals, J. Endod. 11 (1985) 203–211. https://doi.org/10.1016/S0099-2399(85)80061-3.

[44] J.B. Roane, C. Sabala, Clockwise or counterclockwise, J. Endod. 10 (1984) 349–353. https://doi.org/10.1016/S0099-2399(84)80153-3.

[45] G.S. Ibelli, J.M. Barroso, A. Capelli, J.C.E. Spanó, J.D. Pécora, Influence of cervical preflaring on apical file size determination in maxillary lateral incisors, Braz. Dent. J. 18 (2007) 102–106. https://doi.org/10.1590/s0103-64402007000200003.

[46] I. Hülsmann, M., & Schinkel, Influence of several factors on the success or failure of removal of fractured instruments from the root canal, Dent. Traumatol. 15 (1999) 252–258.

[47] L. Tang, T.Q. Sun, X.J. Gao, X.D. Zhou, D.M. Huang, Tooth anatomy risk factors influencing root canal working length accessibility, Int. J. Oral Sci. 3 (2011) 135–140. https://doi.org/10.4248/IJOS11050.

[48] A. Jain, A. Saxena, A. Awat, S. Ajaypratap, S. Jain, Current challenges and strategies in the preparation of root canal systems, highlighting the role of niti rotary instruments: an overview, World J. Pharm. Res. 10 (2021) 885–901. https://doi.org/10.20959/wjpr20214-20147.

[49] E. Spoorthy, N. Velmurugan, S. Ballal, S. Nandini, Comparison of irrigant penetration up to working length and into simulated lateral canals using various irrigating techniques, Int. Endod. J. 46 (2013) 815–822. https://doi.org/10.1111/iej.12065.

[50] T. Aslan, E. Esim, Y. Üstün, H. Dönmez Özkan, Evaluation of Stress Distributions in Mandibular Molar Teeth with Different Iatrogenic Root Perforations Repaired with Biodentine or Mineral Trioxide Aggregate: A Finite Element Analysis Study, J. Endod. 47 (2021) 631–640. https://doi.org/10.1016/j.joen.2020.11.018.

[51] N. Sakkir, K.A. Thaha, M.G. Nair, S. Joseph, R. Christalin, Management of dilacerated and s-shaped root canals - An endodontist's challenge, J. Clin. Diagnostic Res. 8 (2014) 22–24. https://doi.org/10.7860/JCDR/2014/9100.4520.

[52] G.I. Eleftheriadis, T.P. Lambrianidis, Technical quality of root canal treatment and detection of iatrogenic errors in an undergraduate dental clinic, Int. Endod. J. 38 (2005) 725–734. https://doi.org/10.1111/j.1365-2591.2005.01008.x.

[53] F.G. Gorni, A. Andreano, F. Ambrogi, E. Brambilla, M. Gagliani, Patient and Clinical Characteristics Associated with Primary Healing of Iatrogenic Perforations after Root Canal Treatment: Results of a Long-term Italian Study, J. Endod. 42 (2016) 211–215. https://doi.org/10.1016/j.joen.2015.11.006.

[54] G. Aidasani, S. Mulay, Management of iatrogenic errors: Furcal perforation, J. Int. Clin. Dent. Res. Organ. 10 (2018) 42. https://doi.org/10.4103/jicdro.jicdro_2_18.

[55] O. Amza, B. Dimitriu, I. Suciu, R. Bartok, M. Chirila, Etiology and Prevention of an Endodontic Iatrogenic Event: Instrument Fracture, J. Med. Life. 13 (2020) 378–381.

https://doi.org/10.25122/jml-2020-0137.

[56] J.Y. Blum, P. Machtou, S. Esber, J.P. Micallef, Analysis of forces developed during root canal preparation with the balanced force technique, Int. Endod. J. 30 (1997) 386–396. https://doi.org/10.1046/j.1365-2591.1997.00102.x.

[57] K. Gulabivala, S. Abdo, M. Sherriff, J.D. Regan, The influence of interfacial forces and duration of filing on root canal shaping, Endod. Dent. Traumatol. 16 (2000) 166–174. https://doi.org/10.1034/j.1600-9657.2000.016004166.x.

[58] O.A. Peters, C.I. Peters, K. Schönenberger, F. Barbakow, ProTaper rotary root canal preparation: Assessment of torque and force in relation to canal anatomy, Int. Endod. J. 36 (2003) 93–99. https://doi.org/10.1046/j.1365-2591.2003.00628.x.

[59] F.B. &O. A.P. W. Hubscher, Root-canal preparation with FlexMaster: asessment of torque and force in relation to canal anatomy, Int. Endod. J. 36 (2003) 1–8.

[60] A. Diop, N. Maurel, M. Oiknine, E. Patoor, P. Machtou, A Novel Platform for In Vitro Analysis of Torque, Forces, and Three-dimensional File Displacements During Root Canal Preparations: Application to ProTaper Rotary Files, J. Endod. 35 (2009) 568–572. https://doi.org/10.1016/j.joen.2008.12.017.

[61] H. Kim, G.S. Cheung, C. Lee, Comparison of Forces Generated During Root Canal Shaping and Residual Stresses of Three Nickel – Titanium Rotary Files by Using a Three-Dimensional Finite-element Analysis, J. Endod. 34 (2008) 743–747. https://doi.org/10.1016/j.joen.2008.03.015.

[62] C. Boessler, F. Paque, O.A. Peters, The Effect of Electropolishing on Torque and Force During Simulated Root Canal Preparation with ProTaper Shaping Files, J. Endod. 35 (2009) 102–106. https://doi.org/10.1016/j.joen.2008.09.008.

[63] A. Arias, R. Singh, O.A. Peters, Torque and force induced by ProTaper universal and ProTaper next during shaping of large and small root canals in extracted teeth, J. Endod. 40 (2014) 973–976. https://doi.org/10.1016/j.joen.2013.11.019.

165

[64] D. Tokita, A. Ebihara, M. Nishijo, K. Miyara, T. Okiji, Dynamic Torque and Vertical Force Analysis during Nickel-titanium Rotary Root Canal Preparation with Different Modes of Reciprocal Rotation, J. Endod. 43 (2017) 1706–1710. https://doi.org/10.1016/j.joen.2017.05.010.

[65] S. Kimura, A. Ebihara, K. Maki, M. Nishijo, D. Tokita, T. Okiji, Effect of Optimum Torque Reverse Motion on Torque and Force Generation during Root Canal Instrumentation with Crown-down and Single-length Techniques, J. Endod. 46 (2020) 232–237. https://doi.org/10.1016/j.joen.2019.11.007.

[66] A. Nayak, P.K. Kankar, N. Jain, P.K. Jain, Force and vibration correlation analysis in the self-adjusting file during root canal shaping: An in-vitro study, J. Dent. Sci. 13 (2018) 184–189. https://doi.org/10.1016/j.jds.2018.01.002.

[67] A. Nayak, P.K. Kankar, P.K. Jain, N. Jain, Fracture prediction of the self adjusting file using force and vibration signature analysis, Springer Proc. Phys. 224 (2019) 643–649. https://doi.org/10.1007/978-3-030-19894-7_49.

[68] M. Thu, A. Ebihara, S. Adel, T. Okiji, Analysis of torque and force induced by rotary nickel-titanium instruments during root canal preparation: A systematic review, Appl. Sci. 11 (2021) 3079. https://doi.org/10.3390/app11073079.

[69] G. Levy, I. Rizoiu, S. Friedman, H. Lam, Pressure waves in root canals induced by Nd: YAG laser, J. Endod. 22 (1996) 81–84. https://doi.org/10.1016/S0099-2399(96)80278-0.

[70] S.C. Lea, A.D. Walmsley, P.J. Lumley, Analyzing Endosonic Root Canal File Oscillations : An In Vitro Evaluation, J. Endodonotics. 36 (2010) 880–883. https://doi.org/10.1016/j.joen.2009.12.027.

[71] B. Verhaagen, S. Lea, G.J. De Bruin, L.W.M. Van Der Sluis, A.D. Walmsley, M. Versluis, Oscillation characteristics of endodontic files: Numerical model and its validation, IEEE Trans. Ultrason. Ferroelectr. Freq. Control. 59 (2012) 2448–2459. https://doi.org/10.1109/TUFFC.2012.2477.

[72] H.S. Jeon, Y. J., Kim, J. W., Cho, K. M., Park, S. H., & Chang, Vibration characteristics of endodontic motors with different motion: reciprocation and conventional rotation, J. Korean Dent. Assoc. 2011 (2011) 2–5.

[73] D.M. Choi, J.W. Kim, S.H. Park, K.M. Cho, S.W. Kwak, H.C. Kim, Vibrations Generated by Several Nickel-titanium Endodontic File Systems during Canal Shaping in an Ex Vivo Model, J. Endod. 43 (2017) 1197–1200. https://doi.org/10.1016/j.joen.2017.03.010.

[74] A. Nayak, P.K. Kankar, P.K. Jain, N. Jain, Force and vibration generated in apical direction by three endodontic files of different kinematics during simulated canal preparation: An in vitro analytical study, Proc. Inst. Mech. Eng. Part H J. Eng. Med. 233 (2019) 839–848. https://doi.org/10.1177/0954411919854574.

[75] S.-J. Park, S.-H. Park, K.-M. Cho, H.-J. Ji, E.-H. Lee, J.-W. Kim, Comparison of vibration characteristics of file systems for root canal shaping according to file length, Restor. Dent. Endod. 45 (2020) 1–10. https://doi.org/10.5395/rde.2020.45.e51.

[76] C.M. Mörch, S. Atsu, W. Cai, X. Li, S.A. Madathil, X. Liu, V. Mai, F. Tamimi, M.A. Dilhac, M. Ducret, Artificial Intelligence and Ethics in Dentistry: A Scoping Review, J. Dent. Res. 100 (2021) 1452–1460. https://doi.org/10.1177/00220345211013808.

[77] N. Boreak, Effectiveness of Artificial Intelligence Applications Designed for Endodontic Diagnosis, Decision-making, and Prediction of Prognosis A Systematic Review, J. Contemp. Dent. Pract. 21 (8) (2020) 926–934.

[78] W.J. Park, Jun-Beom Park, History and application of artificial neural networks in dentistry Wook, Eur. J. Dent. 12 (2018) 594–601. https://doi.org/10.4103/ejd.ejd.

[79] M. Hung, M.W. Voss, M.N. Rosales, W. Li, W. Su, J. Xu, J. Bounsanga, B. Ruiz-Negrón, E. Lauren, F.W. Licari, Application of machine learning for diagnostic prediction of root caries, Gerodontology. 36 (2019) 395–404.

https://doi.org/10.1111/ger.12432.

[80]   M. Song, S.G. Kim, S.J. Lee, B. Kim, E. Kim, Prognostic factors
        of clinical outcomes in endodontic microsurgery: A prospective
        study, J. Endod. 39 (2013) 1491–1497.
        https://doi.org/10.1016/j.joen.2013.08.026.

[81]   D. Pinto, A. Marques, J.F. Pereira, P.J. Palma, J.M. Santos, Long-
        Term Prognosis of Endodontic Microsurgery —, Medicina (B.
        Aires). 56 (2020) 1–19.

[82]   Y. Qu, Z. Lin, Z. Yang, H. Lin, X. Huang, L. Gu, Machine
        learning models for prognosis prediction in endodontic
        microsurgery, J. Dent. 118 (2022) 103947.
        https://doi.org/10.1016/j.jdent.2022.103947.

[83]   A.A. Azim, H. Albanyan, K.A. Azim, L. Piasecki, The Buffalo
        study: Outcome and associated predictors in endodontic
        microsurgery- a cohort study, Int. Endod. J. 54 (2021) 301–318.
        https://doi.org/10.1111/iej.13419.

[84]   J.J. Hwang, Y.H. Jung, B.H. Cho, M.S. Heo, An overview of deep
        learning in the field of dentistry, Imaging Sci. Dent. 49 (2019) 1–
        7. https://doi.org/10.5624/isd.2019.49.1.1.

[85]   H. Il Choi, S.K. Jung, S.H. Baek, W.H. Lim, S.J. Ahn, I.H. Yang,
        T.W. Kim, Artificial Intelligent Model with Neural Network
        Machine Learning for the Diagnosis of Orthognathic Surgery, J.
        Craniofac. Surg. 30 (2019) 1986–1989.
        https://doi.org/10.1097/SCS.0000000000005650.

[86]   A. Aminoshariae, J. Kulild, V. Nagendrababu, Artificial
        Intelligence in Endodontics: Current Applications and Future
        Directions, J. Endod. 47 (2021) 1352–1357.
        https://doi.org/10.1016/j.joen.2021.06.003.

[87]   T.M.A. Lilian Toledo Reyes, Jessica Klöckner Knorst, Fernanda
        Ruffo Ortiz, Scope and challenges of machine learning-based
        diagnosis and prognosis in clinical dentistry: A literature review,
        J. Clin. Transl. Res. 7 (2021) 523–539.
        https://doi.org/10.18053/jctres.07.202104.012.

[88]   M.A. Saghiri, K. Asgar, K.K. Boukani, M. Lotfi, H. Aghili, A.

Delvarani, K. Karamifar, A.M. Saghiri, P. Mehrvarzfar, F. Garcia-Godoy, A new approach for locating the minor apical foramen using an artificial neural network, Int. Endod. J. 45 (2012) 257–265. https://doi.org/10.1111/j.1365-2591.2011.01970.x.

[89] M.A. Saghiri, F. Garcia-Godoy, J.L. Gutmann, M. Lotfi, K. Asgar, The Reliability of artificial neural network in locating minor apical foramen: A cadaver study, J. Endod. 38 (2012) 1130–1134. https://doi.org/10.1016/j.joen.2012.05.004.

[90] S. Kositbowornchai, S. Plermkamon, T. Tangkosol, Performance of an artificial neural network for vertical root fracture detection: An ex vivo study, Dent. Traumatol. 29 (2013) 151–155. https://doi.org/10.1111/j.1600-9657.2012.01148.x.

[91] M. Fukuda, K. Inamoto, N. Shibata, Y. Ariji, Y. Yanashita, S. Kutsuna, K. Nakata, A. Katsumata, H. Fujita, E. Ariji, Evaluation of an artificial intelligence system for detecting vertical root fracture on panoramic radiography, Oral Radiol. 36 (2020) 337–343. https://doi.org/10.1007/s11282-019-00409-x.

[92] T. Hiraiwa, Y. Ariji, M. Fukuda, Y. Kise, K. Nakata, A. Katsumata, H. Fujita, E. Ariji, A deep-learning artificial intelligence system for assessment of root morphology of the mandibular first molar on panoramic radiography, Dentomaxillofacial Radiol. 48 (2019) 1–7. https://doi.org/10.1259/dmfr.20180218.

[93] K. Orhan, I.S. Bayrakdar, M. Ezhov, A. Kravtsov, T. Özyürek, Evaluation of artificial intelligence for detecting periapical pathosis on cone-beam computed tomography scans, Int. Endod. J. 53 (2020) 680–689. https://doi.org/10.1111/iej.13265.

[94] Nayak A., Kankar.P.K. Jain P.K., Progress and Issues Related to Designing and 3D Printing of Endodontic Guide, in: G.S. (eds) Chandrasekhar U., Yang LJ. (Ed.), Innov. Des. Anal. Dev. Pract. Aerosp. Automot. Eng. (I-DAD 2018), Springer Singapore, 2019: pp. 331–337. https://doi.org/https://doi.org/10.1007/978-981-13-2718-6_30.

[95] A.G. Ismail, M.H.A. Zaazou, M. Galal, N.O.M. Kamel, M.A. Nassar, Finite element analysis comparing WaveOne Gold and ProTaper Next endodontic file segments subjected to bending and torsional load, Bull. Natl. Res. Cent. 43 (2019) 6–11. https://doi.org/10.1186/s42269-019-0215-6.

[96] T. Özyürek, M. Gündoğar, G. Uslu, K. Yılmaz, S. Staffoli, G. Nm, G. Plotino, A. Polimeni, Cyclic fatigue resistances of Hyflex EDM, WaveOne gold, Reciproc blue and 2shape NiTi rotary files in different artificial canals, Odontology. 106 (2018) 408–413. https://doi.org/10.1007/s10266-018-0340-y.

[97] P. Ausiello, S. Ciaramella, F. Garcia-Godoy, M. Martorelli, R. Sorrentino, A. Gloria, Stress distribution of bulk-fill resin composite in class II restorations, Am. J. Dent. 30 (2017) 227–232.

[98] J.P.M. Tribst, A.M. de O. dal Piva, R. Lo Giudice, A.L.S. Borges, M.A. Bottino, E. Epifania, P. Ausiello, The influence of custom-milled framework design for an implant-supported full-arch fixed dental prosthesis: 3D-FEA sudy, Int. J. Environ. Res. Public Health. 17 (2020) 1–12. https://doi.org/10.3390/ijerph17114040.

[99] A.L.S. Borges, A.L. De Lima, L.M. Campaner, M.A. Bottino, A.M. De Oliveira Dal Piva, J.P.M. Tribst, Influence of occlusal anatomy on acrylic resin CAD/CAM crowns fracture load and stress distribution, Dent. 3000. 9 (1) (2021). https://doi.org/10.5195/D3000.2021.118.

[100] M. Martorelli, P. Ausiello, A novel approach for a complete 3D tooth reconstruction using only 3D crown data, Int. J. Interact. Des. Manuf. 7 (2013) 125–133. https://doi.org/10.1007/s12008-012-0166-8.

[101] Z.H. Jin, M.D. Peng, Q. Li, The effect of implant neck microthread design on stress distribution of peri-implant bone with different level: A finite element analysis, J. Dent. Sci. 15 (2020) 466–471. https://doi.org/10.1016/j.jds.2019.12.003.

[102] M.M. Dinc, P. Turkoglu, F. Selvi, Biomechanical evaluation of stress distributions at the implant-abutment complex and peri-

implant bone around mandibular dental implants with different neck geometries and inclinations, Proc. Inst. Mech. Eng. Part H J. Eng. Med. 4 (2021) 1–11. https://doi.org/10.1177/09544119211022985.

[103] Y. Shen, H.M. Zhou, Y.F. Zheng, B. Peng, M. Haapasalo, Current challenges and concepts of the thermomechanical treatment of nickel-titanium instruments, J. Endod. 39 (2013) 163–172. https://doi.org/10.1016/j.joen.2012.11.005.

[104] K.S. Shim, S. Oh, K. Kum, Y.C. Kim, K.K. Jee, S.W. Chang, Mechanical and Metallurgical Properties of Various Nickel-Titanium Rotary Instruments, Biomed Res. Int. 2017 (2017). https://doi.org/10.1155/2017/4528601.

[105] V.S. Thakur, Investigation on Laser Assisted Post Processing of Wire Arc Additive Manufacturing of NiTi Shape Memory Alloys, M Tech. Thesis, Indian institute of technology Indore, 2019.

[106] V.S. Thakur, M. Manikandan, S. Singh, S. Mishra, A. Kaithwas, S.S. Mani Prabu, I.A. Palani, Laser Polishing of Wire Arc Additive Manufactured SS316L, in: M. S. Shunmugam and M. Kanthababu (eds.) (Ed.), Adv. Addit. Manuf. Joining, Lect. Notes Multidiscip. Ind. Eng., Springer Singapore, 2020: pp. 127–135. https://doi.org/10.1007/978-981-32-9433-2_10.

[107] J. Zupanc, N. Vahdat-Pajouh, E. Schäfer, New thermomechanically treated NiTi alloys – a review, Int. Endod. J. 51 (2018) 1088–1103. https://doi.org/10.1111/iej.12924.

[108] J. Ye, Y. Gao, Metallurgical characterization of M-Wire nickel-titanium shape memory alloy used for endodontic rotary instruments during low-cycle fatigue, J. Endod. 38 (2012) 105–107. https://doi.org/10.1016/j.joen.2011.09.028.

[109] I.A. Palani, S.S. Mani Prabu, M. Manikandan, V.S. Thakur, A. Sahu, S. Singh, C.P. Paul, Investigation on actuation characteristics of tailor-made NiTi shape memory alloy structures fabricated through wire arc additive manufacturing (WAAM) technique, in: ASM Int. - Int. Conf. Shape Mem. Superelastic

Technol. SMST 2019, 2019: pp. 135–136.

[110] M. Tonutti, D.S. Elson, G.Z. Yang, A.W. Darzi, M.H. Sodergren, The role of technology in minimally invasive surgery: State of the art, recent developments and future directions, Postgrad. Med. J. 93 (2017) 159–167. https://doi.org/10.1136/postgradmedj-2016-134311.

[111] B. Molina, G. Glickman, P. Vandrangi, M. Khakpour, Evaluation of root canal debridement of human molars using the GentleWave System, J. Endod. 41 (2015) 1701–1705. https://doi.org/10.1016/j.joen.2015.06.018.

[112] T.O. Kim, G.S.P. Cheung, J.M. Lee, B.M. Kim, B. Hur, H.C. Kim, Stress distribution of three NiTi rotary files under bending and torsional conditions using a mathematic analysis, Int. Endod. J. 42 (2009) 14–21. https://doi.org/10.1111/j.1365-2591.2008.01481.x.

[113] A. Nayak, P.K. Jain, P.K. Kankar, N. Jain, Effect of volumetric shrinkage of restorative materials on tooth structure: A finite element analysis, Proc. Inst. Mech. Eng. Part H J. Eng. Med. 235 (2021) 493–499. https://doi.org/10.1177/0954411921990138.

[114] A. Nayak, P.K. Jain, P.K. Kankar, N. Jain, Computer-aided design – based guided endodontic : A novel approach for root canal access cavity preparation, Proc. Inst. Mech. Eng. Part H J. Eng. Med. 232(8) (2018) 787–795. https://doi.org/10.1177/0954411918788104.

[115] R. Arbab-Chirani, V. Chevalier, S. Arbab-Chirani, S. Calloch, Comparative analysis of torsional and bending behavior through finite-element models of 5 Ni-Ti endodontic instruments, Oral Surgery, Oral Med. Oral Pathol. Oral Radiol. Endodontology. 111 (2011) 115–121. https://doi.org/10.1016/j.tripleo.2010.07.017.

[116] L. De Arruda Santos, J.B. López, E.B. De Las Casas, M.G. De Azevedo Bahia, V.T.L. Buono, Mechanical behavior of three nickel-titanium rotary files: A comparison of numerical simulation with bending and torsion tests, Mater. Sci. Eng. C. 37

(2014) 258–263. https://doi.org/10.1016/j.msec.2014.01.025.

[117] M. Prados-Privado, R. Rojo, C. Ivorra, J.C. Prados-Frutos, Finite element analysis comparing WaveOne, WaveOne Gold, Reciproc and Reciproc Blue responses with bending and torsion tests, J. Mech. Behav. Biomed. Mater. 90 (2019) 165–172. https://doi.org/10.1016/j.jmbbm.2018.10.016.

[118] A.G. Padgelwar, Stress Analysis of Human Tooth Using Ansys, Int. J. Eng. Sci. Comput. 6 (2016) 4379–4384. https://doi.org/10.4010/2016.1005.

[119] M. Mahmoudi, A.R. Saidi, M.A. Hashemipour, P. Amini, The use of functionally graded dental crowns to improve biocompatibility: a finite element analysis, Comput. Methods Biomech. Biomed. Engin. 21 (2018) 161–168. https://doi.org/10.1080/10255842.2018.1431219.

[120] E.W. Zhang, G.S.P. Cheung, Y.F. Zheng, A mathematical model for describing the mechanical behaviour of root canal instruments, Int. Endod. J. 44 (2011) 72–76. https://doi.org/10.1111/j.1365-2591.2010.01801.x.

[121] M.R. Javanmardi, Implicit and Explicit Time Integration Methods for Nonlinear Structural Dynamics, in: 9th Internatioional Congr. Civ. Eng. Isfahan Univ. Technol. (IUT), Isfahan, Iran, 2017: p. 1227.

[122] M.I. El-Anwar, A.O. Mandorah, S.A. Yousief, T.A. Soliman, T.M. Abd El-Wahab, A finite element study on the mechanical behavior of reciprocating endodontic files, Brazilian J. Oral Sci. 14 (2015) 52–59. https://doi.org/10.1590/1677-3225v14n1a11.

[123] M.T. Malazi, E.T. Eren, J. Luo, S. Mi, G. Temir, Three-dimensional fluid-structure interaction case study on elastic beam, J. Mar. Sci. Eng. 8 (2020) 714. https://doi.org/10.3390/JMSE8090714.

[124] J. Prakash, S.K. Gupta, P.K. Kankar, An analytical approach to evaluate the maximum load carrying capacity for pin-mounted telescopic hydraulic cylinder, Proc. Inst. Mech. Eng. Part C J. Mech. Eng. Sci. 234 (2020) 3919–3934.

https://doi.org/10.1177/0954406220916524.

[125] B.D. Rundquist, A. Versluis, How does canal taper affect root stresses?, Int. Endod. J. 39 (2006) 226–237. https://doi.org/10.1111/j.1365-2591.2006.01078.x.

[126] M. Vincent, P. Xolin, A. Gevrey, F. Thiebaud, T. Ben Zineb, Experimental and numerical analysis of Penetration/Removal response of endodontic instrument made of single crystal Cu-based SMA : comparison with NiTi SMA instrument, Smart Mater. Struct. 26 (2017) 045014 (15 pp). https://doi.org/https://doi.org/10.1088/1361-665X/aa5f0b.

[127] V. Roda-Casanova, Á. Zubizarreta-Macho, F. Sanchez-Marin, Ó.A. Ezpeleta, A.A. Martínez, A.G. Catalán, Computerized generation and finite element stress analysis of endodontic rotary files, Appl. Sci. 11 (10) (2021) 4329. https://doi.org/10.3390/app11104329.

[128] C. Pirani, O. Ruggeri, P.P. Cirulli, G.A. Pelliccioni, M.G. Gandolfi, C. Prati, Metallurgical analysis and fatigue resistance of WaveOne and ProTaper Nickel-Titanium instruments, Odontology. 102 (2014) 211–216. https://doi.org/10.1007/s10266-013-0113-6.

[129] S. Singh, N. Mirdha, P.H. Shilpa, R.V.C. Tiwari, M.S.M. Abdul, S. Sainudeen, Shaping Ability of 2Shape and WaveOne Gold Files Using Cone-Beam Computed Tomography, J. Int. Soc. Prev. Community Dent. 9 (2019) 245. https://doi.org/10.4103/JISPCD.JISPCD_411_18.

[130] T. Özyürek, M. Gündoğar, K. Yılmaz, G. Uslu, Bending resistance and cyclic fatigue life of Reciproc Blue, WaveOne Gold, and Genius files in a double (S-shaped) curved canal., J. Dent. Res. Dent. Clin. Dent. Prospects. 11 (2017) 241–246. https://doi.org/10.15171/joddd.2017.042.

[131] S. Singhrao, S. K., Harding, A., Simmons, T., Robinson, S., Kesavalu, L., & Crean, Oral Inflammation, Tooth Loss, Risk Factors, and Association with Progression of Alzheimer's Disease Sim K. Singhrao, J. Alzheimer's Dis. 44 (2014) 1–43.

[132] D. Kandelman, P.E. Petersen, H. Ueda, Oral health , general health , and quality of life in older people, Spec. Care Dent. Assoc. Wiley Period. Inc. 8 (2008) 224–236. https://doi.org/10.1111/j.1754-4505.2008.00045.x.

[133] M. Jones, J.Y. Lee, R. Gary Rozier, Oral health literacy among adult patients seeking dental care, J. Am. Dent. Assoc. 138 (2007) 1199–1208. https://doi.org/10.14219/jada.archive.2007.0344.

[134] A. Zanza, M. Seracchiani, D. Di Nardo, R. Reda, G. Gambarini, L. Testarelli, A Paradigm Shift for Torsional Stiffness of Nickel-Titanium Rotary Instruments: A Finite Element Analysis, J. Endod. 47 (2021) 1149–1156. https://doi.org/10.1016/j.joen.2021.04.017.

[135] R. Garberoglio, C. Becce, ENDODONTICS Smear layer removal by root canal irrigants, Oral Surgery, Oral Med. Oral Pathol. 78 (1994) 359–367.

[136] L.B. Peters, P.R. Wesselink, J.F. Buijs, A.J. Van Winkelhoff, Viable bacteria in root dentinal tubules of teeth with apical periodontitis, J. Endod. 27 (2001) 76–81. https://doi.org/10.1097/00004770-200102000-00002.

[137] M. Taubman, A.I. Spielman, The birth of the most important 18th century dental text: Pierre Fauchard's Le chirurgien dentist, J. Dent. Res. 86(10) (2007) 922–926.

[138] Z. Metzger, E. Teperovich, R. Cohen, R. Zary, F. Paqué, M. Hülsmann, The Self-adjusting File (SAF). Part 3: Removal of Debris and Smear Layer-A Scanning Electron Microscope Study, J. Endod. 36 (2010) 697–702. https://doi.org/10.1016/j.joen.2009.12.037.

[139] M.B. Mcguigan, C. Louca, H.F. Duncan, Clinical decision-making after endodontic instrument fracture, Nat. Publ. Gr. 214 (2013) 395–400. https://doi.org/10.1038/sj.bdj.2013.379.

[140] P. Louis I. Grossman, D.D.X., Dr.med.dent., Philadelphia, Guidelines for the prevention of fracture of root canal instruments, Oral Surgery, Oral Med. Oral Pathol. 28 (1969) 746–752. https://doi.org/10.1016/0030-4220(69)90423-X.

[141] M.B. McGuigan, C. Louca, H.F. Duncan, Endodontic instrument fracture: Causes and prevention, Br. Dent. J. 214 (2013) 341–348. https://doi.org/10.1038/sj.bdj.2013.324.

[142] M. Gerek, E.D. Başer, M.B. Kayahan, H. Sunay, R.F. Kaptan, G. Bayirli, Comparison of the force required to fracture roots vertically after ultrasonic and Masserann removal of broken instruments, Int. Endod. J. 45 (2012) 429–434. https://doi.org/10.1111/j.1365-2591.2011.01993.x.

[143] R. Hof, V. Perevalov, M. Eltanani, R. Zary, The Self-adjusting File (SAF). Part 2 : Mechanical Analysis, J. Endod. 36 (2010) 691–696. https://doi.org/10.1016/j.joen.2009.12.028.

[144] S. Bürklein, J.P. Stüber, E. Schäfer, Real-time dynamic torque values and axial forces during preparation of straight root canals using three different endodontic motors and hand preparation, Int. Endod. J. 52 (2019) 94–104. https://doi.org/10.1111/iej.12980.

[145] E. Schäfer, S. Bürklein, Impact of nickel-titanium instrumentation of the root canal on clinical outcomes: A focused review, Odontology. 100 (2012) 130–136. https://doi.org/10.1007/s10266-012-0066-1.

[146] H. Zhou, B. Peng, Y.-F. Zheng, An overview of the mechanical properties of nickel-titanium endodontic instruments, Endod. Top. 29 (2013) 42–54. https://doi.org/10.1111/etp.12045.

[147] P.L. Mirceska M, The role of rotary systems in endodontic in endodontic treatment, Maced. Dent. Rev. 41 (2018) 66–72.

[148] R.L. Poole, S.C. Lea, J.E. Dyson, A.C.C. Shortall, A.D. Walmsley, Vibration characteristics of dental high-speed turbines and speed-increasing handpieces, J. Dent. 36 (2008) 488–493. https://doi.org/10.1016/j.jdent.2008.03.006.

[149] C. Schrader, O.A. Peters, Analysis of torque and force with differently tapered rotary endodontic instruments in vitro, J. Endod. 31 (2005) 120–123. https://doi.org/10.1097/01.don.0000137634.20499.1d.

[150] Z. Khalilak, A. Fallahdoost, B. Dadresanfar, G. Rezvani, Comparison of extracted teeth and simulated resin blocks on

apical canal transportation, Iran. Endod. J. 3 (2008) 109.

[151] E. Schäfer, Irrigation of the root canal, Endod. Pract. Today. 1(1) (2019) 11–27.

[152] M. Tanomaru-FIlho, F.F.E. Torres, G.M. Chávez-Andrade, L.M. Miano, J.M. Guerreiro-Tanomaru, Intermittent or continuous ultrasonically activated irrigation: micro-computed tomographic evaluation of root canal system cleaning, Clin. Oral Investig. 20 (2016) 1541–1546. https://doi.org/10.1007/s00784-015-1645-7.

[153] J. Webber, Shaping canals with confidence : WaveOne GOLD single-file, Int. Dent. - Africa Ed. 6 (2015) 34–40.

[154] J.D. West, The endodontic glidepath: Secret to rotary safety, Dent. Today. 29 (2010) 86–93.

[155] J.J. Mecholsky, A.A. Barrett, C.T. Jones, K.M. Pace, U.P. Nair, Fractographic analysis of separated endodontic file designs, J. Mater. Sci. Mater. Med. 31 (2020). https://doi.org/10.1007/s10856-020-06432-3.

[156] C. Chi, Y. Deng, J. Lee, Fracture resistance of dental nickel e titanium rotary instruments with novel surface treatment : Thin film metallic glass coating, J. Formos. Med. Assoc. (2016) 1–7. https://doi.org/10.1016/j.jfma.2016.07.003.

[157] S. Drukteinis, V. Peciuliene, R. Bendinskaite, V. Brukiene, R. Maneliene, E. Nedzinskiene, Shaping ability, cyclic fatigue resistance and fractographic analysis of hybrid and reciprocating nickel titanium endodontic instruments, Metals (Basel). 10 (2020) 3–5. https://doi.org/10.3390/met10020172.

[158] I.H. Abu-Tahun, S.W. Kwak, J.H. Ha, H.C. Kim, Microscopic Features of Fractured Fragment of Nickel-Titanium Endodontic Instruments by Two Different Modes of Torsional Loading, Scanning. 2018 (2018) 5. https://doi.org/10.1155/2018/9467059.

[159] L. Reimer, Scanning Electron Microscopy: Physics of Image Formation and Microanalysis, Second Edition, Measurement Science and Technology, 2000. https://doi.org/https://doi.org/10.1088/0957-0233/11/12/703.

[160] A. Nayak, P.K. Jain, P.K. Kankar, N. Jain, On comprehensive

analysis of root canal shaping ability of three endodontic files of different kinematics, Proc. Inst. Mech. Eng. Part H J. Eng. Med. (2021). https://doi.org/10.1177/09544119211014670.

[161] A. Nayak, Guided Endodontics and Vibration Signature Analysis of Root Canal Shaping: Experimental and Computational Study, PhD Thesis, PDPM IIITDM, Jabalpur, 2021.

[162] J. Prakash, P.K. Kankar, Health prediction of hydraulic cooling circuit using deep neural network with ensemble feature ranking technique, Meas. J. Int. Meas. Confed. 151 (2020) 107225. https://doi.org/10.1016/j.measurement.2019.107225.

[163] P.K. Kankar, S.C. Sharma, S.P. Harsha, Fault diagnosis of ball bearings using continuous wavelet transform, Appl. Soft Comput. J. 11 (2011) 2300–2312. https://doi.org/10.1016/j.asoc.2010.08.011.

[164] J. Prakash, P.K. Kankar, Determining the Working Behaviour of Hydraulic System Using Support Vector Machine, Lect. Notes Mech. Eng. (2021) 781–791. https://doi.org/10.1007/978-981-15-8025-3_74.

[165] J. Marzec, L. Marzec, P. Martus, D. Zips, A.C. Müller, MATLAB®-based fitting method to evaluate survival fractions after multimodal treatment, Clin. Transl. Radiat. Oncol. 10 (2018) 36–41. https://doi.org/10.1016/j.ctro.2018.03.003.

[166] Y. Zhao, D. Wang, X. Chen, Mathematical analysis of the fitting curves in reconstruction of 3D models, Procedia Eng. 15 (2011) 3546–3550. https://doi.org/10.1016/j.proeng.2011.08.664.

[167] W.J.P. Iii, System Dynamics, 2015. https://doi.org/10.1016/b978-0-08-100036-6.00017-0.

[168] A.C. Mathieson, Nonlinear Characterisation Of Power Ultrasonic Devices Used In Bone Surgery, PhD Thesis, University of Glasgow, 2012. http://theses.gla.ac.uk/3135/.

[169] M. Goldberg, S. Dahan, P. MacHtou, Centering ability and influence of experience when using waveone single-file technique in simulated canals, Int. J. Dent. (2012). https://doi.org/10.1155/2012/206321.

[170] S. Sharma, V. Rajkumar, S. Sarin, S. Sarin, C.S. Chugh, K. Harmeet, Biomechanical preparation of teeth: A comprehensive review, HECS Int. J. Community Heal. Med. Res. 3 (2017) 89–92.

[171] G.P. Nason, B.W. Silverman, The Stationary Wavelet Transform and some Statistical Applications, (1995) 281–299. https://doi.org/10.1007/978-1-4612-2544-7_17.

[172] A. Singhal, P. Singh, B. Fatimah, R.B. Pachori, An efficient removal of power-line interference and baseline wander from ECG signals by employing Fourier decomposition technique, Biomed. Signal Process. Control. 57 (2020) 101741. https://doi.org/10.1016/j.bspc.2019.101741.

[173] R.R. Sharma, R.B. Pachori, Baseline wander and power line interference removal from ECG signals using eigenvalue decomposition, Biomed. Signal Process. Control. 45 (2018) 33–49. https://doi.org/10.1016/j.bspc.2018.05.002.

[174] X. Zhang, R., Wang, H. Q., Wu, J. M., Guo, H. X., & Guo, Comparison of denoising methods for rolling bearing vibration signals: a case study using SWT, EMD, and WPT, Chinese J. Mech. Eng. 31 (2018) 7. https://doi.org/doi: 10.1007/s11771-017-3627-6.

[175] Y. Wang, Z. He, Y. Zi, Enhancement of signal denoising and multiple fault signatures detecting in rotating machinery using dual-tree complex wavelet transform, Mech. Syst. Signal Process. 24 (2010) 119–137. https://doi.org/10.1016/j.ymssp.2009.06.015.

[176] Z. May, M.K. Alam, N.A.A. Rahman, M.S. Mahmud, N.A. Nayan, Denoising of hydrogen evolution acoustic emission signal based on non-decimated stationary wavelet transform, Processes. 8 (2020) 1–19. https://doi.org/10.3390/pr8111460.

[177] M. Vafaeian, B., Naderi, M., Saeedi, P., & Maghazei, Comparative analysis of denoising techniques for gear fault diagnosis: A case study on stationary wavelet transform, empirical mode decomposition and Fourier transform, Mech.

Syst. Signal Process. 156 (2021) 107824.

[178] S. Tabassum, F.R. Khan, Failure of endodontic treatment: The usual suspects, Eur. J. Dent. 10 (2016) 144–147. https://doi.org/10.4103/1305-7456.175682.

[179] H. Jafarzadeh, P. V. Abbott, Ledge Formation: Review of a Great Challenge in Endodontics, J. Endod. 33 (2007) 1155–1162. https://doi.org/10.1016/j.joen.2007.07.015.

[180] S. Mallishery, P. Chhatpar, K.S. Banga, T. Shah, P. Gupta, The precision of case difficulty and referral decisions: an innovative automated approach, Clin. Oral Investig. 24 (2020) 1909–1915. https://doi.org/10.1007/s00784-019-03050-4.

[181] F.H. Alberto Fernández, Salvador García, Mikel Galar, Ronaldo C. Prati, Bartosz Krawczyk, Learning From Imbalanced Data sets, 2018. https://doi.org/10.4018/978-1-5225-7598-6.ch030.

[182] J.A. Sáez, J. Luengo, J. Stefanowski, F. Herrera, SMOTE-IPF: Addressing the noisy and borderline examples problem in imbalanced classification by a re-sampling method with filtering, Inf. Sci. (Ny). 291 (2015) 184–203. https://doi.org/10.1016/j.ins.2014.08.051.

[183] W.P. Chawla, N. V., Bowyer, K. W., Hall, L. O., & Kegelmeyer, SMOTE: synthetic minority over-sampling technique, J. Artif. Intell. Res. 16 (2002) 321–357. https://doi.org/10.1002/eap.2043.

[184] F. Hu, H. Li, A novel boundary oversampling algorithm based on neighborhood rough set model: NRSBoundary-SMOTE, Math. Probl. Eng. 2013 (2013). https://doi.org/10.1155/2013/694809.

[185] C. Bunkhumpornpat, K. Sinapiromsaran, C. Lursinsap, Safe-level-SMOTE: Safe-level-synthetic minority over-sampling technique for handling the class imbalanced problem, Lect. Notes Comput. Sci. (Including Subser. Lect. Notes Artif. Intell. Lect. Notes Bioinformatics). 5476 LNAI (2009) 475–482. https://doi.org/10.1007/978-3-642-01307-2_43.

[186] B.H. Han, H., Wang, W. Y., & Mao, Borderline-SMOTE: a new over-sampling method in imbalanced data sets learning, in: Int. Conf. Intell. Comput., 2005: pp. 878–887.

https://doi.org/10.1007/978-3-319-68385-0_20.

[187] T. Zhu, Y. Lin, Y. Liu, Synthetic minority oversampling technique for multiclass imbalance problems, Pattern Recognit. 72 (2017) 327–340. https://doi.org/10.1016/j.patcog.2017.07.024.

[188] H. He, Y. Bai, E.A. Garcia, S. Li, ADASYN: Adaptive synthetic sampling approach for imbalanced learning, Proc. Int. Jt. Conf. Neural Networks. (2008) 1322–1328. https://doi.org/10.1109/IJCNN.2008.4633969.

[189] S.S. Islam, M.S. Haque, M.S.U. Miah, T. Bin Sarwar, R. Nugraha, Application of machine learning algorithms to predict the thyroid disease risk: an experimental comparative study, PeerJ Comput. Sci. 8 (2022) e898. https://doi.org/10.7717/peerj-cs.898.

[190] J. Sun, J. Lang, H. Fujita, H. Li, Imbalanced enterprise credit evaluation with DTE-SBD: Decision tree ensemble based on SMOTE and bagging with differentiated sampling rates, Inf. Sci. (Ny). 425 (2018) 76–91. https://doi.org/10.1016/j.ins.2017.10.017.

[191] J. Prakash, P.K. Kankar, Health prediction of hydraulic cooling circuit using deep neural network with ensemble feature ranking technique, Measurement. (2019) 107225. https://doi.org/10.1016/j.measurement.2019.107225.

[192] P.K. Kankar, S.C. Sharma, S.P. Harsha, Fault diagnosis of ball bearings using machine learning methods, Expert Syst. Appl. 38 (2011) 1876–1886. https://doi.org/10.1016/j.eswa.2010.07.119.

[193] H. Manning, C., Raghavan, P., & Schütze, Introduction to Information Retrieval, Nat. Lang. Eng. 16 (2010) 100–103. https://doi.org/10.1108/00242530410565256.

[194] J.P. Griffis, J. C., Allendorfer, J. B., & Szaflarski, Voxel-based Gaussian naïve Bayes classification of ischemic stroke lesions in individual T1-weighted MRI scans, J. Neurosci. Methods. 257 (2016) 97–108. https://doi.org/10.1016/j.jneumeth.2015.09.019.Voxel-based.

[195] A.H. Jahromi, M. Taheri, A non-parametric mixture of Gaussian naive Bayes classifiers based on local independent features, 19th CSI Int. Symp. Artif. Intell. Signal Process. AISP 2017. 2018-Janua (2018) 209–212. https://doi.org/10.1109/AISP.2017.8324083.

[196] D. Li, S. Hu, W. He, B. Zhou, J. Peng, K. Wang, The area prediction of western North Pacific Subtropical High in summer based on Gaussian Naive Bayes, Clim. Dyn. (2022) 1–18. https://doi.org/10.1007/s00382-022-06252-x.

[197] T. Benkedjouh, K. Medjaher, N. Zerhouni, S. Rechak, Remaining useful life estimation based on nonlinear feature reduction and support vector regression, Eng. Appl. Artif. Intell. 26 (2013) 1751–1760. https://doi.org/10.1016/j.engappai.2013.02.006.

[198] O. Altay, M. Ulas, K.E. Alyamac, Prediction of the Fresh Performance of Steel Fiber Reinforced Self-Compacting Concrete Using Quadratic SVM and Weighted KNN Models, IEEE Access. 8 (2020) 92647–92658. https://doi.org/10.1109/ACCESS.2020.2994562.

[199] V.N. Vapnik, The Nature of Statistical Learning Theory, Second, Springer science & business media, 2000.

[200] I. Dagher, Quadratic kernel-free non-linear support vector machine, J. Glob. Optim. 41 (2008) 15–30. https://doi.org/10.1007/s10898-007-9162-0.

[201] J.M. Johnson, A. Yadav, Fault Detection and Classification Technique for HVDC Transmission Lines Using KNN, in: Inf. Commun. Technol. Sustain. Dev., 2018: pp. 245–253. https://doi.org/10.1007/978-981-10-3920-1_25.

[202] C. Chethana, Prediction of heart disease using different KNN classifier, in: Proc. - 5th Int. Conf. Intell. Comput. Control Syst. ICICCS 2021, 2021: pp. 1186–1194. https://doi.org/10.1109/ICICCS51141.2021.9432178.

[203] M. Kaushal, B.S. Khehra, A. Sharma, Soft Computing based object detection and tracking approaches: State-of-the-Art survey, Appl. Soft Comput. 70 (2018) 423–464.

https://doi.org/10.1016/j.asoc.2018.05.023.

[204] Y. Li, L. Li, Y. Fang, H. Peng, N. Ling, Bagged Tree and ResNet-Based Joint End-to-End Fast CTU Partition Decision Algorithm for Video Intra Coding, Electronics. 11 (2022) 1–27. https://doi.org/10.3390/electronics11081264.

[205] D. Rani, N.S. Gill, P. Gulia, J.M. Chatterjee, An Ensemble-Based Multiclass Classifier for Intrusion Detection Using Internet of Things, Comput. Intell. Neurosci. 2022 (2022) 1–16. https://doi.org/10.1155/2022/1668676.

[206] Mariette Awad and Rahul Khanna, Efficient Learning Machines: Theories, Concepts, and Applications for Engineers and System Designers, Apress, 2015.

[207] Harvey Motulsky & Arthur Christopoulos, Fitting Models to Biological Data using Linear and Nonlinear Regression. A practical guide to curve fitting, 2003. https://doi.org/10.1016/j.mineng.2004.06.019.

[208] G. Michau, Y. Hu, T. Palmé, O. Fink, Feature learning for fault detection in high-dimensional condition monitoring signals, Proc. Inst. Mech. Eng. Part O J. Risk Reliab. 234 (2020) 104–115. https://doi.org/10.1177/1748006X19868335.

[209] M.Z. Barbosa, I. B., Scelza, P., Pereira, A. M. B., Ferreira, F. G., Bagueira, R., Adeodato, C. S. R., & Scelza, Progressive structural deterioration of an endodontic instrument – A preliminary micro-computed tomography study, Eng. Fail. Anal. 104 (2019) 105–111. https://doi.org/https://doi.org/10.3390/app10186201.

[210] G. La Rosa, F. Lo Savio, E. Pedullà, E. Rapisarda, A new torquemeter to measure the influence of heat-treatment on torsional resistance of NiTi endodontic instruments, Eng. Fail. Anal. 82 (2017) 446–457. https://doi.org/10.1016/j.engfailanal.2017.08.005.

[211] M. Martinez Olmedo, F.J. Iglesias Godino, P. Fernández Liétor, F.A. Corpas Iglesias, J.M. Gómez de Salazar Caso de los Cobos, Corrosion and fracture analysis in screws of dental implants prostheses. New coatings, Eng. Fail. Anal. 82 (2017) 657–665.

https://doi.org/10.1016/j.engfailanal.2017.04.040.

[212] G. Douzas, F. Bacao, F. Last, Improving imbalanced learning through a heuristic oversampling method based on k-means and SMOTE, Inf. Sci. (Ny). 465 (2018) 1–20. https://doi.org/10.1016/j.ins.2018.06.056.

[213] X. Gao, X. Xin, Z. Li, W. Zhang, Predicting postoperative pain following root canal treatment by using artificial neural network evaluation, Sci. Rep. 11 (2021) 1–8. https://doi.org/10.1038/s41598-021-96777-8.

[214] M. Kataya, S. Ibrahim, G.E.H. Eid, I. El-Mahallawi, Correlating cutting efficiency and debris retention of endodontic files to their design features using AutoCAD measurements, Eng. Fail. Anal. 18 (2011) 1775–1783. https://doi.org/10.1016/j.engfailanal.2011.03.030.

[215] D. Bruellmann, S. Sander, I. Schmidtmann, The design of an fast Fourier filter for enhancing diagnostically relevant structures - endodontic files, Comput. Biol. Med. 72 (2016) 212–217. https://doi.org/10.1016/j.compbiomed.2016.03.019.

[216] D. Katircioglu-Öztürk, H.A. Güvenir, U. Ravens, N. Baykal, A window-based time series feature extraction method, Comput. Biol. Med. 89 (2017) 466–486. https://doi.org/10.1016/j.compbiomed.2017.08.011.

[217] T.F. Guo X, Peng C, Zhang S, Yan J, Duan S, Wang L, Jia P, A Novel Feature Extraction Approach Using Window Function Capturing and QPSO-SVM for Enhancing Electronic Nose Performance _ Enhanced Reader.pdf, Sensors. 15 (2015) 15198–15217. https://doi.org/10.3390/s150715198.

[218] V. Vapnik, S.E. Golowich, A. Smola, Support vector method for function approximation, regression estimation, and signal processing, Adv. Neural Inf. Process. Syst. (1997) 281–287.

[219] G. Guo, J.S. Zhang, Reducing examples to accelerate support vector regression, Pattern Recognit. Lett. 28 (2007) 2173–2183. https://doi.org/10.1016/j.patrec.2007.04.017.

[220] M.D. Anis, Towards Remaining Useful Life Prediction in

Rotating Machine Fault Prognosis: An Exponential Degradation Model, in: 2018 Cond. Monit. Diagnosis, C. 2018 - Proc., IEEE, 2018: pp. 18–23. https://doi.org/10.1109/CMD.2018.8535765.

[221] R.R. Zhou, N. Serban, N. Gebraeel, Degradation modeling applied to residual lifetime prediction using functional data analysis, Ann. Appl. Stat. 5 (2011) 1586–1610. https://doi.org/10.1214/10-AOAS448.

[222] Z. Li, X. Zhang, T. Kari, W. Hu, Health assessment and remaining useful life prediction of wind turbine high-speed shaft bearings, Energies. 14 (2021). https://doi.org/10.3390/en14154612.

[223] N. Li, Y. Lei, J. Lin, S.X. Ding, An Improved Exponential Model for Predicting Remaining Useful Life of Rolling Element Bearings, IEEE Trans. Ind. Electron. 62 (2015) 7762–7773. https://doi.org/10.1109/TIE.2015.2455055.

[224] Z. Zhang, X. Si, C. Hu, X. Kong, Degradation modeling-based remaining useful life estimation: A review on approaches for systems with heterogeneity, Proc. Inst. Mech. Eng. Part O J. Risk Reliab. 229 (2015) 343–355. https://doi.org/10.1177/1748006X15579322.

[225] N. Gebraeel, Sensory-updated residual life distributions for components with exponential degradation patterns, IEEE Trans. Autom. Sci. Eng. 3 (2006) 382–393. https://doi.org/10.1109/TASE.2006.876609.

[226] D. Wagner, ABSTRACTS 46 ème Congrès Société Biomécanique, in: Comput. Methods Biomech. Biomed. Engin., 2021: pp. S1–S325. https://doi.org/10.1080/10255842.2021.1978758.

[227] S.A. Ghaznavi Bidgoli, A. Sharifi, M. Manthouri, Automatic diagnosis of dental diseases using convolutional neural network and panoramic radiographic images, Comput. Methods Biomech. Biomed. Eng. Imaging Vis. 9 (2021) 447–455. https://doi.org/10.1080/21681163.2020.1847200.

[228] B. Thanathornwong, S. Suebnukarn, Y. Songpaisan, K.

Ouivirach, A system for predicting and preventing work-related musculoskeletal disorders among dentists, Comput. Methods Biomech. Biomed. Engin. 17 (2014) 177–185. https://doi.org/10.1080/10255842.2012.672565.

[229] D. Wang, K.L. Tsui, Q. Miao, Prognostics and Health Management: A Review of Vibration Based Bearing and Gear Health Indicators, IEEE Access. 6 (2017) 665–676. https://doi.org/10.1109/ACCESS.2017.2774261.

[230] A. Sharma, M. Amarnath, P.K. Kankar, Life assessment and health monitoring of rolling element bearings: an experimental study, Life Cycle Reliab. Saf. Eng. 7 (2018) 97–114. https://doi.org/10.1007/s41872-018-0044-x.

[231] S.Y. You, K.S. Bae, S.H. Baek, K.Y. Kum, W.J. Shon, W. Lee, Lifespan of one nickel-titanium rotary file with reciprocating motion in curved root canals, J. Endod. 36 (2010) 1991–1994. https://doi.org/10.1016/j.joen.2010.08.040.

[232] M.B. Mcguigan, C. Louca, H.F. Duncan, The impact of fractured endodontic instruments on treatment outcome, Nat. Publ. Gr. 214 (2013) 285–289. https://doi.org/10.1038/sj.bdj.2013.271.

[233] A. Gesi, P. Mareschi, T. Doldo, M. Ferrari, Apical dimension of root canal clinically assessed with and without periapical lesions, Int. J. Dent. 2014 (2014) 4. https://doi.org/10.1155/2014/374971.

[234] A.R. PradeepKumar, H. Shemesh, C. van Loveren, S. JothiLatha, F. Shireen, R. VijayaBharathi, A. Kishen, Impact of apical extent of root canal filling on vertical root fracture: a case–control study, Int. Endod. J. 52 (2019) 1283–1289. https://doi.org/10.1111/iej.13134.

[235] C. Boutsioukis, C. Gogos, B. Verhaagen, M. Versluis, E. Kastrinakis, The effect of apical preparation size on irrigant flow in root canals evaluated using an unsteady Computational Fluid Dynamics model, (2010) 874–881. https://doi.org/10.1111/j.1365-2591.2010.01761.x.

[236] O.A. Peters, M.S. Ficd, Current Challenges and Concepts in the Preparation of Root Canal Systems : A Review, (2004).

[237] L.E. Gregoris Rabelo, M. dos R. Bueno, M.V.C. da Costa, C.R. de Musis, C.R. de A. Estrela, O.A. Guedes, G. Gavini, C. Estrela, Blooming artifact reduction using different cone-beam computed tomography software to analyze endodontically treated teeth with intracanal posts, Comput. Biol. Med. 136 (2021). https://doi.org/10.1016/j.compbiomed.2021.104679.

[238] P. Harikrishnan, Finger Imaging by RadioVisioGraphy Digital Dental Radiography Imaging System, J. Hand Microsurg. 08 (2016) 181–182. https://doi.org/10.1055/s-0036-1593856.

[239] D. V. Ilić, L.S. Stojanović, Application of radiovisiography (digital radiology) in dental clinical practice, Vojnosanit. Pregl. 69 (2012) 81–84. https://doi.org/10.2298/VSP1201081I.

[240] J. Shan, A.W. Tucker, L.R. Gaalaas, G. Wu, E. Platin, A. Mol, J. Lu, O. Zhou, Stationary intraoral digital tomosynthesis using a carbon nanotube X-ray source array, Dentomaxillofacial Radiol. 44 (2015) 1–9. https://doi.org/10.1259/dmfr.20150098.

[241] K. Yoshiura, E. Nakayama, M. Shimizu, T.K. Goto, T. Chikui, T. Kawazu, K. Okamura, Effects of the automatic exposure compensation on the proximal caries diagnosis, Dentomaxillofacial Radiol. 34 (2005) 140–144. https://doi.org/10.1259/dmfr/88681265.

[242] A. Kumar, A. Parey, P.K. Kankar, Polymer Gear Fault Classification Using EMD-DWT Analysis Based on Combination of Entropy and Hjorth Features, Indian J. Pure Appl. Phys. 60 (2022) 339–346. https://doi.org/10.56042/ijpap.v60i4.58431.

[243] C. Pécora, J. D., Capelli, A., Guerisoli, D. M. Z., Spanó, J. C. E., Estrela, Influence of cervical preflaring on apical file size determination, Int. Endodo. 38 (2005) 430–435. https://doi.org/10.1590/S1980-65232012000200008.

[244] P.N.R. Nair, U. Sjögren, G. Krey, K.E. Kahnberg, G. Sundqvist, Intraradicular bacteria and fungi in root-filled, asymptomatic human teeth with therapy-resistant periapical lesions: A long-term light and electron microscopic follow-up study, J. Endod. 16

(1990) 580–588. https://doi.org/10.1016/S0099-2399(07)80201-9.